

Numerical Study of Isothermal Gas-liquid Two-phase Bubbly Flow

Cong Li
B.Eng.

A dissertation submitted in fulfilment of the requirement for the
degree of **Doctor of Philosophy** in

Nov. 2011

School of Aerospace, Mechanical and Manufacturing Engineering
Royal Melbourne Institute of Technology (RMIT)
University

Declaration

I, Cong Li, submit the dissertation titled “*Numerical Study of Isothermal Gas-liquid Two-phase Bubbly Flow*” in the fulfilment of the requirement for the degree of Doctor of Philosophy and certify that the work presented in this work is, to the best of my knowledge and belief, original except where acknowledgement has been made; the material has not been submitted previously, either in whole or in part, for a degree at this or any other university.

The author consents to the thesis being made available for photocopying and loan if accepted for the award of the degree

Cong Li
Nov. 2011

Acknowledgements

I firstly want to expresses my gratitude to Australian government and RMIT University for their sponsorship and support. Particular thanks are extended to School of Graduate Research and Student Union.

I would like to thank the School of Aerospace, Mechanical and Manufacturing Engineering, RMIT University. And sincere gratitude is expressed to my supervisors, Professor Jiyuan Tu and Dr Sherman Cheung for their time, assistance and work in guiding this research. Their help in developing my knowledge in computational fluid dynamics could not be underestimated.

I also would like to express gratitude to Dr William Yang of Commonwealth Scientific and Industrial Research Organization (CSIRO) and Dr Guan Heng Yeoh of Australian Nuclear Science and Technology Organization (ANSTO), for their kindly encouragement in exploration of image proccession and guidance in scientific writing, respectively.

I also would like to thank members of RMIT CFD group who always provided help whenever it needed.

Particular thanks are for the my friends who supported me in my difficult time - Dianne C., Kim M., Udeshika W., Deep S., Deju L., and Asintha N. Your help is unforgettable. A special thank to my parents for their patience, care and encouragement throughout my studying years.

Abstract

With the development of computer capability and advancement of modelling software, the technology of computational fluid dynamics (CFD) has been gradually recognized and utilized in engineering field to help seeking practical industrial solutions of gas-liquid two-phase flow. Among various numerical models for two-phase flow, the two-fluid model which traces two phases separately by using two sets of transport equations can be considered as the most accurate one. However, the numerical descriptions of interfacial actions bridging these two phases become to critical aspects to transport equations. The interfacial process descriptions named closure terms generally include three aspects, referred as turbulence model, interfacial driving force and interfacial area concentration (interfacial area per unit). In current study, the capability of Two-fluid model and its closure terms has been investigated to simulate vertical and horizontal bubbly flow conditions. An additional population balance model has been adopted to trace the interaction mechanisms between bubbles/bubbles and bubbles/eddies. There are three major aims for this current work: i) to assess the capability of an experimental drag coefficient correlation in terms of local void fraction and to compare this model with Ishii-Zuber drag coefficient model. ii) to estimate the performance of population balance model-Average Bubble Number Density (ABDN) model on horizontal bubbly flow where the internal local parameters are highly asymmetrically distributed along the radius direction. iii) to value the qualification of recently developed Direct Quadrature Methods of Moments (DQMOM) model which transforms the description of Particle Size Distribution (PSD) problem into lower-order moments of the size distribution (Cheung et al 2009 b).

Due to extensive expectations of simulating practical industrial scenarios under highly concentrated gas bubbly flows, plentiful researches have been carried out to explore neighbouring influence on drag reduction in a highly packaged swarm of bubbles. In this study, the performance of an experimental drag coefficient correlation proposed by Simonnet et al., (2007) by considering representation such neighbouring effects in terms of local void fraction has been assessed. This model has been compared with a densely distributed fluid particles drag model proposed by model Ishii-Zuber which is widely

utilized in commercial software packages. With the purpose of assessing the performance of these two drag force models, three primitive variables including gas void fraction, Sauter mean bubble diameter and gas velocity have been chosen as the aspects to validated against the experimental data of Hibiki et al. (2001). Both drag force models have achieved general satisfactory predicted results comparing with measured data. With extensive understanding of drag reduction caused by closely packed neighbouring bubbles, the latest coefficient model proposed by Simonnet et al. (2007) shows considerably better performance (Li et al. 2008 and 2009 a, b).

In order to predict the details of interfacial area concentration (IAC), extra set of population balance equations have been utilized to describe the bubble size distribution. Under certain amount of gas volume, IAC is inversely proportional to bubble size. There are extensive literatures regarding population balance model (PBM) applications in vertical bubbly flow; however such applications are seldom reported in horizontal bubbly flow where the local parameters are extremely asymmetrical distributed due to migration caused by buoyant force. With the purpose to investigate the performance of single averaged quantities PBM approach based on Average Bubble Number Density (ABND) model in prediction of bubbly flow phenomenon in horizontal pipe, predicted local radial distributions of void fraction, interfacial area concentration and gas velocity have been validated against the experimental data of Kocamustafaogullari et al. (1994 a) under four flow conditions with average gas volume fraction ranging from 4.4% to 20%. Satisfactory agreements have been generally achieved. Some discrepancies between the numerical predictions and experimental measurements have nonetheless been noticed at certain locations of the pipe. One of the reasons might be the insufficient resolution of the turbulent model in fully accommodating the strong turbulence in this current pipe orientation. And the inclusions of additional interfacial force such as the prevalent bouncing force among bubbles may need to be considered in future work in order to improve the PBM capability of prediction of horizontal gas-liquid bubbly flow (Li et al. 2010 a, b).

Population balance Model (PBM) plays important role to provide information regarding detailed bubble size distribution which could not be specified by general two-fluid model. Traditionally, the class method represented by the MUltiple SIze Group

(MUSIG) model has been considered as one of the most straightforward methods to investigate the population balance equation (PBE) by discretizing the continuous size range into a series number of discrete size classes. Nevertheless, a substantial number of equations may be required to adequately track the possible wide range of bubble sizes which leads to significantly expensive computational effort. Comparing with MUSIG model, the main advantage of Direct Quadrature Methods of Moments (DQMOM) is that the number of moments to be solved is generally very small. In this thesis, the DQMOM model has been developed and implemented into the commercial ANSYS CFX software to accommodate coalescence and breakage of gas bubbles. The simulation results have been validated with experimental data of MTLOOP measured by Lucas et al. (2005) and TOPFLOW measured by Prasser et al. (2007).

Publication

1. **Cong Li**, G H Yeoh, Sherman C P Cheung and Jiyuan Tu, “Modelling Horizontal Gas-Liquid Flow using Averaged Bubble Number Density Approach”, *Journal of Computational Multiphase Flows*, 2010, 2(2), 89-99.
2. **Cong Li**, Sherman C P Cheung, G H Yeoh and Jiyuan Tu, “On Modelling Horizontal Gas-liquid Bubbly Flow using Population Balance Approach” *The 17th Australasian Fluid Mechanics Conference, December 2010, Auckland, New Zealand*.
3. **Cong Li**, Sherman C P Cheung, G H Yeoh, and Jiyuan Tu, “A study of drag force in isothermal bubbly flow” *Journal of Computational Multiphase Flows*, 2009, 1(4), 295-309.
4. **Cong Li**, Sherman C P Cheung, G H Yeoh, and Jiyuan Tu, “Influence of drag forces of a swarm of bubbles in isothermal bubbly flow conditions” *The 7th International Conference on Computational Fluid Dynamics in the Minerals and Process Industries, December 2009, Melbourne, Australia*.
5. **Cong Li**, Sherman C P Cheung, Jiyuan Tu and G H Yeoh, “3-D Numerical simulation of isothermal upward bubbly flow: A study of drag force in multi-bubble system based on ABND model” *2008 ANSYS Australia User Conference, November 2008, Sydney, Australia*

Table of Contents

	<u>Page</u>
DECLARATION.....	I
ACKNOWLEDGEMENTS.....	II
ABSTRACT	III
PUBLICATION	VI
TABLE OF CONTENTS.....	VII
LIST OF FIGURES	XI
LIST OF TABLES	XIII
NOMENCLATURE.....	XIV
CHAPTER 1 INTRODUCTION.....	1
1.1 BACKGROUND.....	1
1.2 MOTIVATION AND AIM.....	4
1.3 SCOPE AND OUTLINE OF THE THESIS	6
CHAPTER 2 LITERATURE REVIEW.....	8
2.1 GAS-LIQUID TWO-PHASE FLOW PATTERNS AND REGIME MAP IN VERTICAL AND HORIZONTAL PIPES	8
2.1.1 <i>Flow Patterns and Regime Map in Vertical Pipe Flow</i>	8
2.1.2 <i>Flow Pattern and Regime Map in Horizontal Pipe Flow</i>	11
2.2 CHARACTERISTIC OF ISOTHERMAL BUBBLY FLOW IN BUBBLE COLUMN	14
2.3 POPULATION BALANCE MODELLING FOR ISOTHERMAL BUBBLY FLOW	16
2.4 BUBBLE INTERACTION MECHANISMS.....	22
CHAPTER 3 NUMERICAL FORMULATION AND POPULATION BALANCE MODEL.....	25
3.1 POPULATION BALANCE MODEL	25
3.1.1 <i>Population Balance Equation</i>	25
3.1.2 <i>Bubble Interaction Mechanisms</i>	26
3.1.2.1 Mechanisms of coalescence	26
3.1.2.2 Mechanisms of breakage.....	30

3.1.3	<i>The Methods of Population Balance Model</i>	32
3.1.3.1	Method of Moments (MOM) Approach	33
3.1.3.2	Class Method.....	35
3.2	INTER-PHASE MOMENTUM TRANSFER.....	37
3.2.1	<i>Drag force</i>	37
3.2.2	<i>Lift force</i>	38
	Where $D_s = (6V / \pi)^{1/3}$ is Sauter mean bubble diameter.	39
3.2.3	<i>Wall lubrication force</i>	39
3.2.4	<i>Virtual mass force</i>	39
3.2.5	<i>Turbulence dispersion force</i>	40
3.3	TURBULENCE MODELLING FOR TWO-FLUID MODEL	40
3.4	TWO-FLUID MODEL AND CLOSURE TERM.....	43
CHAPTER 4 NUMERICAL INVESTIGATION OF INFLUENCE OF INTERFACIAL FORCES ON BUBBLY FLOW		45
4.1	INTRODUCTION.....	45
4.2	MATHEMATICAL MODEL.....	49
4.2.1	<i>Interfacial Momentum Transfer due to Drag</i>	49
4.2.2	<i>Averaged Bubble Number Density (ABND) model</i>	51
4.2.3	<i>Coalesce and Break-up kernels</i>	51
4.3	NUMERICAL AND EXPERIMENTAL DETAILS	53
4.4	RESULT AND DISCUSSION.....	55
4.4.1	<i>Void fraction distribution</i>	55
4.4.2	<i>Sauter mean bubble diameter</i>	57
4.4.3	<i>Time-averaged gas velocity</i>	59
4.5	CONCLUSIONS	61
CHAPTER 5 ON MODELLING HORIZONTAL GAS-LIQUID BUBBLE FLOW USING POPULATION BALANCE APPROACH.....		63
5.1	INTRODUCTION.....	63
5.2	NUMERICAL DETAILS.....	65
5.3	RESULTS AND DISCUSSION.....	67
5.3.1	<i>Time averaged gas void fraction</i>	67
5.3.2	<i>Time averaged Interfacial Area Concentration (IAC)</i>	70

5.3.3	<i>Time averaged gas velocity</i>	70
5.4	CONCLUSION.....	71
CHAPTER 6 ON MODELLING VERTICAL GAS-LIQUID BUBBLE FLOW USING DIRECT QUADRATURE METHOD OF MOMENTS (DQMOM) APPROACH..... 72		
6.1	INTRODUCTION AND MATHEMATICAL FORMULATIONS.....	72
6.2	MATHEMATICAL MODELS	75
6.2.1	<i>DQMOM models</i>	75
6.2.2	<i>Source and Sink terms for DQMOM models</i>	77
6.3	DESCRIPTION OF THE EXPERIMENT SETUP	77
6.3.1	<i>Descriptions of the MTLOOP and TOPFLOW Experimental Setup</i>	78
6.3.2	<i>Different bubble size evolution caused by different injection methods</i> ...	80
6.4	NUMERICAL DETAILS.....	81
6.5	DISCUSSION	82
6.5.1	<i>Bubble void fraction distribution</i>	83
6.5.2	<i>Bubble Size Distribution</i>	85
6.6	CONCLUSION.....	87
CHAPTER 7 EXPERIMENTAL SETUP AND DIGITAL IMAGE DATA PROCESSION 88		
7.1	EXPERIMENTAL METHODS FOR MEASURING LOCAL BUBBLE DIAMETER DISTRIBUTIONS	88
7.2	EXPERIMENTAL SETUP AND ITS IMPROVEMENT BY USING SIDE-LIGHT ILLUMINATION METHOD WITH TWO FLASHES.....	91
7.2.1	<i>Experimental Setup Details</i>	91
7.2.2	<i>Experimental Setup Improvement</i>	92
7.2.2.1	Back-light illumination Configuration.....	92
7.2.2.2	Side-light illumination with one flash Configuration	93
7.2.2.3	Side-light illumination with two flashes Configuration.....	96
7.3	IMAGE PROCESSION	96
7.3.1	<i>Literature review of identification algorithms of overlapped objects</i>	98
7.3.2	<i>Overlapped Object Recognition (OOR) Method</i>	101
7.3.2.1	Edge Detection	101
7.3.2.2	Threshold	103

7.3.2.3	Detection of Joint Point.....	103
7.3.2.4	Tracing the Boundaries	106
7.3.2.5	Clustering Algorithms.....	108
7.4	DISCUSSION AND CONCLUSION	108
7.4.1	<i>Illumination methods with two side flashes</i>	108
7.4.2	<i>Overlapped Object Recognition</i>	110
CHAPTER 8	CONCLUSION.....	113
8.1	NUMERICAL INVESTIGATION OF INFLUENCE OF INTERFACIAL FORCE ON BUBBLE FLOW	113
8.2	ON MODELLING HORIZONTAL GAS-LIQUID BUBBLY FLOW USING ABND BASED POPULATION BALANCE APPROACH.....	114
8.3	ON MODELLING VERTICAL GAS-LIQUID BUBBLE FLOW USING DIRECT QUADRATURE METHOD OF MOMENTS (DQMOM) APPROACH.....	115
8.4	SIDE-LIGHT ILLUMINATION METHOD WITH TWO FLASHES AND OVERLAPPED OBJECT RECOGNITION (OOR) METHOD.....	116
8.5	RECOMMENDATIONS ON CFD DEVELOPMENT AND FUTURE RESEARCHES ON TWO-PHASE FLOW	117
REFERENCES	119	

List of Figures

FIGURE 2-1 FLOW PATTERNS OF AIR-WATER TWO-PHASE FLOW IN A VERTICAL PIPE.....	9
FIGURE 2-2 FLOW REGIME MAP FOR AIR-WATER TWO-PHASE FLOW IN A VERTICAL PIPE PROPOSED BY MISHMA AND ISHII (1984).	10
FIGURE 2-3 FLOW PATTERNS OF AIR-WATER TWO-PHASE FLOW IN A HORIZONTAL PIPE	12
FIGURE 2-4 FLOW REGIME MAP OF AIR-WATER TWO-PHASE FLOW IN A HORIZONTAL PIPE PROPOSED BY TAITEL AND DUKLER (1976)	13
FIGURE 2-5 DEMONSTRATION OF BUBBLY FLOW CHARACTERISTICS IN ISOTHERMAL BUBBLY FLOW.	15
FIGURE 2-6 AN EXAMPLE OF THE INTERNAL AND EXTERNAL COORDINATES OF POPULATION BALANCE FOR GAS-LIQUID BUBBLY FLOWS.....	18
FIGURE 2-7 GRAPHICAL PRESENTATIONS OF CLASS METHODS (CM).....	20
FIGURE 2-8 GRAPHICAL PRESENTATIONS OF THE QUADRATURE METHOD OF MOMENTS (QMOM).....	21
FIGURE 2-9 THE SCHEMATIC ILLUSTRATION OF BUBBLE COALESCENCE AND BREAK- UP MECHANISMS	24
FIGURE 4-1 STREAMLINE OF LIQUID VELOCITY AROUND A SINGLE BUBBLE AND A NUMBER OF BUBBLES	46
FIGURE 4-2 GEOMETRY DETAILS OF HIBIKI ET AL. (2001) EXPERIMENT.....	52
FIGURE 4-3 MAP OF TUBE FLOW REGIME AND TRANSITION FLOW CONDITIONS STUDIED IN THE PRESENT STUDY (CHEUNG ET AL 2007 A).....	53
FIGURE 4-4 MESH DISTRIBUTION OF COMPUTATIONAL MODEL: HIBIKI ET AL. (2001) EXPERIMENT.....	55
FIGURE 4-5 PREDICTED RADIAL VOID FRACTION DISTRIBUTION AND EXPERIMENT DATA OF HIBIKI ET AL. (2001).....	56
FIGURE 4-6 PREDICTED SAUTER MEAN BUBBLE DIAMETER DISTRIBUTION AND EXPERIMENT DATA OF HIBIKI ET AL. (2001).	58
FIGURE 4-7 PREDICTED RADIAL GAS VELOCITY PROFILE AND EXPERIMENT DATA OF HIBIKI ET AL. (2001).	60

FIGURE 4-8 ERROR PERCENTAGE OF PREDICTED TIME AVERAGED GAS VELOCITY COMPARING WITH EXPERIMENTAL DATA OF HIBIKI ET AL. (2001).....	62
FIGURE 5-1 A SIMPLIFIED SCHEMATIC BUBBLE MOTIONS IN HORIZONTAL PIPE FLOW: UNDER THE COMBINATION OF RADIAL AND AXIAL FORCE, BUBBLES TRAVEL NEITHER VERTICALLY NOR HORIZONTALLY	64
FIGURE 5-2 (A) GEOMETRY DETAILS OF KOCAMUSTAFAOGULLARI AND HUANG (1994) EXPERIMENT AND (B) MESH DISTRIBUTION OF COMPUTATIONAL MODEL FOR CROSS SECTION.....	66
FIGURE 5-3 PREDICTED TIME AVERAGED GAS VOID FRACTION DISTRIBUTIONS AND EXPERIMENTAL DATA OF KOCAMUSTAFAOGULLARI AND HUANG (1994) AT LOCATION OF $L/D = 253$	67
FIGURE 5-4 PREDICTED TIME AVERAGED INTERFACIAL AREA CONCENTRATION (IAC) DISTRIBUTIONS AND EXPERIMENTAL DATA OF KOCAMUSTAFAOGULLARI AND HUANG (1994) AT LOCATION OF $L/D = 253$	68
FIGURE 5-5 PREDICTED GAS VELOCITY DISTRIBUTIONS AND EXPERIMENTAL DATA OF KOCAMUSTAFAOGULLARI AND HUANG (1994) AT LOCATION OF L/D $= 253$	69
FIGURE 6-1 SCHEMATIC ILLUSTRATION OF MTLOOP EXPERIMENT	78
FIGURE 6-2 SCHEMATIC ILLUSTRATION OF TOPFLOW EXPERIMENT	79
FIGURE 6-3 PREDICTED RADIAL VOID FRACTION DISTRIBUTION AND EXPERIMENT DATA OF MTLOOP MEASURED BY LUCAS ET AL., (2005).....	82
FIGURE 6-4 PREDICTED RADIAL VOID FRACTION DISTRIBUTION AND EXPERIMENT DATA OF TOPFLOW MEASURED BY PRASSER ET AL (2007).....	83
FIGURE 6-5 PREDICTED BUBBLE SIZE DISTRIBUTION AND EXPERIMENT DATA OF MTLOOP MEASURED BY LUCAS ET AL., (2005).	84
FIGURE 6-6 PREDICTED BUBBLE SIZE DISTRIBUTION AND EXPERIMENT DATA OF TOPFLOW MEASURED BY PRASSER ET AL (2007).	86

List of Tables

TABLE 4-1 FLOW SCENARIOS AND ITS INLET BOUNDARY CONDITION DETAILS IN SIMULATION OF HIBIKI ET AL. (2001) EXPERIMENT.	54
TABLE 5-1 FLOW SCENARIOS AND ITS INLET BOUNDARY CONDITION DETAILS IN SIMULATION OF KOCAMUSTAFAOGULLARI AND HUANG (1994 A) EXPERIMENT.	65
TABLE 6-1 INFORMATION OF INLET FLOW CONDITIONS EMPLOYED IN SIMULATION OF MTLOOP AND TOPFLOW EXPERIMENT	81

Nomenclature

A	Cross-section area
C_D	Drag coefficient,
C_L	Lift coefficient
C_{TD}	Turbulence dispersion coefficient
C_{RC}	Random collision coefficient
C_{TI}	Turbulent impact coefficient
d_H	Maximum bubble horizontal dimension
D_s	Bubble Sauter mean diameter
D_B, D_C	Mass loss rate due to breakage and coalescence
E_o	Eötvos number
E_{dg}	Modified Eötvos number
f	Bubble size distribution
F_i	Total interfacial force
$F_{l \rightarrow g}^{\text{drag}}$	Drag force
$F_{l \rightarrow g}^{\text{lift}}$	Lift force
$F_{l \rightarrow g}^{\text{lubrication}}$	Wall lubrication force
$F_{l \rightarrow g}^{\text{dispersion}}$	Turbulent dispersion force
g	Gravitational acceleration
h	Film thickness
m	moment
n	Average number density of gas phase
P_B, P_C	Mass production rate due to breakage and coalescence
R	Sink and source terms
Re_g	Local Reynolds number

S	Mass transfer rate due to coalescence and breakage
t	Bubble contact time
\bar{u}	Velocity vector
V	Volume
We	<i>Weber number</i>
We_{cr}	Critical Weber number
X	Spatial locations

Greek Symbols

α	Volume fraction
α_{max}	Maximum allowable volume fraction
ε	Turbulence kinetic energy dissipation
ρ	Density
σ	Surface tension
ϕ_n^{RC}	Bubble number density change rate due to random collision
ϕ_n^{TI}	Bubble number density changes rate due to impact of turbulent eddies
ξ	Abcissa
ω	Weight
Ψ	Coalescence frequency
Ω	Break-up frequency
η	Collision frequency
ι	Coalescence efficiency
ξ	Fundamental parameter in PBE
ν	Viscosity
ς	Dimensionless size of eddies
φ	Shear rate
ζ	Weighted abscissas
δ	Standard deviation of coordinates

Subscripts

<i>g</i>	Gas phase
<i>gl</i>	Transfer of quantities from liquid phase to gas phase
<i>i</i>	Bubble size class
<i>j</i>	Velocity group
<i>l</i>	Liquid
<i>lg</i>	Transfer of quantities from gas phase to liquid phase

Chapter 1 Introduction

The purpose of this chapter is providing a brief description of this research work starting with introduction of background and obstacles in simulations of bubbly flow. Then, motivation and aim of this work have been subsequently explained. An outline is summarized to accommodate an overview of this thesis at the end of this chapter.

1.1 Background

Multiphase flow has been extensively existed in various industrial applications and academia researches, and particularly the bubbly gas-liquid two-phase flow can be considered as one of the most widely applied flow conditions. The characteristics of bubbly two-phase flow can be recognize as the existing of individual bubbles dispersed in a continuous liquid carrier phase and the maximum bubble size is extremely much smaller than the pipe diameter (Ekambara et al. 2008). It can be classified as isothermal or thermal bubbly flow depending on the occurrence of interfacial energy transfer between dispersed bubble phase and continuous liquid phase.

Bubbly two-phase flow is of great importance in many industrial applications. In nuclear and thermal engineering, dispersed small bubbles have opportunity to offer large interfacial areas enhancing efficiency of heat and mass transfer. In the various industrial applications such as chemical process, plenty of contacting equipments are running under dispersed bubbly flow conditions in order to achieve maximum interfacial areas for the purpose of specified particles attachment (i.e. mineral particles in flotation cell or oil sands in hydro- transport). As such, a lack of fundamental knowledge in this area can reduce industrial production capability; and can even have terrible tragedies when it comes to nuclear safety.

Generally speaking, there are three methods to investigate the bubbly flow mechanism, namely experimental, numerical and theoretical approaches. With the continuous strengthening of computer power and advancement of commercial modelling software, a rapidly increasing number of studies have exerted on the modelling of bubbly two-

phase flow using advanced computational fluid dynamics (CFD) methods in the last decade. These geometrical sizes and flow parameters of simulation studies are often set up to similar to experimental work aiming at identifying the hydrodynamic behaviour, heat and mass transfer, flow regime and mixing behaviour in practical industrial applications. By considering application of CFD, the time and cost in design and production will be significantly reduced compared to experimental based approach. Another feature of CFD approach is that it can provide rather detailed, visualized and comprehensive “microscopic” or “local” information which might be difficult to obtain through experimental methods. Furthermore, the CFD has another unique advantage when applying to simulate certain flow conditions which are not suitable for experimental tests (such as nuclear accident scenarios). It facilitates scientists and engineers to gain more knowledge and insight about design and operation of dangerous reactor devices.

In the numerical research of bubbly two-phase flow, due to the existence of the relative motion of one phase with respect to the other caused by differences of density and viscosity between two phases, two separate velocity fields should be considered in any research of two-phase flow problems. A general transient two-phase flow problem can be formulated by using a two-fluid model or a mixture model (Ishii 1975). The two-fluid model considered each phase separately by formulating two sets of conservation equations governing the balances of mass, momentum and energy of each phase with interfacial transfer terms appearing in each of the equations to bridge the different phasic effects. A simple mixture model such as the drift-flux model (Zuber 1967) can be obtained by replacing the two momentum equations by a mixture momentum equation and a relative velocity correlation. Such simple mixture model can decrease computational cost by reducing two momentum equations to one mixture momentum equation; however, it is difficult to obtain the relative velocity correlations which can appropriately and simultaneously represent the dynamic behaviors of both phases under a wide range of flow conditions. In order to obtain a model which can be widely adopted in various spans of industrial applications, the two-fluid model has been considered and investigated in the current study.

In the research of isothermal bubbly flow without heat and energy transfer, the two-fluid model can be simplified as only mass and momentum conservation equations of each phase with interfacial transport terms. As highlighted in the early work by Ishii (1975), the interfacial transports of mass, momentum usually have closely relationship to three important aspects: the liquid turbulences, the interfacial driving forces and interfacial area concentration a_{if} (interfacial area per unit volume).

Many if not most flows of engineering in nature significance are turbulences where fluctuations exist in the flow field in time and space. Principally, the transport equations can describe the turbulence without extra information. However, the direct simulation would require extremely expensive computational power which is at many orders of magnitude higher than available in the foreseeable future (ANSYS. CFX-11 User Manual). In order to practically describe flow turbulence with affordable computational price, turbulent flow has been considered consisted by average characteristics with additional time-varying fluctuating component. Equations only solve the mean flow quantities regardless the need for the resolution of the turbulent fluctuations. This method significantly reduces computational efforts. Nevertheless, the averaging procedure introduces additional unknown terms containing products of the fluctuation quantities which are difficult to determinate directly and so become research focuses for decade years. More information can be found in our group's previous research (Tian 2007). The focuses of current research have been concentrated on other two aspects of two-fluid model including interfacial driving forces and interfacial area concentration.

The interfacial driving force is an important closure term of two-fluid model which represent the momentum transfer between these two individual phases. The interfacial driving force has been formulated through the interfacial transfer term of momentum conservation equation. Currently, the interfacial driving force usually includes drag force, lateral lift force, wall lubrication force and turbulent dispersion force. Among all interfacial driving forces, drag force can be considered as the most important one since it represents the relative motions between two different phases and the relative motions are the fundamental information to calculate other interfacial forces.

Interfacial area concentration a_{if} describing the available interfacial area per unit volume for the interfacial transport of mass, momentum is a critical parameter for efficiency of heat transfer and production of industrial facilities. The interfacial area concentration can mathematically represented by the bubble number in certain spatial volume called bubble number density. And the variation of bubble number density occurs when bubbles merge together and/or break up, which can be described by the population balance model. A population balance in gas-liquid bubbly flow system focuses on tracking the changes of bubbles number in finite space under the consideration of bubbles coalescence and breakage due to interactions among bubbles and between bubbles and turbulent eddies. Traditionally, population balance is implemented by using the Class Method (CM), in which a series number of discrete size classes are utilized to approximate the continuous bubble size range. For each class, a scalar equation is solved to trace the population changes caused by intra/inter-group bubble coalescence and breakage. Recently, the method of moments (MOM) and its extensional application approach have attracted abundant interest from academic researchers and industrial engineers. As reported in plenty of literatures, the MOM and its extensional methods which condense population balance model (PBM) substantially by only tracking the evolution of a small number of moments can be considered as other promising methods in viably attaining practical solutions for the industrial application purpose.

1.2 Motivation and Aim

Since the interfacial driving forces and the interfacial area concentration play significantly important roles of linking gas and liquid phases by describing the interactions between these two separately considered phases as discussed before, the current study has been concentrated on a better understanding of interfacial driving force and population balance approach. Three main objectives were completed in the thesis.

First of all, the effort on improvement of the most important interfacial driving force, drag force, has exerted in current study. An experimental drag coefficient correlation in terms of local void fraction proposed by Simonnet et al., (2007) has been implemented

into ANSYS CFX commercial software via the CFX Expression Language (CEL). With the purpose of value the performance of this experimental model, the numerical prediction results of time averaged void fraction, Sauter mean bubble diameter distribution and gas velocity have been validated against the experimental data conducted by Hibiki et al. (2001). These predictions of experimental drag model are compared with the traditionally and widely utilized drag coefficient formulations of Ishii and Zuber (1979) as well. Satisfactory agreements are achieved for both models, however the model of Simioonet et al. (2007) shows considerably better performance in predicting the degradation of drag force incurred by neighbouring bubbles due to its addition consideration for closely packed bubbles (Li et al. 2009 a and b).

The second aim of this thesis is to assess the capability of PBM in simulation highly asymmetrical distributed bubbly flow in horizontal configuration. Horizontal bubbly flow commonly exists in many industrial systems; however, this flow orientation received less attention in the literature than vertical bubbly flow (Ekambara et al 2008). Due to buoyant influence, the migration of dispersed bubbles towards the top in horizontal pipe causes a highly asymmetric internal phase distribution, which adds more complexity than vertical bubbly flow in experimental observation and numerical simulation. In this study, the ABND model has been estimated in horizontal orientation bubbly flow conditions and validated against the experimental data of Kocamustafaogullari and Huang (1994 a). Generally speaking, the numerical model performs reasonably prediction comparing with measured experimental data. The results delivered a encouraging message that that average bubble number density (ABND) has the possibility to provide reasonable prediction in even highly non-symmetric internal phase distribution flow conditions (Li et al. 2010 a and b).

Thirdly, a recently developed population balance approach, the Direct Quadrature Method Of Moment (DQMOM) constituted by Marchisio and Fox (2005) has been implemented into ANSYS CFX commercial software via the CFX User Routines with Fortran language in the work of this thesis. DQMOM model, stemmed from MOM method, is an alternative approach to solve population balance model by transforming problem into lower-order of moments of the Particle Size Distribution (PSD). In this

current research, these predicted local radial distributions of time averaged void fraction and time averaged Sauter mean bubble diameter were validated against experimental data of MTLOOP and TOPFLOW. The results of satisfactory agreement between the numerical simulation and experimental measurement provide this valuable information that the DQMOM model can be considered as one promising population balance approach for industrial application since it has the capability to obtain reasonable prediction with affordable computational cost.

1.3 Scope and Outline of the thesis

The contents of the remaining seven chapters are as follows:

In Chapter 2, the simple patterns of gas-liquid two-phase flows in vertical and horizontal pipes and their flow regime maps have been introduced firstly. Particularly interests have been focus on characteristics of isothermal bubbly flow. The concept of population balance model and its interaction mechanisms have been explained in Chapter 2 as well.

Chapter 3 addresses the mathematical and numerical methodology. This chapter explains the principles of population balance model, interfacial force model and turbulent model which are useful formulations to solve two-fluid model and its three closure terms.

The primary aim of Chapter 4 is to assess the capability of an empirical model formulated by Simonnet et al. (2007) and to compare it with commonly used Ishii and Zuber (1979) model. These two models are validated against experimental data performed by Hibiki et al. (2001).

In chapter 5, a simple population balance model - Average Bubble Number Density (ABND) approach has been applied to simulate the internal phase distributions of air-water bubbly flow in a 50.3mm i.d. horizontal pipeline where the local parameters are highly asymmetrically distributed. With the aim of assessing the model performance under a wide range of flow scenarios, four individual flow conditions with average gas

volume fraction from 4.4% to 20% have been modeled. The predicted local radial distributions of void fraction, Interfacial Area Concentration (IAC) and gas velocity are validated against the experimental data of Kocamustafaogullari and Huang (1994).

In chapter 6, the capability of a recently developed population balance approach, the Direct Quadrature Method Of Moment (DQMOM) proposed by Marchisio and Fox (2005) has been investigated by validating against experimental results of MTLOOP and TOPFLOW. In this chapter, the background of Method Of Moment (MOM) approach have been introduced firstly. Then more detailed information regarding experimental and numerical setup is provided. Following discussion of predicted numerical results and measured experimental data, the future research recommendations are advised at the end of this chapter.

An experimental research of isothermal bubbly two-phase flow has been described in chapter 7. Firstly, main approaches for measuring local bubble size distribution have been simply introduced and particular interest has been focused on the photograph research methods in present study. Then, the experimental setup and its improvement of side-light illumination method with two flashes are explained. Furthermore, the Overlapped Object Recognition (OOR) method is demonstrated to abstract the mathematical information of overlapped bubbles by searching joint points through convolution.

Last but not least, the conclusion and recommendations are made in Chapter 8. Further research orientation is also suggested.

Chapter 2 Literature Review

Chapter 2 started with description of gas-liquid two-phase flow physical morphologies and their regime distribution in a two-dimensional map, namely flow patterns and regime map respectively, in vertical pipes as well as horizontal pipes. Particular information about characteristics of bubbly flow and transition phenomenon from bubbly flow to slug flow has been further provided. The numerical approach referred as population balance model is recognized by many scientists to have the potential capability to simulate the complex bubbly flow characteristics involving bubble deformation, mergence and breakage. The principle of population balance model and its history have been generally introduced.

2.1 Gas-liquid two-phase flow patterns and regime map in vertical and horizontal pipes

The morphology of gas and liquid phases distributing themselves into each others is well known as fundamental and essential information, since the underlying mechanisms of heat transfer vary dramatically from one distribution to another. In early stage research of gas-liquid two-phase flow, importance of flow structure has been widely aware; thereby research focuses have predominately concentrated on recognizing and description of flow mixture (Yang et al. 2004). Through abundant of visualization experiments on gas-liquid two-phase flow, the flow structures have been identified into several classes, which are referred to as flow patterns. When further research interesting has been laid down on the transformation from one flow pattern to another, the regime map of flow patterns is considered important knowledge as well.

2.1.1 Flow Patterns and Regime Map in Vertical Pipe Flow

Through much experimental visualization in gas-liquid two-phase flow in vertical configuration, some commonly observed flow structures have been identified and classified, which have been depicted in Figure 2-1.

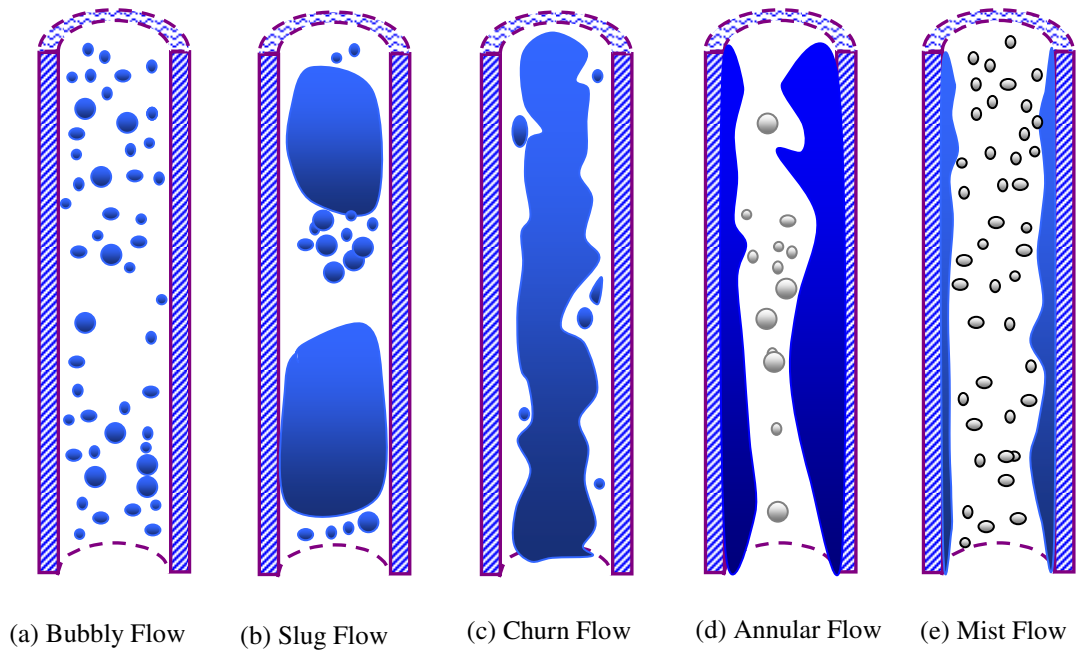


Figure 2-1 Flow patterns of air-water two-phase flow in a vertical pipe

As demonstrated in Figure 2-1 (a), when the gas void fraction is low but the relative velocities between two-phase are considerably high, the strong turbulence caused by high relative velocities can easily break such small amount gas volume, resulting gas phase is dispersed as the form of nearly spherical and discrete bubbles in the continuous liquid phase. The bubbles may have various sizes; however they are much smaller than the diameter of the tube. This flow structure called bubbly flow.

With increasing gas void fraction, the bubbles are so fully packed with each other in limited spatial locations of tube that the tendency of small bubbles colliding and coalescing to form large bubbles has been significantly increased. In slug flow condition illuminated in Figure 2-1 (b), these large bubbles, namely Taylor bubbles, are almost the same in dimension to tube diameter and have bullet shape. Slugs of liquid are observed to separate Taylor bubbles and may include some small bubbles. These small bubbles are easily sucked by Taylor bubbles because of the effecting of weak entrainment.

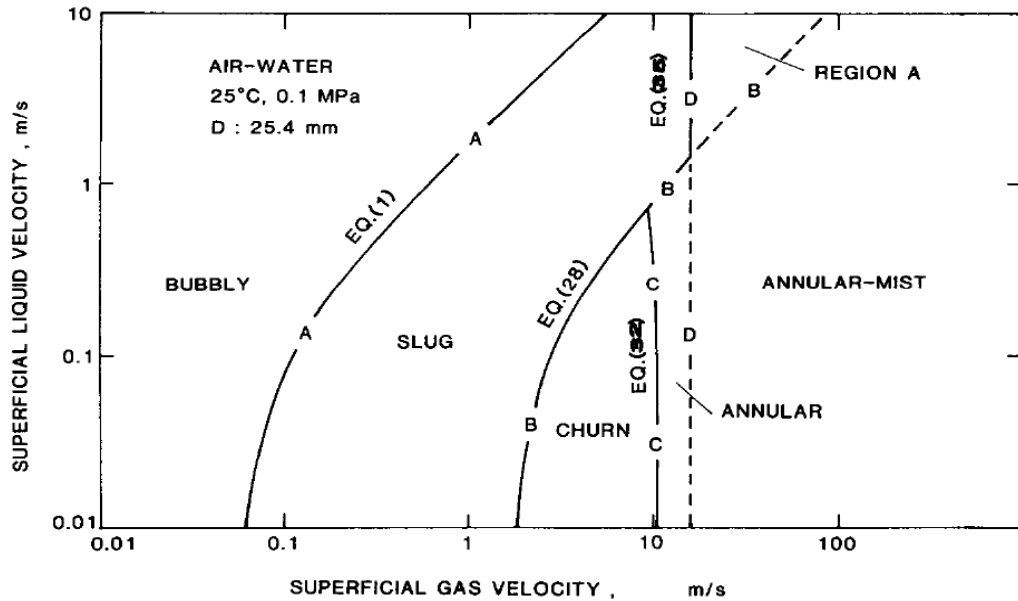


Figure 2-2 Flow regime map for air-water two-phase flow in a vertical pipe proposed by Mishma and Ishii (1984).

Continuously increasing the gas void fraction, the Taylor bubbles are connected with each other to expelled liquid from the center of tube to form liquid film next to tube wall. However, the liquid film is under unstable structure and presented in an oscillatory routine. The liquid phase flows up and down depending on the compromised results between gravity and shear forces acting on the thin film of liquid. The gravity and shear forces are in relative parity and effect in opposing directions on the liquid film. This flow pattern is referred as churn flow as depicted in Figure 2-1 (c), which is an intermediate regime between the slug flow/annular flow regimes and may not observed at all flow conditions with various sizes of tubes.

When the dominant force on the liquid film is from the interfacial shear force as the result of increasing relative velocities between two phases, the gas phase occupies the center of tube as a continuous phase, while the liquid film becomes thin forming an annular ring of liquid on the wall. Comparing with churn flow, this flow pattern, namely annular flow (depicted in Figure 2-1 (d)), is in a particularly stable flow condition with frequency waves and ripples on the liquid film surface. Few liquid droplets may be entrained into the gas corn.

Under very high gas void fraction, the strong interfacial shear force compels the thinness of liquid film and destroys the stability of flow structure, resulting more and more liquid is entrained into the continuous gas phase core as the format of droplets. In this mist flow pattern depicted in Figure 2-1 (e), it is difficult to see the small droplet or mist without special treatment, such as lighting and/or magnification.

After collecting information of fluid properties and visualizing the flow pattern through a transparent window on test section, a next step of research is usually undertaken for a way to map the transition boundaries between the regimes in a two-dimensional plot by utilizing obtained flow information through experiments. Many flow-regime maps have been proposed through this approach. Mishima and Ishii (1984) further developed theory of flow-regime criteria for upward gas-liquid flow in vertical pipe and proposed a flow-regime map by using a direct geometrical parameter void fraction. The widely applied Mishima and Ishii (1984) upward gas-liquid flow regime map in vertical pipe is demonstrated in Figure 2-2.

2.1.2 Flow Pattern and Regime Map in Horizontal Pipe Flow

The two-phase flow patterns in horizontal configuration are more complicated than those in vertical flows since gravity force/buoyant force is perpendicular to the flow main direction which influences that gas/liquid phase dominantly occupies the top/bottom of tube or even straightforward stratifying in some flow patterns in horizontal flows. Figure 2-3 demonstrates the flow patterns in horizontal tube.

As depicted in Figure 2-3 (a), the bubbly flow in horizontal tube has the similar flow pattern with the one in vertical tube but the bubbles have high tendency to migrate to the upper half of the tube under the influence of buoyancy. This flow condition typically occurs under high liquid velocity whose strong turbulence can possibly counteract coalesce of bubbles fully packaging with each other in the vicinity of upper tube wall.

With increasing the gas flow rate and reducing the liquid velocity, the fully packed bubbles next to the upper tube wall to form big elongated gas bubbles, which is referred as plug flow and shown in Figure 2-3 (b).

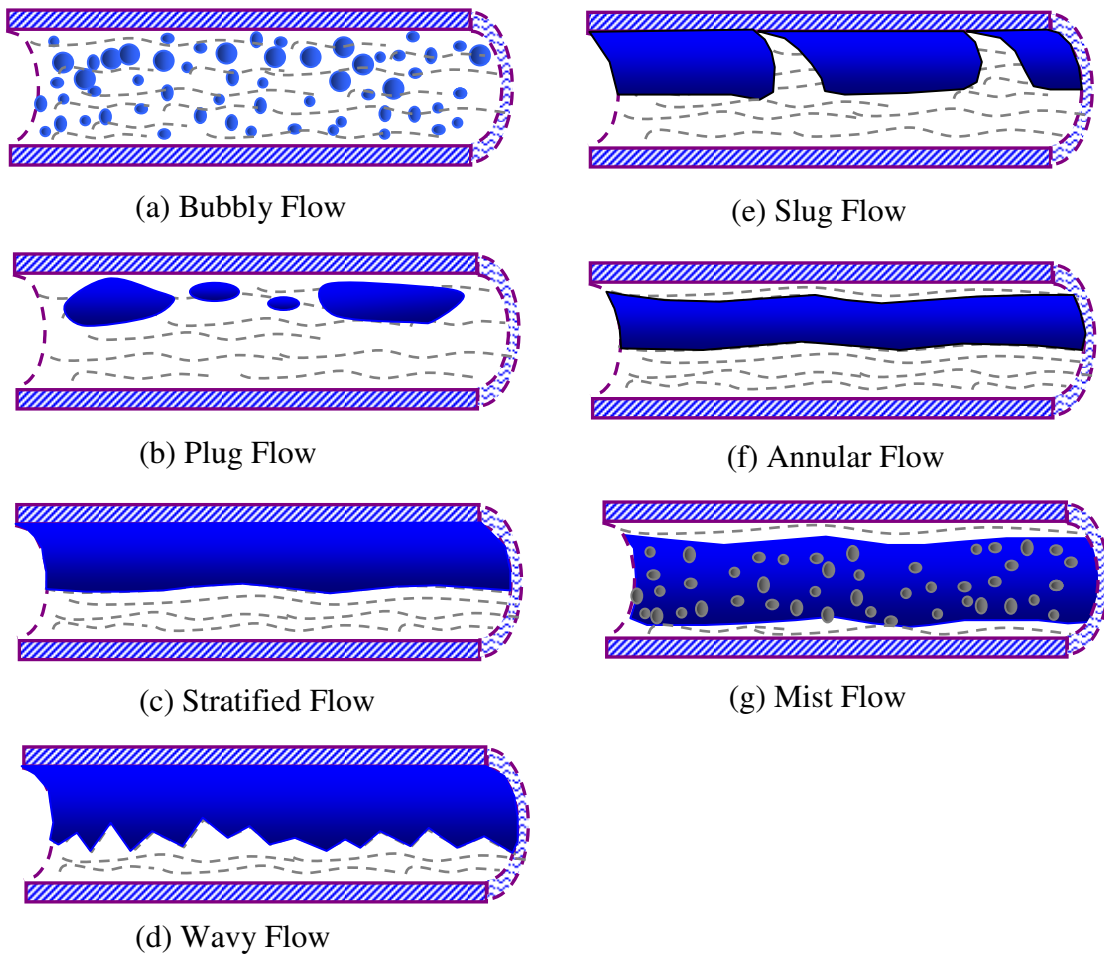


Figure 2-3 Flow patterns of air-water two-phase flow in a horizontal pipe

A complete separation of these two phases happens when liquid and gas phases are both under circumstance of low velocities. A stable horizontal interface is normally observed in this so called stratified flow pattern, which is shown in Figure 2-3 (c).

Increasing the gas velocity in a stratified flow, the interfacial shear force caused by the strong relative velocity engages partial stratified liquid phase into gas phase to form waves on the interfacial surface. The phenomenon of the waves is notable; however, their crests do not touch the top of the tube, as illuminated in Figure 2-3 (d). This flow structure is called wavy flow.

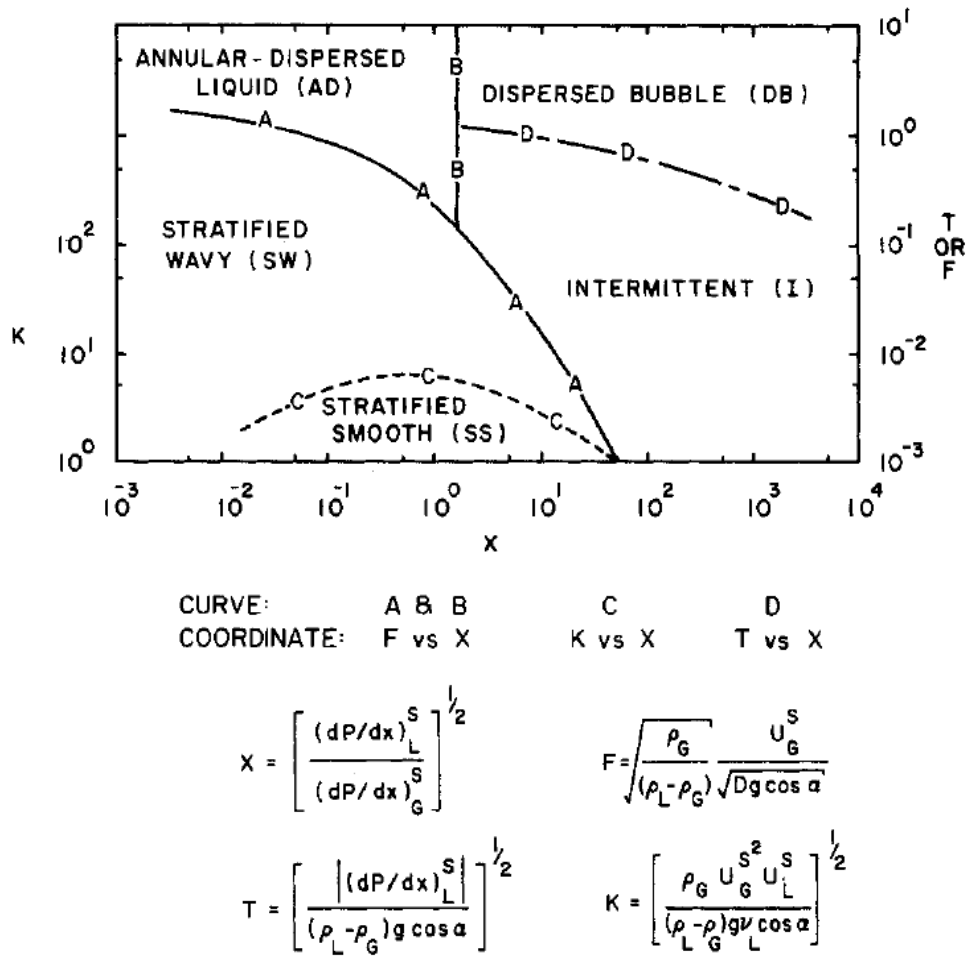


Figure 2-4 Flow regime map of air-water two-phase flow in a horizontal pipe proposed by Taitel and Dukler (1976)

When these interfacial waves become large enough to wet the top of the tube, the slug flow condition occurs. As illuminated in Figure 2-3 (e), the large amplitude waves continuously touch the top wall leaving thin liquid films behind in gas phase. And the continuous gas phase has been separated by these thin liquid films and broken down to elongated bubbles. The diameters of these bubbles are similar to the diameter of tube.

With even larger gas flow rate, a continuous annular liquid film is formed around the inner surface of tube, which is named as annular flow. The annular flow in horizontal has similar characteristics with that in vertical flow; however the thickness of liquid

film around horizontal tube perimeter is not equal with thicker at the bottom than the top, as demonstrated in Figure 2-3 (f).

At very high gas velocities, small droplets may be stripped from the annulus liquid films in vicinity of wall because of interfacial shear force and entrained into the continuous gas core in tube (Figure 2-3 (g)).

When clarifying the flow regimes through experimental data, the choosing of coordination had to be carefully considered. Without supporting of theoretical basis, this approach of locating experimental data on plot strongly depended on the particular data which were prepared for the map. Thus, the theories of transition mechanisms in gas-liquid two-phase flow in horizontal pipe were required to develop. Based on physically realistic mechanisms of transitions between different flow regimes, Taitel and Dukler (1976) proposed analytical prediction of the transition criteria from a flow regime to another and plotted transition lines on a two-dimensional map, which is depicted in Figure 2-4. More details can be found in Taitel and Dukler (1976).

2.2 Characteristic of Isothermal Bubbly Flow in Bubble Column

Comparing with other flow regimes mentioned above, bubbly flow can provide large interfacial areas and has various industrial applications. In nuclear engineering, many types of equipment are running under bubbly flow condition since its large interfacial areas provide the capability to enhance heat and mass transfer between two phases. Another example of bubbly flow application is in flotation cell of mineral procession for the purpose of separation mineral particles from slurry. In the flotation cell, the useful mineral particles attach on the surface of injected bubbles in the bottom of tank and rise up to tank surface with bubbles under the effect of bubble buoyant force separating from the waste which has been left in the bottom of tank. Thereby, the interfacial surface between two phases is proportional to mineral procession efficiency. In order to understand fundamental principle of bubbly flow, a simplified geometry of bubble column is possibly needed to investigate initially.

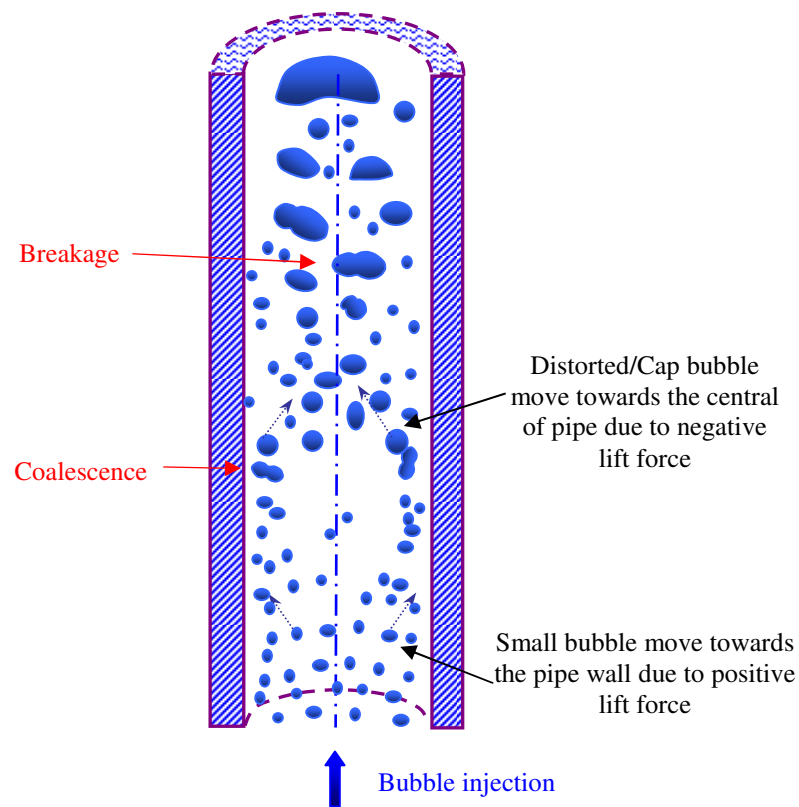


Figure 2-5 Demonstration of bubbly flow characteristics in isothermal bubbly flow.

In isothermal bubbly flow, there is no heat transferring from the outside of pipe into inside flow field and no vapor bubbles being generated into liquid phase, thus characteristics of isothermal gas-liquid two-phase flow fully depend on the bubble mechanistic behaviors such as bubble coalescence and bubble breakage under various combinations of gas and liquid velocities. Physical phenomenon of bubble coalescence and breakage on the bubbly-to-slug transition regime in a simplified bubble column has been illuminated in Figure 2-5. The bubbly-to-slug flow condition is a coalescence dominated flow condition. In upward flow condition, the small bubbles (under 5.5 mm for air-water flows at 25°C) and liquid phase are injected at the bottom of the bubble column through spargers. As the result of effects from the positive lift force created by lateral velocity gradient and local vortexes, the small bubbles have a tendency of migration towards to the wall of pipe causing high void fraction in the vicinity of wall. By increasing the gas flow rate, the number of bubbles in limited space next to wall has been climbed and the bubbles are fully packaged with each other, whereby the

possibilities of bubble coalescence to form large bubbles mount up. The large bubbles (above 5.5mm), pushed by negative lift force, migrate to the center of pipe to form larger Taylor bubbles. It is worthy to be aware that the bubble coalescence and breakage happen simultaneously; however effects of bubble coalescence are dominate in certain flow conditions. The flow transition from bubbly-to-slug regime is a typical example. The mechanistic behaviors of bubbly flow in breakage dominant flow condition will be detailed in Chapter 6.

2.3 Population balance modelling for isothermal bubbly flow

Generally speaking, two methods have been utilized to describe bubbly two-phase fluid flow characteristics, namely the Lagrangian approach and Eulerian approach respectively. By using Lagrangian approach, a bubble has been selected and is followed as it moves through space with time. The interest of Lagrangian approach is to trace the motion of this single object and its path line. Instead of focusing on track of single bubble, the Eulerian approach is used to obtain an overall information about the distribution of dispersed phase by investigation on average performance of whole bubbles group.

Since the actions of coalescence and breakage among bubbles generally and frequently happen, it is almost impossible to trace the path line of single object because of creation or disappearing of this object. On the other hand, the efficiency of industrial application depends on averaged interfacial area concentrations between these two phases instead of performance of single bubble. Thereby, a widely applied concept from Eulerian approach referred as population balance has been studied following by mounting academic and industrial interests.

The concern of population balance on any system is to track the number changes of entities whose presence or occurrence indicates the overall performance of the system under investigation (Ramkrishna, 2000). Depending on the convenience of applications, the tracked variables may change to other extensive measurements rather than number such as interfacial area, volume or mass. And the entities can be solid particles, liquid

droplets, bubbles or even more abstractly events (Cheung et al. 2009 a). Mathematically, the variable describing an entity has to be represented in “external” as well as “internal” coordinates. The “external” coordinate is utilized to locate the entity’s physical position which is governed by flow convection and diffusion, while the “internal” coordinate is referred to essential properties of the entity such as number, size, surface area, velocity and so on (Ramkrishna and Mahoney, 2002). A simple example of the internal and external coordinates involved in the population balance for gas-liquid bubbly flows is shown in Figure 2-6. Usually, the external and internal coordinates of an entity are represented by a finite dimensional state space and the total number of entities in a state space would maintain the same (even though the number varies depending on the selected domain) if there are only physical motion of entities. However, in some process such as nucleation of particles, aggregation, bubble coalescence & breakage and so on, the number in such state space may change due to “birth” processes creating new bubbles and “death” process destroying existing bubbles. The population balance model is developed to deal with the displacement of entities by consideration of their motion in state space and the birth-and-death processes (Ramkrishna and Mahoney, 2002).

Population balance models have long history with respect to applications in specific fields as reported by Cheung et al. (2009 a). The original concept of population balance model came from Boltzmann equation proposed by Ludwig Boltzmann more than a century ago to address the spatial locations and velocities of molecules in a defined space. However, the gradual maturation and consequent application of population balance models using diverse types of varieties as internal coordinates is actually recent years’ work. Hulburt and Katz (1964) and Randolph and Larson (1964), (1971) have presented a treatment of population balance to deal with crystallization. Hidy and Brock (1970), Friedlander (2000) have applied population balance model to solve particle distribution in aerocolloidal systems. A most recently book published by Ramkrishna (2000) concluded various generic issues in application of population balance model.

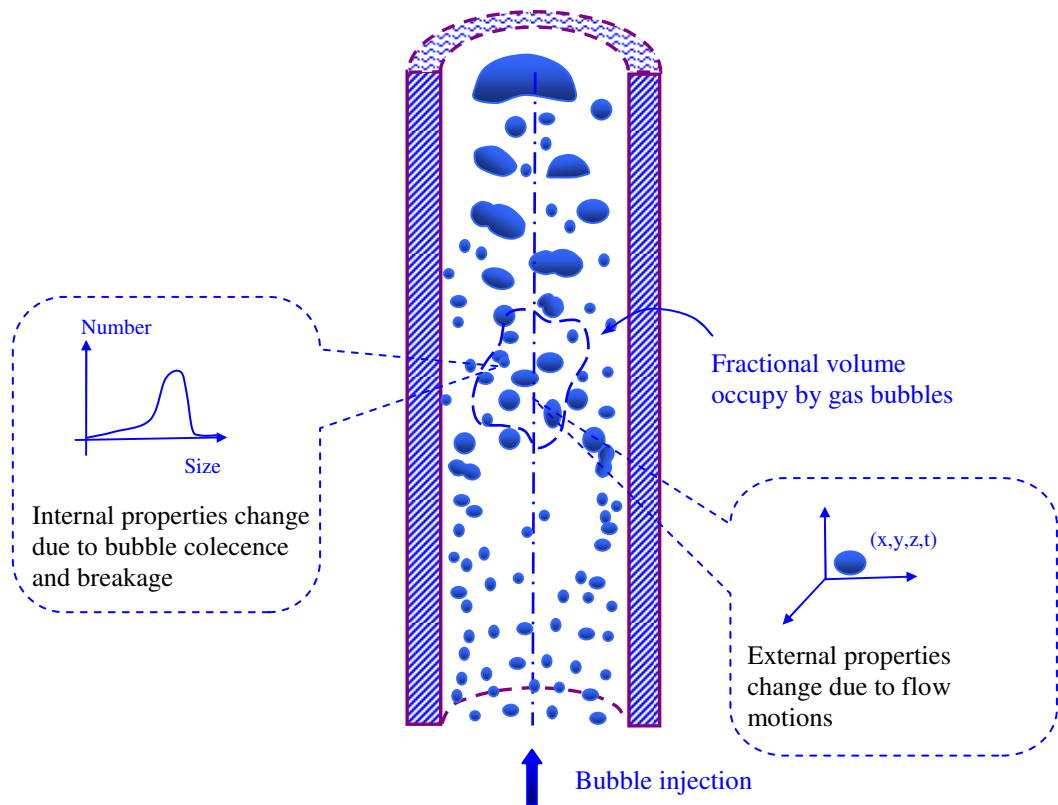


Figure 2-6 An example of the internal and external coordinates of population balance for gas-liquid bubbly flows

Till this stage, only few cases with simplified coalescence and breakage kernels can be mathematically analysis with population balance model due to complexity of bubble dynamics (Scott, 1968; McCoy and Madras, 2003). Generally speaking, two types of methods, namely Class Method and Method of Moments are commonly utilized in industrial application.

The traditional class method (CM) has long standing history of development and straightforward implementation in many commercial CFD software packages. In this method, the bubbles main characteristic has been directly simulated using primitive variable. The fundamental ideal of CM is discretion continuous bubble size range into a series discrete size classes. A scalar equation is solved to represent the population changes due to bubble coalescence and breakage in inter group as well as extra groups.

A graphical representation of CM is depicted in Figure 2-7. As it can be seen, the position of each size group among size range in CM are fixed and aligned during solution of scalar equations, however, the size fraction of each group can be flexibly changed to represent the population changes in this size group. Depending on the number of groups, CM can be classified as single average quantities approach and Multiple Size Group (MUSIG) approach.

In the single average quantities approach, the overall changes of the particle population are represented by only an average quantity, by which the computational time has been reduced in solving PBE. It provides an attractive feature for practical application in industrial fields. The first single average quantities approach has been derived by Kocamustafaogullari and Ishii (1995) using primitive variable of interfacial area concentration (IAC). According to their study, the interfacial transfer mechanisms is a dominant factor and an interfacial area concentration (IAC) transport equation has been derived for tracking the interfacial area changes between gas and liquid phase in bubbly flow problems. And an equivalent formulation, an Average Bubble Number Density (ABND) equation has been proposed recently in our group previous studies (Yeoh and Tu, 2006; Cheung et al., 2007 a).

A more complex model referred as Multiple Size Group (MUSIG) model is developed to handle poly-dispersed multiphase flow. By poly-dispersed multiphase flow, it means that the dispersed phase has a large variation in size which is difficult to be described by single average quantity (ANSYS CFX-11 User Manual). Depending on assumptions of same or different velocities in same size group, the MUSIG model has been classified as homogeneous or inhomogeneous MUSIG model. In the homogeneous MUSIG model, M groups of size fractions have been utilized to approximate the continuous particle size distribution (PSD) and the transformation of each size fractions has been expressed by a transport equation with its source kernels controlling the inter-group fraction transfer due to the mechanisms of bubble mergence and break-up. The various applications of homogeneous MUSIG model in simulation of bubbly flow have been reported in abundant studies such as Pochorecki et al. (2001), Olmos et al. (2001), Frank et al. (2004), Yeoh and Tu (2005) and Cheung et al. (2007 a and b). Recently, Krepper

et al (2005) developed inhomogeneous MUSIG model, which considered the practicability of velocities difference in each group by sub-dividing the dispersed phase into N groups of velocity fields. This flexibility further developed the possibility of simulating complex gas-liquid two-phase flow in transition regime from bubbly flow to slug flow where different bubble shapes exist simultaneously.

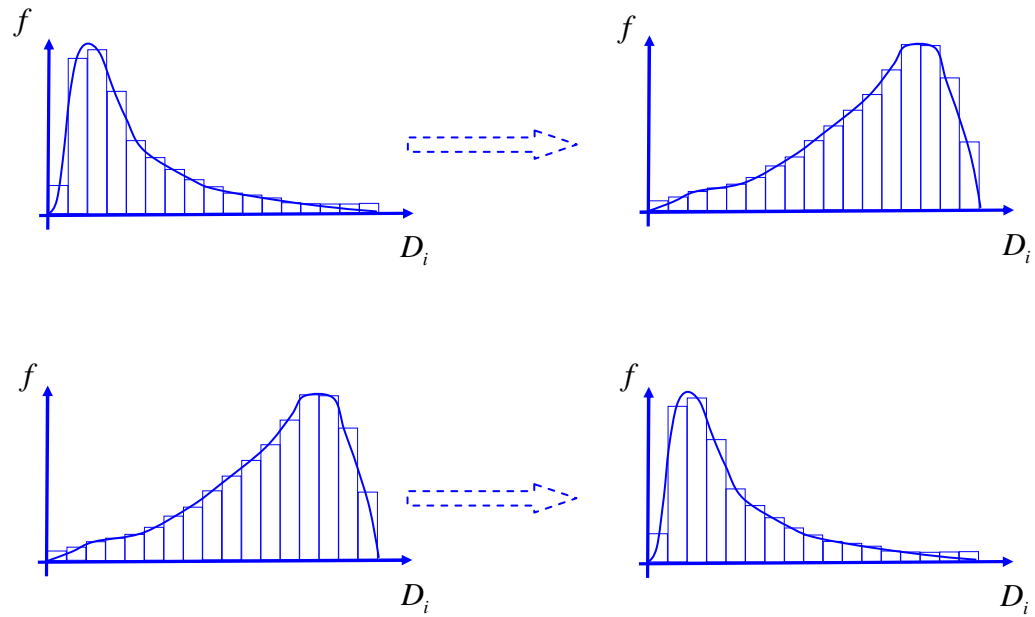


Figure 2-7 Graphical presentations of Class Methods (CM)

Another possible way of solving the PBE is by means of the method of moments (MOM) which was firstly introduced by Hulburt and Katz (1964). The beautiful ideal behind the MOM is to transform the Particle Size Distribution (PSD) problem substantially by only tracking the evolution of a small number of moments (normally 4-6). Therefore, it becomes numerical economy which is a critical value in modelling complex industrial systems when the bubble dynamics is strongly coupled with already time-consuming simulations of turbulence multiphase flows. However, the method of moments suffers severe restriction of integral types and is only applicable to a limited number of problems. On the other hand, the moment equation gives no information about the shape of the distribution for internal parameters, such as bubble diameter, surface area, which denotes a closure problem (Hulburt and Katz, 1964).

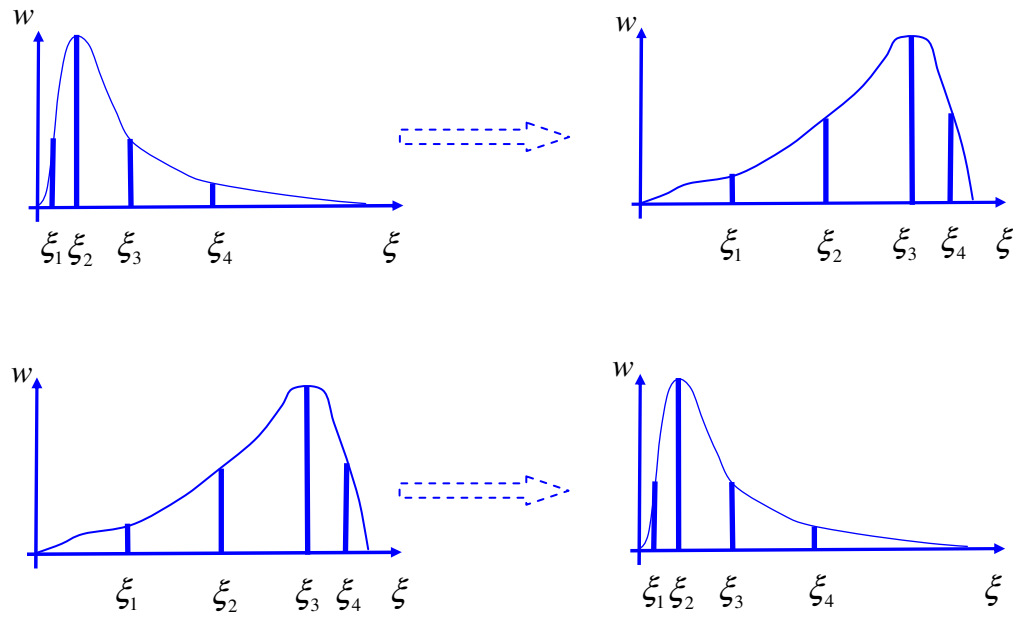


Figure 2-8 Graphical presentations of the Quadrature Method of Moments (QMOM)

In order to circumvent this limitation, McGraw (1997) proposed a modification of the MOM through method of quadrature approximation, namely Quadrature Method of Moments (QMOM). For the integral of equations (Navier–Stokes equations or General dynamic equations) whose each individual term could not be directly expressed by function of moments, this QMOM creates formulations including new variables, referred as the abscissas and weights to present this integral by means of n -point Gaussian quadrature approximation. Then the abscissas and weights can be further specified in terms of the low-order moments. The A graphical representation of the QMOM in approximating the PSD is depicted in Figure 2-8. Different from CM method in which the position of each size group is fixed and aligned, the position of each abscissa can flexibly move according to the mechanical dynamics causing by bubble coalescence and breakage. This feature is extremely useful when it calculate the flow characteristics of poly-dispersed multiphase flow. In order to cover wide range of bubble size, a general 20 groups of bubble size have been generated in CM method, however, only 4 sets of abscissa and weights are needed in QMOM method since the abscissa can freely slide to represent the small bubbles as well as large bubbles. QMOM

has been extensively validated for several problems with different internal coordinates. One of the main limitations of QMOM is that each moment adopted to represent the PSD is solved by single average velocity which is apparently non-physical in the context of the multiphase flows. Moreover, by tracking only the moments of the PSD, it does not provide information of connection between internal coordinates and phase velocities. With the aim to address these issues, the Direct Quadrature Method of Moments (DQMOM) has been proposed and validated by Marchisio and Fox (2005) where the Dirac delta function has been utilized in size distribution functions. The principle behind the DQMOM centres on tracking the primitive variables appearing in the quadrature approximation, instead of moments of PSD. Therefore, the evaluation of the abscissas and weights are solved by matrix operations. More information will be provided in Chapter 3 and Chapter 6.

In summary, the class method has attracted numerous academic attentions and various industrial applications because of its rather straightforward implementation within commercial CFD software packages. However, the extra computational effort is costed in order to achieve sufficient numerical accuracy. On the other hand, the MOM represents a rather sound treatment for solving PBE with limited computational burden. But further validations against experimental data and assessments of the various approaches of method of moments are still required in future research owing to the considerably short development history.

2.4 Bubble Interaction Mechanisms

The interfacial area concentration is a key parameter to straightforward to represent the interaction between the gas and liquid phases. In order to fully describe the interaction of coalescence and breakage between these two phases, amount of focus has been concentrated on interactions among bubbles and between bubbles and turbulent eddies.

In order to briefly demonstrate the mechanisms responsible for bubbles coalescence and breakup, the simple classification of Wu et al. (1998) has been introduced here.

- Coalescence through random collision driven by turbulent eddies

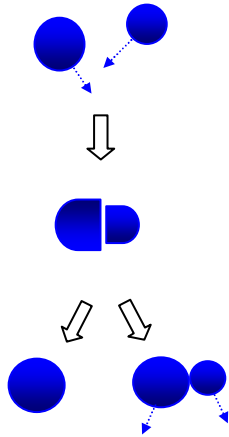
- Coalescence due to the acceleration of the following bubble in the wake of the preceding bubble
- Break-up due to the impact of turbulent eddies
- shearing-off of small bubbles from larger cap bubbles
- breakup of large cap bubbles due to interfacial instabilities

In the case of low void fraction conditions where no cap bubbles are present, the first three major phenomenological mechanisms have been considered and the appropriate mechanistic models have subsequently been established. However in realistic applications more complicated coalescence and breakup kernels of first three major phenomenological mechanisms are applied. More information can be found in Chapter 3.

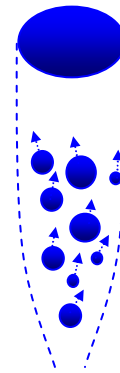
The schematic illustrations of these mechanisms are shown in Figure 2-9.

Coalescence Mechanism

Random Collision

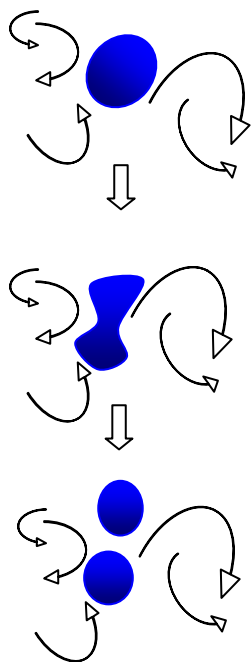


Wake Entrainment

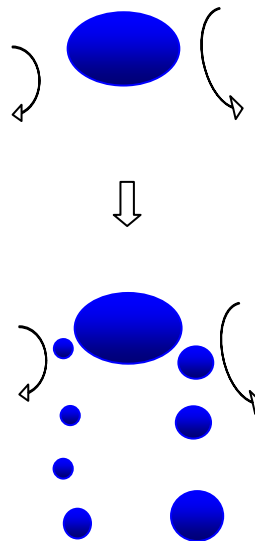


Break-up Mechanism

Turbulent Impact



Shearing-off



Surface Instability

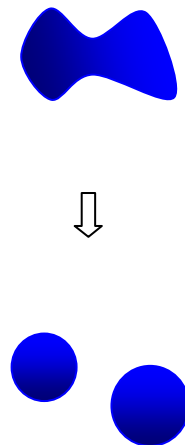


Figure 2-9 the Schematic Illustration of Bubble Coalescence and Break-up Mechanisms

Chapter 3 Numerical Formulation and Population Balance Model

This chapter firstly provides detailed information of population balance model, interfacial force model and turbulent model. Then the widely applied two-fluid model in multi-phase flow is explained and its three important closure terms, referred as bubble size distribution, interfacial momentum transfer and turbulent viscosity are highlighted. These three closure terms can be separately solved through the models which are introduced at the beginning of this chapter.

3.1 Population Balance Model

3.1.1 Population Balance Equation

The purpose of population balance equation (PBE) is to describe particle physical location (external coordinates) as well as to determinate particle characteristics (internal coordinates) in certain state space. As the Boltzman equation laid the foundation of PBE, such equation is generally expressed in the similar format of Boltzman equation to predict the particle size distribution (PSD) as follow:

$$\frac{\partial f(\xi, X, t)}{\partial t} + \nabla \cdot (u(\xi, X, t) f(\xi, X, t)) = S(\xi, X, t) \quad (3.1)$$

where $f(\xi, X, t)$ is the PSD function including internal vector ξ referring particle characteristics and external variables X and t presenting spatial position and physical time respectively. $u(\xi, X, t)$ is velocity vector in external space. The net source or sink term $S(\xi, X, t)$ indicates the particle number changes due to merging and breakage processes (ANSYS CFX-11 User Manual).

$$S(\xi, X, t) = B_C - D_C + B_B - D_B$$

$$B_C = \frac{1}{2} \int_0^\xi \Psi(\xi' - \xi; \xi) f(\xi' - \xi, X, t) f(\xi', X, t) d\xi \quad (3.2)$$

$$D_C = f(\xi', X, t) \int_0^\infty \Psi(\xi'; \xi) f(\xi, X, t) dt$$

$$B_B = \int_{\xi'}^{\infty} \Omega(\xi; \xi') f(\xi, X, t) d\xi$$

$$D_B = f(\xi, X, t) \int_0^{\xi} \Omega(\xi'; \xi) d\xi$$

Where B_C and D_C represent the birth rate and death rate respectively due to coalescence with other smaller particles. Similarly, B_B and D_B delegate the birth rate and death rate because of breakage process from larger particles. Particularly, a great quantity studies have been focused on coalescence frequency $\Psi(\xi'; \xi)$ and breakup frequency $\Omega(\xi'; \xi)$ and its extension of net source or sink term since accuracy of these description plays major influence on prediction of two-phase flow structure and particle size distribution.

3.1.2 Bubble Interaction Mechanisms

3.1.2.1 Mechanisms of coalescence

In two-phase flow condition, the coalescence and breakup are happening simultaneously and both taking responsibility for the evolution of geometrical structure and bubble size distribution; however, the coalescence phenomenon is considered more complicated than breakup process (Chesters, 1991). The activities of coalescence are involved not only interactions between bubbles themselves when they are closed packaged, but also those between bubbles and the surrounding turbulent eddies. Shinnar and Church (1960) proposed the most popular bubble coalescence theory, namely film drainage model. Their research stated that, when the collision happens between two bubbles, there is a thin sheet of liquid trapping between them. Coalescence only happens after the liquid film drains out to a critical thickness by molecular attraction force between two colliding interfaces. However, Howarth (1964) argued that the molecular attraction force is too weak to influence bubble coalescence comparing with the turbulent force. He proposed energetic collisions theory and reported that coalescence immediately happens without liquid film existing and thinning when the relative velocities between two colliding bubbles are above a certain critical level. In recent work, Lehr et al. (2002) found out that small approach velocities cause high coalescence efficiency. Among all theories, the collision can be considered as the first stage of coalescence and it is

decided by their relative velocity. Nevertheless, not every collisions end up to coalescence and most of them bounce back from each other after collision. Therefore, the coalescence frequency is expressed as follow as a function of collision frequency (it is referred from relative velocities between bubbles) and coalescence efficiency (it is description of possibility of coalescence from collision) as reported by Liao et al. 2010.

$$\Psi(\xi'; \xi) = \eta(\xi'; \xi) \iota(\xi'; \xi) \quad (3.3)$$

where $\eta(\xi'; \xi)$ is collision frequency and $\iota(\xi'; \xi)$ presents coalescence efficiency.

3.1.2.1.1 Collision frequency

The motion of collision occurs due to a various reasons in turbulent flow and till now five collision mechanisms are considered and reported by researchers (Liao and Lucas 2010). They are 1) Turbulent random motion-induced collisions, 2) Buoyancy-induced collision, 3) Wake-entrainment, 4) Velocity gradient/shear-induced collisions, 5) Capture in a turbulent eddy.

In a turbulent bubbly flow, the collision resulting from the random movement of bubbles because of turbulent fluctuation is considered as the most dominated factor. Based on the assumption of random movement similarity between gas molecules and fluid particles, the collision frequency can be expressed as follow according to the kinetic gas theory of Kennard (1938):

$$\eta_{tur}(\xi'; \xi) = A(\xi'; \xi) u_{rel}(\xi'; \xi) \quad (3.4)$$

Where the cross-sectional area of the colliding particles is defined by:

$$A(\xi'; \xi) = \frac{\pi}{4} [\xi' + \xi]^2 \quad (3.5)$$

Many researchers (Coulaloglou and Tavlarides, 1977; Lee et al., 1987; Prince and Blanch, 1990; Luo, 1993) considered the relative velocity between colliding bubbles is similar to the relative velocities of their equal-sized eddies since much small eddy does not have enough energy to influence bubble motion and much large eddies only carry bubbles without effecting their motions. Thereby, the relative velocity between two bubbles is proportional to the mean-square root of equivalent eddy-velocities.

$$\begin{aligned}
u_{rel}(\xi'; \xi) &= [u_{t\xi'}^2 + u_{t\xi}^2]^{\frac{1}{2}} \\
u_{t\xi'} &= \sqrt{2\epsilon^{\frac{1}{3}} \xi'^{\frac{1}{3}}} \\
u_{t\xi} &= \sqrt{2\epsilon^{\frac{1}{3}} \xi^{\frac{1}{3}}}
\end{aligned} \tag{3.6}$$

Moreover, Prince and Blance (1990) argued that the difference in bubble rise velocities due to different bubble size and consequent buoyant force might be one of reasons for bubble collision. A format of buoyancy-induced collision model was proposed by Friedlander (1977).

$$\eta_{buo}(\xi'; \xi) = S(\xi'; \xi) u_{brel}(\xi'; \xi) \tag{3.7}$$

where $S(\xi'; \xi)$ can be by using equation (3.5). The relative velocity for equation (3.7) is calculated from the rise velocity cause by buoyant force according to Clift et al. (1978)

$$\begin{aligned}
u_{brel}(\xi'; \xi) &= |u_{buo\xi'} - u_{buo\xi}| \\
u_{buo\xi'} &= \sqrt{\frac{2.14\sigma}{\rho_l \xi'} + 0.505g\xi'} \\
u_{buo\xi} &= \sqrt{\frac{2.14\sigma}{\rho_l \xi} + 0.505g\xi}
\end{aligned} \tag{3.8}$$

In the last few decades, there were many researches reported experimental observation of wake-entrainment. When the small bubbles enter the wake region of a large leading cap bubble, the small bubbles have high tendency to be accelerated colliding with such leading bubble. A wake entrainment modeling in a vertical pipe was proposed by Wu et al. (1998) under the assuming a uniform bubble size distribution.

$$\eta_{wake}(\xi; \xi) = -0.0073 \left(\frac{\xi g \Delta \rho}{3C_D \rho_l} \right)^{\frac{1}{2}} \frac{\alpha_g^2}{\xi^4} \tag{3.9}$$

The particles may collide with each other due to shear force from velocity gradients. A shear-induced collisions frequency model was proposed by Friedlander (1977).

$$\eta_{shear}(\xi; \xi') = \frac{1}{6} (\xi + \xi')^3 \varphi \tag{3.10}$$

Where φ is the shear rate.

Chesters (1991) reported that the viscous might become dominant force for collision if the bubble size is much small compared with the size of the energy dissipating eddies. Considering this flow phenomenon, local shear of the flow in turbulent eddies will become to the dominate factor to influence collision frequency.

$$\eta_{eddy}(\xi; \xi') = 0.07725(\xi + \xi')^3 \sqrt{\varepsilon / \nu} \quad (3.11)$$

Where $\sqrt{\varepsilon / \nu}$ is the shear strain-rate in the smallest eddy (Chesters, 1991)

3.1.2.1.2 Coalescence efficiency

Abundant of experiments discover that not every collision lead to coalescence and actually most of them turn out detach from each other after contact. In order to describe the chance of coalescence process from collision contact, the concept of coalescence efficiency is introduced. There were three models which have been widely utilized to calculate the coalescence efficiency, namely, film drainage model, energy model, critical approach velocity model (Liao et al. 2010).

The film drainage model determines the coalescence efficiency by consideration of the contact time and the drainage time, which are two key characteristic parameters to decide the occurring of intervening liquid film between bubbles thinning down to a critical thickness. Coulaloglou (1975) proposed a simplified format for film drainage model

$$t_{drain}(\xi'; \xi) = \exp\left(-\frac{t_{draine}(\xi'; \xi)}{t_{contact}(\xi'; \xi)}\right) \quad (3.12)$$

Till now, the film drainage model can be considered as the most popular one and a number of researches have been focus calculation of the contact time and drainage time. Among them, the Prince and Blanch (1990) model simplified the film drainage model and have been variously applied in industry.

$$t_{draine}(\xi'; \xi) = \left(\frac{\rho_l r_{eq}^3}{16\sigma}\right)^{1/2} \ln\left(\frac{h_o}{h_f}\right) \quad (3.13)$$

$$t_{contact}(\xi'; \xi) = \frac{(\xi_{eq}(\xi'; \xi) / 2)^{2/3}}{\varepsilon^{1/3}}$$

where h_o is the initial film thickness, h_f is the critical film thickness when rupture occurs, and $\xi_{eq}(\xi'; \xi) = 2 / \left[\frac{1}{2} \left(\frac{2}{\xi} + \frac{2}{\xi'} \right) \right]^{-1}$ is the equivalent diameter.

Howarth (1964) firstly concerned that significant percentage of coalescence are results from immediate collisions and later this assumption was confirmed by experimental observation of Park and Blair (1975) and Kuboi et al. (1972). The experiments discovered that the increasing energy of collision increases the possibility of bubble coalescence. Sovova (1981) proposed an energy model to calculate coalescence efficiency by considering the interfacial energy $E_\sigma(\xi'; \xi)$ and kinetic collision energy $E_{kin}(\xi'; \xi)$

$$\begin{aligned} \iota_{energy}(\xi'; \xi) &= \exp\left(-\frac{E_\sigma(\xi'; \xi)}{E_{kin}(\xi'; \xi)}\right) \\ E_\sigma(\xi'; \xi) &= \sigma \left(V_\xi^{2/3} + V_{\xi'}^{2/3} \right) \\ E_{kin}(\xi'; \xi) &= \frac{\rho_g V_{eq}(\xi'; \xi) u_{rel}(\xi'; \xi)^2}{2} \end{aligned} \quad (3.14)$$

where equivalent volume $V_{eq}(\xi'; \xi) = V_\xi V_{\xi'} / (V_\xi + V_{\xi'})$ is the average volume

From energy model, it is well known that coalescence will happen immediately once the approach velocity of two collision bubbles exceeds a critical value. However, Doubiez (1991) and Duineveld (1994) reported that the gentle approach lead to coalescence as well. A simple expression of critical approach velocity model has been utilized to describe coalescence efficiency

$$\iota_{vel}(\xi'; \xi) = \min\left(\frac{u_{crit}(\xi'; \xi)}{u_{rel}(\xi'; \xi)}\right) \quad (3.15)$$

where $u_{crit}(\xi'; \xi)$ is critical velocity which can be determined experimentally.

3.1.2.2 Mechanisms of breakage

The breakup of a fluid particle is determined by the compromising between external shear force from surrounding turbulent liquid phase and internal surface force and viscous force from bubbles themselves. The liquid turbulent shear attempt to tear down

the bubbles; however the bubble surface tension and viscous force try to maintain its form. A number of researches have been reported to describe the mechanisms of breakage, which can be classified into four main categories, referred as: 1) turbulent induced breakup; 2) viscous shear stress induced breakup; 3) Shear-off process; 4) interfacial surface instability (Liao and Lucas, 2009)

In turbulent flow, the breakup mainly occurs due to turbulent pressure fluctuations along the bubble surface. When the amplitude of the oscillation initiates from dynamic pressure difference around the bubble and approaches to the bubble surface, the surface of bubble losses its stability and deforms to sandglass form with a slim neck connecting two or more prospective daughter particles. Thus the breakup mechanism can be expressed as a balance between dynamic pressure τ_i and its surface stress τ_s , in other word, Weber number (Which can be thought of as a measure of the relative importance of the fluid's inertia compared to its surface tension) $We = \tau_i / \tau_s$. Luo and Svendsen (1996) proposed a turbulent induced breakup model to describe breakup frequency $\Omega_{tur}(\xi'; \xi)$ based on the kinetic gas theory

$$\Omega_{tur}(\xi'; \xi) = 0.923(1 - \alpha_g) \left(\frac{\varepsilon}{\xi'^2} \right)^{1/3} \int_{\xi_{min}}^1 \frac{(1 + \xi)^2}{\xi^{11/3}} e^{-\chi} d\xi$$

$$\chi = \frac{6\sigma \left[\left(\frac{m_\xi}{m_{\xi'}} \right)^{2/3} + \left(1 - \frac{m_\xi}{m_{\xi'}} \right)^{2/3} - 1 \right]}{\rho_l \varepsilon_l^{2/3} \xi'^{5/3} \xi^{11/3}} \quad (3.16)$$

where ξ is the dimensionless size of eddies in the inertial sub-range of isotropic turbulence. The lower limit of the integration is give by

$$\xi_{min} = (11.4 \sim 31.4)(\mu_l / \rho_l)^{1/4} / (\varepsilon^{1/4} \xi') \quad (3.17)$$

Another consideration of bubble breakup mechanism is due to viscous shear force and Capillary number, defined as the ratio of viscous stress over the surface tension, is introduced to calculate breakup frequency

$$Ca = \frac{\tau_v}{\tau_s} = \frac{\mu_l \xi \varphi}{2\sigma} \quad (3.18)$$

where φ is the shear rate. The increasing of capillary number means that the viscous stress is more dominate than surface tension. When the capillary number is over certain critical level, the stability of bubble gradually reduces and finally breakup occurs. And the critical capillary number Ca_{cr} is decided by the viscosity ratio and the flow type (Taylor, 1934; Grace, 1982)

In the air-water system, small bubbles have tendency to shear off from the cap/slug bubbles due to the movement of gases in the interfacial layer penetrating into the liquid film around gas phase edge (Liao et al 2009). For this shearing mechanism, the breakup frequency is determined by the total sheared-off volume and the generated bubble size. Fu and Ishii (2002) have more details.

Once the volume of bubble exceeds a certain limitation, the bubble becomes unstable and easily breakup. Under such consideration, Wang et al. (2005a, b) proposed the breakup frequency.

$$\Omega_{surfinstable}(\xi) = 100 \frac{(\xi - \xi_{cr})^6}{(\xi - \xi_{cr})^6 + \xi_{cr}^6} \quad (3.19)$$

Where ξ_{cr} is the critical bubble diameter set as 27 mm. Assumption of parent bubble breaking into two equal daughter bubbles was made since detailed studies are not available.

3.1.3 The Methods of Population Balance Model

The numerical approaches for solving the population balance equation have been developed for more than 50 years. As reported by Cheung et al (2009 a), Monte Carlo method which developed in early stage has the advantage of flexibility and accuracy since it solves the PBE based on tracking direct particle movements in multidimensional systems. However, it has limited applications in realistic industrial proccession where the information of hundreds of thousands of particles is generally requested and normally the consequently extensive computational cost is not affordable at current stage. Moreover, the implementation of this method into CFD software is not straightforward, which also slow down the application spread of this method. The other two methods,

namely the Method of Moments (MOM) and the Class Method (CM) are widely utilized in academic research and industrial application. More details of these two methods will be discussed as follow.

3.1.3.1 Method of Moments (MOM) Approach

3.1.3.1.1 Method of Moments (MOM) Approach

The principle behind MOM is to transform the problem focus from describing the computational costly particle size distribution function into its corresponding lower-order of moments. The moments of the particle size distribution are defined as:

$$m^{(k)}(X, t) = \int_0^\infty f(\xi, X, t) \xi^k d\xi \quad (3.20)$$

The key to the MOM is that the lower-order moments can be tracked directly without requiring additional knowledge of the distribution. The conventional MOM can be solved by formulating equations for evolution of the moments in closed form, i.e., involving only functions of the moments themselves. However, there is a severe restriction on form of source terms in equation which can be handled by this MOM method, which is probably the main reason for the method only to be applied in a limited number of problems (Hulburt and Katz, 1964).

3.1.3.1.2 Quadrature Method Of Moments (QMOM)

With the purpose of circumventing the limitations of MOM, the quadrature method of moment (QMOM) obtains closure through approximation of the integrals using a much less restrictive quadrature method. The essence of quadrature-based closure exist in the fact that the new abscissas ξ_i and weights w_i which are obtained after approximation of the integrals may be completely specified in terms of the lower-order moments of the unknown distribution function. And the moments themselves may be written in the similar form. For n-point Gaussian quadrature these are:

$$m^{(k)}(X, t) = \int_0^\infty f(\xi, X, t) \xi^k d\xi = \sum_{i=1}^n \xi_i^k w_i \quad (3.21)$$

for $k = 0$ through $2n - 1$.

3.1.3.1.3 Direct Quadrature Method Of Moments (DQMOM)

In order to solve multi-dimensional problems, Marchisio and Fox (2005) further developed MOM by using Dirac Delta function and proposed direct quadrature method of moment (DQMOM) where the quadrature abscissas and weights are formulated in the format of transport equations. Thereby the primitive variables appearing in the quadrature approximation, instead of moments of the PSD, are directly tracked (Cheung et al 2009 b). Thereby, the abscissas and weights are solved by using matrix operations. The fundamental equation of importance in DQMOM is:

$$f(\xi, X, t) \approx \sum_{i=1}^n w_i \delta(\xi - \xi_i(X, t)) \quad (3.22)$$

The aggregate of the distribution is represented by a summation of n Dirac Delta Function, each with a weight w_i centred on abscissas ξ_i . Substitute Eq. (3.31) into PBE and after some mathematical manipulations, transport equations for weights and abscissas are given by:

$$\begin{aligned} \frac{\partial w_i}{\partial t} + \nabla \cdot (u(X, t) w_i) &= a_i \\ \frac{\partial \xi_i}{\partial t} + \nabla \cdot (u(X, t) \xi_i) &= b_i \end{aligned} \quad (3.23)$$

where $\xi_i = w_i \xi_i$ is the weighted abscissas and the terms a_i and b_i are related to the “birth” and “death” rate of population which forms $2n$ linear equations of which unknowns can be evaluated via matrix inversion:

$$(1 - k) \sum_{i=1}^n \xi_i^k a_i + k \sum_{i=1}^n \xi_i^{k-1} b_i = \bar{S}_k(X, t) \quad (3.24)$$

The source term for the k^{th} moment \bar{S}_k is defined by:

$$\bar{S}_k(X, t) = \int_0^\infty \xi^k S(\xi, X, t) d\xi \quad (3.25)$$

3.1.3.2 Class Method

3.1.3.2.1 Multiple Size Group (MUSIG) model

The Multiple Size Group (MUSIG) model can be considered as one of the mostly widely adopted population balance methods because of its straightforward implementation to CFD software as well as its reasonable capability to handle polydispersed multiphase flow. By polydispersed multiphase flow, it means that the dispersed phase has large variations in size. In the MUSIG model, the continuous size range of bubbles is discretized by M groups; the population change of each group due to coalescence and breakage processes of bubbles in the same group or/and between groups is balanced through transport equations of a scalar (i.e number density of bubbles). The mechanisms of bubble coalescence and breakage can be presented via source terms within these transport equations.

Let $N_{(i)}$ represent the particle number of size group i :

$$N_{(i)} = \int_{\xi_{i-1/2}}^{\xi_{i+1/2}} n(\xi, t) d\xi \quad (3.26)$$

By defining the void fraction of size group i to be α_i , the size fraction is presented as $f_{(i)} = \alpha_{(i)} / \alpha_g$. Then, the particle size distribution of MUSIG model is thereby approximated as follow:

$$\frac{\partial \rho_{(i)} \alpha_g f_{(i)}}{\partial t} + \nabla \cdot (\rho_{(i)} \alpha_g f_{(i)} \bar{u}_{g,(i)}) = S_{(i)} \quad (3.27)$$

A further simplification is to assume that all size groups share the same density ρ_g and velocity u_g yielding the homogeneous MUSIG model:

$$\frac{\partial \rho_g \alpha_g f_{(i)}}{\partial t} + \nabla \cdot (\rho_g \alpha_g f_{(i)} \bar{u}_g) = S_{(i)} \quad (3.28)$$

By considering the practicability of the velocities difference between each size group, an inhomogeneous MUSIG model has been developed by Krepper et al. (2005) by subdividing the each group into N number of velocity fields. The PSD equation for the inhomogeneous MUSIG model can be re-expressed in terms of the volume fraction and

size fraction of the bubble size class i , $i \in [1, M]$, of velocity group j , $j \in [1, N]$ according to:

$$\frac{\partial \rho_g \alpha_{g,(i)} f_{(i,j)}}{\partial t} + \nabla \cdot (\rho_g \alpha_{g,(i)} f_{(i,j)} \bar{u}_{g,(i,j)}) = S_{(i,j)} \quad (3.29)$$

with additional relations and constraints:

$$\alpha_g = \sum_{i=1}^M \alpha_{(i)} = \sum_{i=1}^M \sum_{j=1}^N \alpha_{(i,j)} ; \alpha_{(i)} = \sum_{j=1}^N \alpha_{(i,j)} \quad (3.30)$$

$$\alpha_g + \alpha_l = 1 ; \sum_{i=1}^M \sum_{j=1}^N f_{(i,j)} = 1$$

3.1.3.2.2 Single Average Quantities Approach

Under the industrial applications background where only information of overall changes in bubble population is required, the Multiple Size Group (MUSIG) approach can be simplified as a single averaged quantities method by using only one size group to describe the changes of bubble population. Kocamustafaogullari and Ishii (1995) considered the interfacial area concentration (IAC) is a straightforward parameter for assessment the performance of heat and mass transfer and firstly derived a transport equation for tracking the interfacial area between gas and liquid phase in bubbly flow problems. Thereby the interfacial area concentration (IAC) a_{if} = transport equation is expressed as (Ishii et al., 2002) under the assumption of perfect spherical bubble shape:

$$\frac{\partial a_{if}}{\partial t} + \nabla \cdot (\bar{u}_g a_{if}) = \frac{2}{3} \left(\frac{a_{if}}{\alpha_g} \right) \left(\frac{\partial \alpha_g}{\partial t} + \nabla \cdot (\bar{u}_g \alpha_g) \right) + \frac{1}{3\phi} \left(\frac{\alpha_g}{a_{if}} \right)^2 R \quad (3.31)$$

On the other hand, Yeoh and Tu (2006) and Cheung et al. (2007 a and b) argued that the bubble number density should be a premier parameter to demonstrate the bubble population changes and proposed an Average Bubble Number Density (ABND) equation which is equivalent to the formulation of the interfacial area transport equation

$$\frac{\partial n}{\partial t} + \nabla \cdot (\bar{u}_g n) = S \quad (3.32)$$

where S represents the local volume-averaged source and sink rates, which need to be closed through constitutive relations. More details of source and sink terms of ABND model will be provided in Chapter 4.

3.2 Inter-phase Momentum Transfer

The two-fluid model which treats each phase separately in terms of two sets of conservation equations can be considered as one of the most accurate numerical model in the research of two-phase flows (Cheung et al 2009). However, information of interfacial momentum transfer presenting the interfacial actions between gas and liquid phases is required to close these two sets of conservation equations. The interfacial momentum transfer is rather crucial to the modeling of gas-liquid flows since it plays important influence on bubbles diameters and their distributions into liquid phase in bubbly flow. Generally, the interfacial force contains viscous drag force as well as lateral lift force, wall lubrication force, virtual mass force and turbulent dispersion force, which are bond together as non-drag forces. For the liquid phase, the total interfacial force from liquid phase to gas phase is given by:

$$F_{l \rightarrow g} = F_{l \rightarrow g}^{\text{drag}} + F_{l \rightarrow g}^{\text{non-drag}} = F_{l \rightarrow g}^{\text{drag}} + F_{l \rightarrow g}^{\text{lift}} + F_{l \rightarrow g}^{\text{wall lubrication}} + F_{l \rightarrow g}^{\text{virtual mass}} + F_{l \rightarrow g}^{\text{turbulent dispersion}} \quad (3.33)$$

3.2.1 Drag force

In the case of bubbly flow, the viscous drag force is primer parameter governing relative motions between two phases. Generally, the interfacial drag force is a result from shear and form viscous drag of the fluid flow. It can be written

$$F_{l \rightarrow g}^{\text{drag}} = -F_{g \rightarrow l}^{\text{drag}} = \frac{1}{8} C_D a_{if} \rho_l |\bar{u}_g - \bar{u}_l| (\bar{u}_g - \bar{u}_l) \quad (3.34)$$

where C_D is the drag coefficient, $C_D = D / (0.5 \rho_l (\bar{u}_g - \bar{u}_l)^2 A)$. The drag coefficients based on the correlations by Ishii and Zuber (1979) for different flow regimes are normally employed for gas-liquid flows. The function $C_D(Re_b)$, known as the drag coefficient, can be correlated for individual bubbles across several distinct bubbles

Reynolds number regions (ratio of inertial forces to viscous forces $Re = \rho v L / \mu$); known as: stokes, undistorted particle (viscous), Newton, distorted particle and churn turbulent flow regime.

3.2.2 Lift force

In vertical bubbly flows, the small bubbles have the tendency of migration towards the pipe wall; however large bubbles are more likely to move to the pipe centre. This flow phenomenon is considered under the influence of lateral lift force which is caused by the radial velocity gradient. This interfacial force density can normally be proportion to the relative velocity and curl of the velocity vector, which acts perpendicular to the direction of relative motion between two phases:

$$F_{l \rightarrow g}^{\text{lift}} = -F_{g \rightarrow l}^{\text{lift}} = C_L \alpha_g \rho_l (\bar{u}_g - \bar{u}_l) \times (\nabla \times \bar{u}_l) \quad (3.35)$$

The lift coefficient C_L in above equation has various suggestions with constant value from $C_L = 0.01$ to 0.5 . However, the practical flow phenomenon of different migration direction between large bubbles and small bubbles is requested to be represented by flexible lift coefficient instead of constant value. Tomiyama (1998) proposed a lift coefficient correlation in terms of Eotvos number which is used to characterize the

shape of bubbles ($Eo = \frac{g(\rho_l - \rho_g)d^2}{\sigma}$). In this correlation, the negative coefficient

occurs to demonstrate the migration towards the centre of the flow pipe when the bubble diameter is larger than 5.5 mm for air-water system. The lift coefficient can be expressed as:

$$C_L = \begin{cases} \min[0.288 \tanh(0.121 Re_g); f(Eo_{dg})] & Eo_g < 4 \\ f(Eo_{dg}) = 0.00105 Eo_{dg}^3 - 0.0159 Eo_{dg}^2 - 0.0204 Eo_{dg} + 0.474 & 4 \leq Eo_g \leq 10 \\ -0.29 & Eo_g > 10 \end{cases} \quad (3.36)$$

where the modified Eotvos number Eo_{dg} is defined by

$$Eo_{dg} = \frac{g(\rho_l - \rho_g)d_H^2}{\sigma} \quad (3.37)$$

in which D_H is the maximum bubble radial dimension that can be evaluated through the empirical correlation of Wellek et al. (1966).

$$d_H = D_s(1 + 0.163Eo_g^{0.757})^{1/3} \quad (3.38)$$

Where $D_s = (6V/\pi)^{1/3}$ is Sauter mean bubble diameter.

3.2.3 Wall lubrication force

Due to surface tension, bubbles are experimentally observed to concentrate in a region close to the wall, but not immediately adjacent to the wall, which cause a low void fraction at the vicinity of the wall area. According to Antal et al. (1991), another lateral force, namely wall lubrication force should be considered to represent this flow characteristic as:

$$F_{l \rightarrow g}^{\text{lubrication}} = -F_{g \rightarrow l}^{\text{lubrication}} = -\left(C_{w1} + C_{w2} \frac{D_s}{y_w}\right) \frac{\alpha_g \rho_l [(\bar{u}_g - \bar{u}_l) - ((\bar{u}_g - \bar{u}_l) \cdot \bar{n}_w) \bar{n}_w]^2}{D_s} \bar{n}_w \quad (3.39)$$

where y_w is the distance to the nearest wall and \bar{n}_w is the unit normal pointing away from the wall. According to the research of Krepper et al. (2005), $C_{w1} = -0.0064$ and $C_{w2} = 0.016$ are proposed. Moreover, for avoiding attraction force emerges, the force is set zero for large y_w :

$$F_{l \rightarrow g}^{\text{lubrication}} = -F_{g \rightarrow l}^{\text{lubrication}} = 0 \quad \text{if } y_w > \frac{C_{w2}}{C_{w1}} D_s \quad (3.40)$$

3.2.4 Virtual mass force

The virtual mass force is proportional to relative accelerations between two phases as:

$$F_{l \rightarrow g}^{\text{virtualmass}} = -F_{g \rightarrow l}^{\text{virtualmass}} = d\rho_l C_{vm} \left(\frac{D_g u_g}{Dt} - \frac{D_l u_l}{Dt} \right) \quad (3.41)$$

In general, the non-dimensional virtual mass coefficient C_{vm} depends on shape and particle concentration. $C_{vm} = 0.5$ is advised for inviscid flow around an isolated sphere.

3.2.5 Turbulence dispersion force

Considering turbulent assisted bubble dispersion, Antal et al. (1991) proposed turbulence dispersion force in terms of turbulent kinetic energy of liquid phase and gradient of the void fraction of gas phase:

$$F_{l \rightarrow g}^{\text{dispersion}} = -F_{g \rightarrow l}^{\text{dispersion}} = -C_{TD} \rho_l k_l C_D \nabla \alpha_l \quad (3.42)$$

Value of constant C_{TD} has various ranges from 0.1 to 500 (Lopez de Bertodano, 1998, Moraga et al., 2003). Another popular model for the turbulence dispersion force was derived by Burns et al. (2004) based on the consistency of Favre-averaging drag force, which is given by:

$$F_{l \rightarrow g}^{\text{dispersion}} = -F_{g \rightarrow l}^{\text{dispersion}} = C_{TD} C_D \frac{\nu_{t,g}}{\sigma_{t,g}} \left(\frac{\nabla \alpha_l}{\alpha_l} - \frac{\nabla \alpha_g}{\alpha_g} \right) \quad (3.43)$$

where $\nu_{t,g}$ is the turbulent kinematic viscosity for the gas phase and $\sigma_{t,g}$ is the turbulent Schmidt number of the gas phase with an adopted value of 0.9. The C_{TD} is normally set to a value of unity. In the right hand of this equation, the C_D is drag coefficient which essentially describes the interfacial drag movements, thereby this model clearly depends on the details of the drag characteristics and relative interactions. For certain situations where the value of C_{TD} is not clear such as this study, the Favre-averaged turbulent dispersion force model is recommended.

3.3 Turbulence modelling for two-fluid model

Turbulence, which consists of fluctuations in the flow field in time and space, generally exists in realistic flow conditions and significantly influence on the characteristics of the flow. In principle, the Navier-Stokes equations have the capability to solve both laminar and turbulent flows without the aid for additional information (ANSYS CFX-11 User Manual). However, the turbulence is a complex process involving its three dimensions,

unsteady and consists of many scales. By many scales, it means the turbulent flow span a large range of turbulent length and time scales, and would generally involve length scales much smaller than the smallest finite volume mesh. The Direct Numerical Simulation (DNS) requires expensive computer efforts which are far more than availability in the foreseeable future. In order to account for the effects of turbulence without fine mesh and DNS, the statistical turbulence models, which exhibit average characteristics with an additional time-varying fluctuating component, are generally adopted for practical engineering calculations. This method greatly reduces the computational effort; however it introduces additional unknown terms such as Reynolds stresses and Reynolds flux which need to be modelled by extra equations of known quantities in order to achieve closure (ANSYS CFX-11 User Manual). One of widely applied extra equations for Reynolds stresses and Reynolds flux is eddy viscosity model in which the Reynolds stresses are assumed to be proportional to mean velocity gradients. Thereby, the searching of unknown terms Reynolds stresses and Reynolds flux is broken down to calculation of turbulence viscosity $\mu_{t,g}$.

The turbulence phenomenon has been a research interesting for many years and many turbulent models have been proposed, such as k- ϵ model, k- ω model, their extensions Shear Stress Transport (SST) model and so on. In single-phase flow, the standard k- ϵ model is generally used because of its simplicity and stability. However in multi-phase flow, no standard turbulence model is suitable for all flow conditions. Following the researches of Cheung and Yeoh (2007a), the Shear Stress Transport (SST) model developed by Menter (1994) was found superior to the standard k- ϵ model and has been used in this research. k- ω

The SST model is a complex combination of the Wilcox models (Wilcox, D.C. 1988) originally from k- ω) and k- ϵ with a specific blending function. It avoids over prediction of the eddy-viscosity by accounting the transport of the turbulent shear stress and gives highly accurate predictions of the onset and the amount of flow separation under adverse pressure gradients. The ensemble-averaged transport equations of the SST model for bubbly flow can be expressed as:

$$\frac{\partial \rho_l \alpha_l k_l}{\partial t} + \nabla \cdot (\rho_l \alpha_l \bar{u}_l k_l) = \nabla \cdot (\alpha_l (\mu_l + \sigma_k \mu_{t,l}) \nabla k_l) + \alpha_l P_{k,l} - 0.09 \rho_l k_l \omega_l \quad (3.44)$$

$$\frac{\partial \rho_l \alpha_l \omega_l}{\partial t} + \nabla \cdot (\rho_l \alpha_l \bar{u}_l \omega_l) = \nabla \cdot (\alpha_l (\mu_l + \sigma_{\omega} \mu_{t,l}) \nabla \omega_l) - 2 \rho_l \alpha_l (1 - F_1) \sigma_{\omega} \frac{1}{\omega_l} \frac{\partial k_l}{\partial x_j} \frac{\partial \omega_l}{\partial x_j} + \alpha_l \frac{\gamma}{\nu_t} P_{k,l} - \rho_l \beta \omega_l^2$$

Let Θ_1 represent any quantities in Wilcox model (σ_{k1}, \dots) and Θ_0 represent any constant in $k-\epsilon$ model (σ_{k0}, \dots), then $\Theta = F_1 \Theta_1 + (1 - F_1) \Theta_0$ demonstrates the corresponding result of the new model (σ_k, \dots).

When $F_1 = 1$, it is Wilcox model: $\sigma_{k1} = 0.85$, $\sigma_{\omega1} = 0.5$, $\beta_1 = 0.075$, $\gamma_1 = \beta_1 / 0.09 - \sigma_{\omega1} k^2 / 0.3$

When $F_1 = 0$, it is $k-\epsilon$ model: $\sigma_{k0} = 1.0$, $\sigma_{\omega0} = 0.856$, $\beta_0 = 0.0828$, $\gamma_0 = \beta_0 / 0.09 - \sigma_{\omega0} k^2 / 0.3$

And the shear induced turbulent viscosity μ_{ts} can be calculated from ν_t :

$$\mu_{ts} = \nu_t \rho = \frac{0.31 \rho k_l}{\max(0.31 \omega_l, S F_2)} \quad (3.45)$$

$$S = \sqrt{2 S_{ij} S_{ij}}$$

The success of SST model is mostly decided by the use of blending functions of F_1 and F_2 which is based on the distance to the nearest surface d_n and on the flow kinematic viscosity μ_l :

$$F_1 = \tanh(\theta_1^4) \quad ,$$

$$\theta_1 = \min \left[\max \left(\frac{\sqrt{k_l}}{0.09 \omega_l d_n}, \frac{500 \mu_l}{\omega_l d_n^2} \right), \frac{4 \rho_l k_l}{\max \left(\frac{2 \rho_l}{\sigma_{\omega 2} \omega} \nabla k \nabla \omega, 10^{-10} \right) \sigma_{\omega 0} d_n^2} \right] \quad (3.46)$$

$$F_2 = \tanh(\theta_2^2), \quad \theta_2 = \max \left(\frac{2 \sqrt{k_l}}{0.09 \omega_l d_n}, \frac{500 \mu_l}{\omega_l d_n^2} \right)$$

More detail descriptions of these model constants can be found in Menter (1994).

Except the effect of liquid phase shear induced turbulence which even happens in single phase flow, Sato et al (1981) argued that the existing of bubbles phase in multiphase

also contribute to turbulence in liquid field. The Sato's bubble-induced turbulent viscosity model μ_{td} was also employed. The turbulent viscosity of liquid phase is therefore given by:

$$\begin{aligned}\mu_t &= \mu_{ts} + \mu_{td} \\ \mu_{td,l} &= C_{\mu p} \rho_l \alpha_g D_s |\bar{U}_g - \bar{U}_l|\end{aligned}\tag{3.47}$$

In two-fluid model, generally effective turbulent viscosity μ_{te} is required. It is subtotal of phase viscosity and turbulent viscosity.

$$\mu_{te} = \mu + \mu_t\tag{3.48}$$

3.4 Two-Fluid Model and Closure Term

The two-fluid model can be considered as one of the mostly widely utilized method in bubbly flow due to its reasonable compromise between accuracy and computational cost. This model separately uses set of conservation equation to individually represent gas or liquid phase. However, since each phase is not independent of each other, closure terms are required to bridge the transport of mass, momentum, and energy of each phase across the interfaces.

For the isothermal bubbly flow without the mass and heat transfer, the three-dimensional two-fluid model conservation equations can reduce to mass and momentum conservation equations. Denoting the liquid as the continuum phase (α_l) and the gas bubbles phase as disperse phase (α_g), these equations can be written as:

$$\begin{aligned}\frac{\partial(\rho_i \alpha_i)}{\partial t} + \nabla \cdot (\rho_i \alpha_i \bar{u}_i) &= 0 \\ \frac{\partial(\rho_i \alpha_i \bar{u}_i)}{\partial t} + \nabla \cdot (\rho_i \alpha_i \bar{u}_i \bar{u}_i) &= -\alpha_i \nabla P + \alpha_i \rho_i \bar{g} + \nabla \cdot [\alpha_i \mu_{i,te} (\nabla \bar{u}_i + (\nabla \bar{u}_i)^T)] + F_i\end{aligned}\tag{3.49}$$

where F_i and $\mu_{i,te}$ are interfacial force and effective turbulent viscosity, respectively.

The bubble size distributions which can be solved through population balance model is critical information for simulation process of bubbly flow even though it is not directly required by two-fluid model equations. It is a key parameter not only to calculate interfacial force and effective turbulent viscosity but also to assess the efficiency of industrial proccession. Thereby, the accuracies solving population balance model,

interfacial force model and turbulent model in two-fluid model are the key parameters of simulating bubbly flow.

Chapter 4 Numerical Investigation of Influence of Interfacial Forces on Bubbly Flow

The prediction capabilities of two drag coefficient models have been estimated in this chapter by validation against experimental data of vertical isothermal air-water bubbly flow conducted by Hibiki et al. (2001). Coupled with ABND model (Cheung et al. 2007 a and b) the experimental drag formulation proposed by Simonnet et al. (2007) has been implemented into two-fluid model to predict the local bubble distribution and compared with commonly used Ishii and Zuber (1979) drag coefficient model. Particular emphasis is placed on investigations of bubbly-to-slug transitional regime (cap-bubbly flow condition) where the significant deformations of bubbles were observed. Comparing with Ishii and Zuber (1979) model, the Simonnet et al. (2007) formulation considers local void fraction and provides reasonably better performance in prediction of gas velocity. In this chapter, the principles of two drag coefficient formulations have been introduced initially, and then numerical and experimental details have been subsequently explained. After comparison of time averaged void fraction, interfacial area concentration and gas velocities among these two models and experiment results, conclusions and future research direction have been recommended.

4.1 Introduction

Two-fluid model has wide ranges of application backgrounds and can be probably considered to be the most detailed and accurate macroscopic formulation for prediction gas-liquid flow systems. It traces two phases separately and individually through two sets of transport equations. The purpose of this is to maximally express the characteristics of each phase. However, the most important and difficult aspect of two-fluid model is the description of interfacial actions regarding the exchanges of the mass, momentum and energy between these two phases. These so named closure terms determine the interfacial exchange rate and the non-equilibrium degree in mass,

momentum and thermal energy. Thereby, such parameters are the most fundamental and critical aspects which have been attracted plenty of research interest.

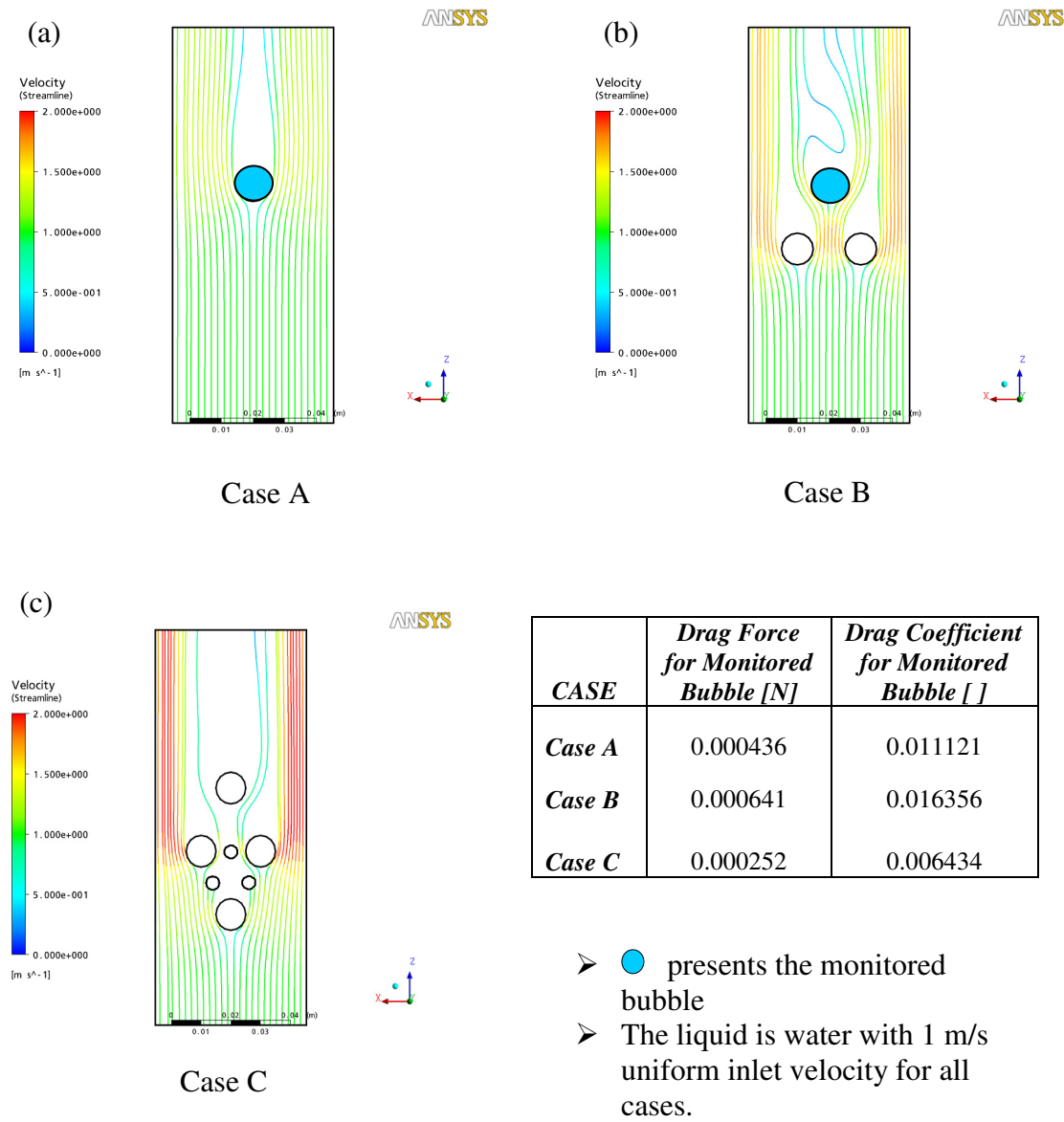


Figure 4-1 Streamline of liquid velocity around a single bubble and a number of bubbles

Without the heat and mass transfer in isothermal bubbly flow system, the complexity of interfacial actions between two phases reduces to consideration of only the momentum exchange term. Generally, there are many interfacial transfers are involved in the conservation momentum equation; however the interfacial drag force, which is a result

of the shear and form drag of the fluid flow, can be considered as the most important and critical one because the well predicted fundamental parameter of relative velocity by interfacial drag force formulations can exploit the possibility of better performances of other parameters and consequently of better predictions of whole system. Herein, some literature reports classified interfacial driving force as drag and non-drag force. Comparing with drag coefficient of solid particle, the scenarios of bubbles are more complicated. As reported by Bertola et al. (2004), the drag coefficient of solid particles determines only by the surrounding flow conditions. And it can be simply described as a primary function of the continuous phase turbulence intensity and particle Reynolds number. However, the characteristics of bubble including the containing of high inertia in liquid phase instead of dispersed phase itself due to extreme difference of density, the possibility of slip on the surface of bubbles (when the degree of continuous phase purification is above certain critical standard) and the tendency of bubble to deform, coalescence and breakup (Magnaudet and Eames 2000).

The mutual interaction among bubbles is also a significantly influent factor and should be considered in drag force formulations (Behzadi et al. 2004; Bertola et al. 2004; and Simonnet et al. 2007). Figure 4-1 illustrates the pressure distributions differences on the research object (blue bubble) between the cases of liquid passing a single bubble and of liquid passing group bubbles. The pressure differences between fronts and backs of research object commonly are regarded as driving factor of drag force. As it can be seen in Figure 4-1, the pressure differences of monitored blue bubble significantly changes with various incoming flow conditions and the incoming flow conditions are affected by bubbles distributions. In Figure 4-1 (b), after passing the other two bubbles, the liquid has been accelerated due to the narrowing of cross section area and thereby the front of monitored blue bubble has been hit by liquid phase with higher velocity comparing with the scenario of liquid passing single bubble in Figure 4-1 (a). The faster velocity carrying stronger energy transforms to higher pressure at stagnant point in front of bubble, which results to more significant drag reduction under the generally consideration of the similar pressure in bubble wake area. However, the drag force in Figure 4-1 (c) is comparatively lower than single bubble case in Figure 4-1 (a) since the observed bubble is in a wake area (low pressure area) of a front bubble (Li et al. 2009 a and b).

Over the years, abundant researches have been focused on calculating the drag force for bubbles under the scenario of fully packaged bubble in liquid phase (high void fraction) and several models have been proposed. In the widely employed Ishii and Zuber (1979) model, the bubbly flow behaviors have been categorized into different flow regimes in terms of bubble shape and subsequently a mixture viscosity drag coefficient formulations are individually developed for each flow regimes. Additionally, another method of searching appropriate drag coefficient multipliers are frequently reported in literature (Rusche and Issa 2000, Behzadi et al. 2004 and Simonnet et al. 2007). In such method, the ratio of the drag coefficient over its single dispersed element value can be expressed as a function of the phase fraction, i.e. $C_D/C_{D_{\infty}} = f(\alpha)$ where $C_{D_{\infty}}$ is the drag coefficient of an isolated bubble in an infinite medium. Recently, Simonnet et al. (2007) has collected exhaustive experimental data and has developed an experimental drag coefficient multiplier. Particular interesting has been focused on prediction of flow characteristics from bubbly-to-slug transitional regime where bubbles are generally highly distorted and closely packed with each other. Such unique characteristics are different from the bubbly flow regime where general spherical bubbles have the possibility to move freely (Hibiki et al., 2001 and Cheung et al., 2007).

The purpose of this work is to assess the prediction performance of recently developed experimental drag coefficient model by Simonnet et al. (2007). The numerical results have been compared with the numerical prediction of commonly utilized Ishii and Zuber (1979) drag coefficient model and the experimental measurement of isothermal gas-liquid bubbly flow in a vertical pipe performed by Hibiki et al. (2001). In order to predict the dynamic changes of the interfacial structure, the population balance model, averaged bubble number density (ABND) (Cheung et al. 2007 a and b) has employed and special emphasis has been centered on investigations of bubbly-to-slug transitional regime (cap-bubbly flow condition).

4.2 Mathematical Model

4.2.1 Interfacial Momentum Transfer due to Drag

The inter-phase momentum transfer between gas and liquid due to the effects of drag force can be formulated by using the interfacial area concentration a_{if} and relative velocity $(\bar{u}_g - \bar{u}_l)$ as (Yeoh and Tu 2004):

$$F_{l \rightarrow g}^{\text{drag}} = -F_{g \rightarrow l}^{\text{drag}} = \frac{1}{8} C_D a_{if} \rho_l |\bar{u}_g - \bar{u}_l| (\bar{u}_g - \bar{u}_l) \quad (4.1)$$

where C_D is the drag coefficient. In the present study, two correlations proposed by Ishii and Zuber (1979) and Simonnet et al. (2007) respectively are employed. The prediction results are validated with experimental data to evaluate these two drag coefficient C_D performance.

The drag coefficient model of Ishii and Zuber (1979) was proposed under the consideration of classification of different flow regimes. The function $C_D(Re_b)$ can be correlated for individual bubbles across several distinct bubbles Reynolds number regions; known as: stokes, undistorted particle (viscous), Newton, distorted particle and churn turbulent flow regime. As implement this model into commercial software ANSYS CFX 11 (ANSYS CFX-11 User Manual), the regimes are simplified as dense spherical particle, dense distorted particle and dense spherical cap regime.

Dense Spherical Particle Regime

$$C_D(\text{sphere}) = \frac{24}{Re_m} (1 + 0.15 Re_m^{0.687}) \quad (4.2)$$

Dense Distorted Particle Regime

$$C_D(\text{ellipse}) = \frac{2}{3} \sqrt{Eo} E \quad (4.3)$$

Dense Spherical Cap Regime

$$C_D(\text{cap}) = \frac{8}{3} E' \quad (4.4)$$

where Re_m is mixture Reynolds number. More information can be found in Ishii and Zuber (1979)

Particularly, in equation (4.3), the dense distorted particle regime drag coefficient model takes the form of a multiplying factor E , which is given in terms of the void fraction as

$$E = \left[\frac{1 + 17.67 f(\alpha_g)^{6/7}}{18.67 f(\alpha_g)} \right]^2 \quad (4.5)$$

Where

$$f(\alpha_g) = \frac{\mu_l}{\mu_m} (1 - \alpha_g)^{1/2} \quad (4.6)$$

And, E_o represents the Eotvos number with the surface tension coefficient σ

$$E_o = \frac{g(\rho_l - \rho_g)D_s^2}{\sigma} \quad (4.7)$$

For dense spherical cap regime, the multiplication factor E' takes however the form:

$$E' = (1 - \alpha_g)^2 \quad (4.8)$$

As implemented within ANSYS CFX 11 (ANSYS, CFX-11 User Manual) the regime selection is based on

$$C_D = \begin{cases} C_D(sphere) & \text{if } C_D(sphere) \geq C_D(ellipse) \\ \min(C_D(ellipse), C_D(cap)) & \text{if } C_D(sphere) \leq C_D(ellipse) \end{cases} \quad (4.9)$$

Recently, Simonnet et al. (2007) investigated abundant experimental data and proposed alternative drag correlation for pure air-water systems which can be written as

$$C_{D\infty} = C_{D\infty} E'' \quad (4.10)$$

where $C_{D\infty}$ is the drag coefficient of an isolated bubble in an infinite medium, which can be represented by the equilibrium between buoyancy, drag and gravitational as

$$C_{D\infty} = \frac{4}{3} \frac{\rho_l - \rho_g}{\rho_l} g D_s \frac{1}{u_\infty^2} \quad (4.11)$$

Where u_∞ is the velocity of an isolated bubble in a quiescent liquid which can be calculated using the correlation of Jamialahmadi et al. (1994):

$$u_\infty = \frac{u_{b1} u_{b2}}{\sqrt{u_{b1}^2 + u_{b2}^2}} \quad (4.12)$$

Where

$$u_{b1} = \frac{1}{18} \frac{\rho_l - \rho_g}{\mu_l} g D_s^2 \frac{3\mu_g + 3\mu_l}{3\mu_g + 2\mu_l}$$

$$u_{b2} = \sqrt{\frac{2\sigma}{D_s(\rho_l - \rho_g)} + \frac{gD_s}{2}} \quad (4.13)$$

In equation (4.10), the multiplication factor E'' according to Simonnet et al. (2007) is

$$E'' = (1 - \alpha_g)[(1 - \alpha_g)^m + (4.8 \frac{\alpha_g}{1 - \alpha_g})^m]^{-2/m} \quad (4.14)$$

Where, m is set a value of 25. The above modification is valid for a wide range of void fractions and across different flow regimes.

4.2.2 Averaged Bubble Number Density (ABND) model

In the current study, the Averaged Bubble Number Density (ABND) model proposed by Yeoh and Tu (2006) and Cheung et al. (2007 a and b) has been employed. The ABND model can be written as follow:

$$\frac{\partial n}{\partial t} + \nabla \cdot (\bar{u}_g n) = \phi_n^{RC} + \phi_n^{TI} + \phi_n^{WE} \quad (4.15)$$

where ϕ_n^{RC} , ϕ_n^{TI} , ϕ_n^{WE} represents the bubble number density changes due to random collision, turbulent induced breakage and wake entrainment. According to Cheung et al. (2007 a and b)'s report, Yao and Morel (2004) source and sink terms provide reasonable better performance than most of other models, thereby the source and sink terms of Yao and Morel (2004) are employed in current study.

4.2.3 Coalesce and Break-up kernels

Yao and Morel (2004) considered two new identical important characteristic time scales including the free travelling time or the interaction time and developed bubble coalescence rate due to bubble random collisions.

$$\phi_n^{RC} = -C_{RC1} \frac{\alpha_g^2 \varepsilon^{1/3}}{D_s^{11/3}} \frac{\exp(-C_{RC2} \sqrt{We/We_{cr}})}{(\alpha_{max}^{1/3} - \alpha_g)/\alpha_{max}^{1/3} + C_{RC3} \alpha_g \sqrt{We/We_{cr}}} \quad (4.16)$$

where the derived constants are $C_{RC1} = 2.86$, $C_{RC2} = 1.017$ and $C_{RC3} = 1.922$, respectively.

For bubble break-up, they argue that bubble breakage is mainly caused by the resonance oscillation. Considering the natural frequency of the oscillating bubbles, the interaction time can be approximated and the rate of bubble breakage is given by:

$$\phi_n^{TI} = 1.6 \frac{\alpha_g (1 - \alpha_g) \varepsilon^{1/3}}{D_s^{11/3}} \frac{\exp(-We_{cr}/We)}{1 + 0.42(1 - \alpha_g) \sqrt{We/We_{cr}}} \quad (4.17)$$

where the constants are: $C_{TI1} = 1.6$ and $C_{TI2} = 0.42$. The critical Weber number of 1.42 is employed (Sevik and Park, 1973). Considering the transition point from the finely dispersed bubbly flow to slug flow, the maximum allowable void fraction is a value of 0.52.

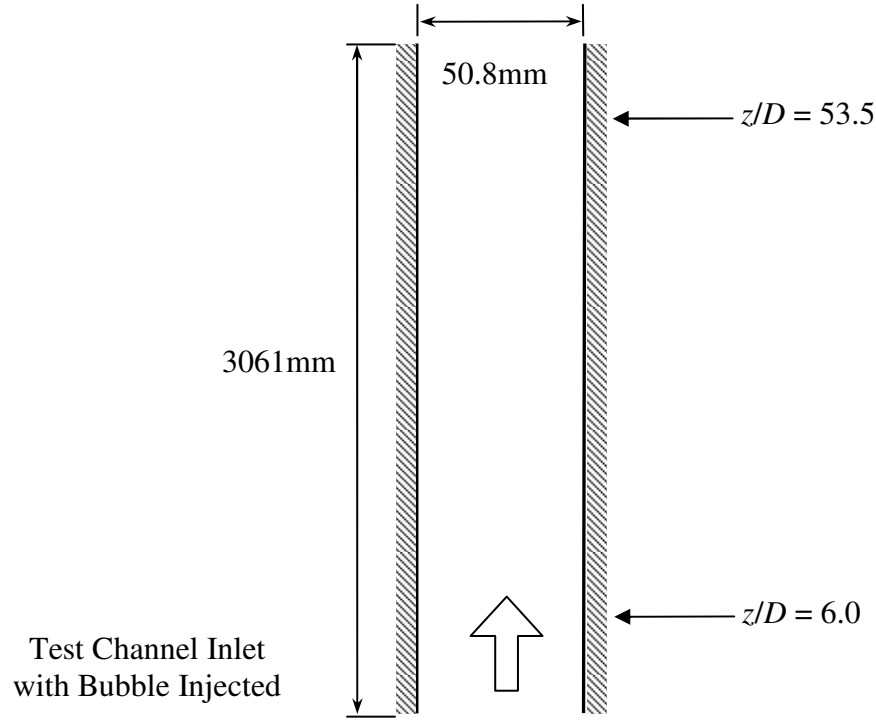


Figure 4-2 Geometry details of Hibiki et al. (2001) experiment

Regarding coalescence caused by wake entrainment, Yao and Morel (2004) stated it only has significant influence in slug flow where a big bullet bubble almost occupy whole cross-section of pipe. In scenario of bubbly flow, it can be neglected. Similar reports can be found in Hibiki and Ishii (2002) model, Cheung et al. (2007 a and b).

4.3 Numerical and Experimental Details

The two numerical models are estimated by validating against experimental data conducted by Hibiki et al. (2001) with a range of superficial liquid velocities $\langle j_f \rangle$ and superficial gas velocities $\langle j_g \rangle$ at the location of $z/D = 6.0$ and 53.5 (see Figure 4.2). Eight bubbly flow conditions, as summarized in Table 4.1, have been employed for validation. As depicted in Figure 4-3, there are four conditions are in bubbly flow and another four represent the characteristics of bubbly-to-slug transitional regime. Particularly in flow condition of $\langle j_f \rangle = 0.986$ m/s and $\langle j_g \rangle = 0.321$ m/s, observation of cap bubbles was reported. As discussed in Ho and Yeoh (2005), the interactions among bubbles-bubbles, bubbles-liquid eddies in bubbly-to-slug transitional flow regime may become comparatively complicated when the coalescence involves cap bubbles, which causes noticeable discrepancy between numerical predictions and experimental measurements.

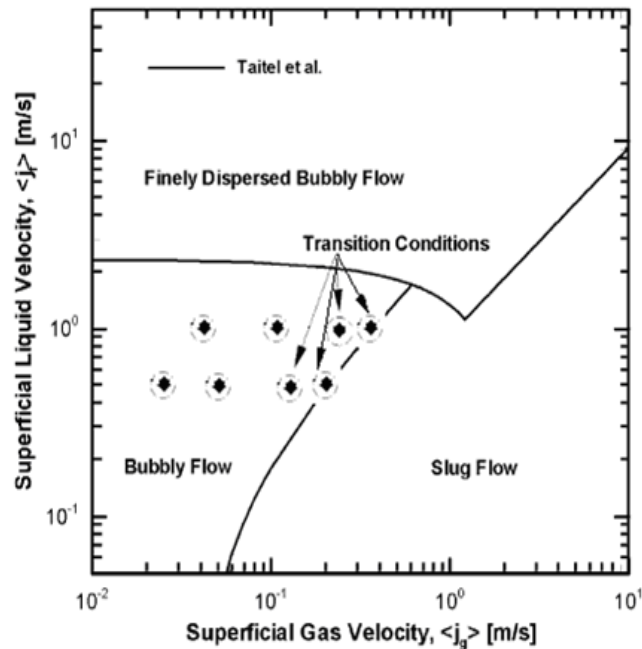


Figure 4-3 Map of tube flow regime and transition flow conditions studied in the present study (Cheung et al 2007 a)

Two sets of transport equations for mass and momentum of each phase coupled with additional Population Balance Equations, Average Bubble Number Density (ABND) model are sought. In the ABND model, the Yao and Morel (2004) coalescence and breakage kernels model has been applied. In order to reduce computational cost, radial symmetry has been assumed; consequently numerical simulations are only performed on a 60 degree radial sector of the pipe with symmetry boundary conditions at both vertical sides, instead of whole pipe domain. The computational mesh and geometry is shown in Figure 4-4. At the inlet of the test section, as the diameter of the injected bubbles are unknown, uniformly distributed superficial liquid and gas velocities, void fraction and bubble size are specified in accordance with the flow condition described. More details of the boundary conditions have been summarized in Table 4.1. The Shear Stress Transport (SST) turbulent model coupled with Sato's bubble-induced turbulent viscosity model (Sato et al., 1981) has been adopted in the current study.

Table 4-1 Flow scenarios and its inlet boundary condition details in simulation of Hibiki et al. (2001) experiment.

Superficial liquid velocity $\langle j_f \rangle$ (m/s)	Superficial gas velocity $\langle j_g \rangle$ (m/s)			
<i>Hibiki et al. (2001) experiment</i>				
0.491	0.0275	0.0556	0.129	0.190
$[\alpha_g]_{z/D=0.0}$ (%)	[5.0]	[10.0]	[20.0]	[25.0]
$[D_S]_{z/D=0.0}$ (mm)	[3.0]	[3.0]	[3.0]	[3.0]
0.986	0.0473	0.113	0.242	0.321^b
$[\alpha_g]_{z/D=0.0}$ (%)	[5.0]	[10.0]	[20.0]	[25.0]
$[D_S]_{z/D=0.0}$ (mm)	[3.0]	[3.0]	[3.0]	[3.0]

^b Cap bubbles were experimental observed in this flow condition

4.4 Result and Discussion

With the purpose of assessing these two models within wide range of flow scenarios, eight different operations have been numerically implemented and validated against experimental data of Hibiki et al. (2001). By comparison of numerical results of gas void fraction, Sauter mean bubble diameter and air velocity with experimental data, values of some adjustable parameters in the model has been set up in order to give reasonable overall outcomes in all study cases. Under the consideration of increased possibility of coalescence between closely package bubbles under high void fraction flow condition, breakage and coalescence calibration factors of 0.1 and 0.6 respectively are applied for the case of high void fraction (transitional flow) while 0.3 of coalescence and 1 of breakage are set up to adjust for comparatively low void fraction (bubbly flow) flow conditions. The similar calibration factors adjustments were reported in research of Chen et al. (2005) and Olmos et al. (2001).

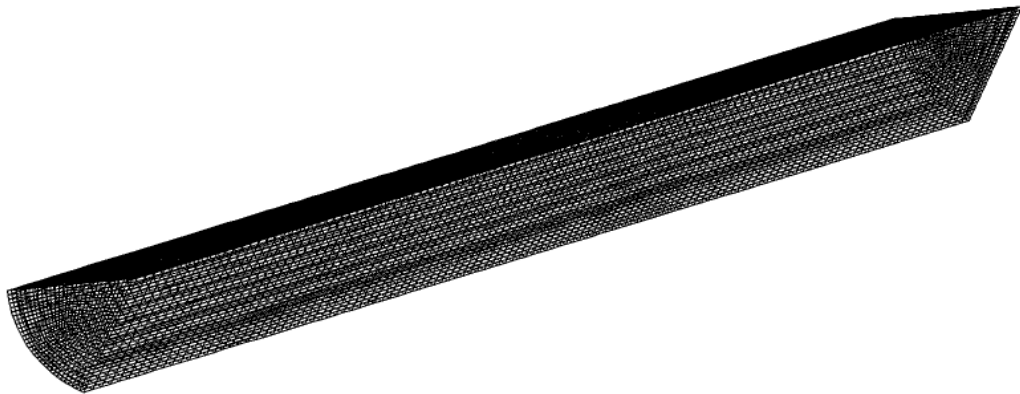


Figure 4-4 Mesh distribution of computational model: Hibiki et al. (2001) experiment.

4.4.1 Void fraction distribution

The Figure 4-5 shows the comparisons of time averaged radial void fraction distribution between simulated predictions by applying drag coefficient correlations of Simonnet et al. (2007) and Ishii and Zuber (1979) and experimental measurements conducted by

Hibiki et al. (2001) at the dimensionless axial position $Z/D = 53.5$. The 0 of radial

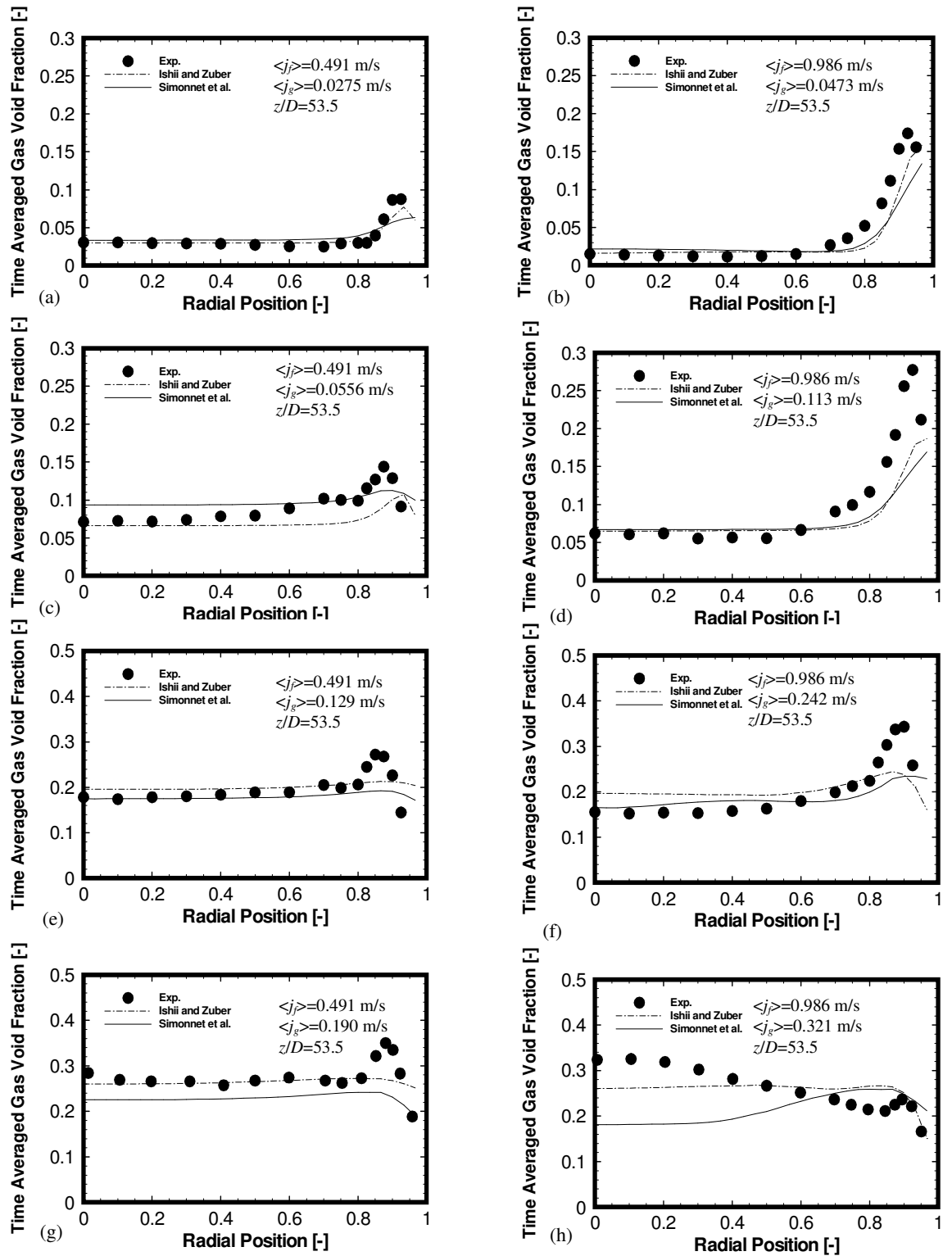


Figure 4-5 Predicted radial void fraction distribution and experiment data of Hibiki et al. (2001).

position means the centre of the pipe and the “1” means the wall of the pipe. Based on phase distribution patterns, Hibiki et al. (2001) classified isothermal bubbly flow into five basic types of radial void fraction distributions: “wall peak”, “intermediate peak”, “corn peak”, “transition” and “flat”. In the present research, wide range of flow patterns of “wall peak”, “intermediate peak” and “transition”. Both drag coefficient correlation models generally provide considerably reasonable good agreement in most of flow conditions comparing with experimental value. For the complex flow condition of $\langle j_f \rangle = 0.986$ m/s and $\langle j_g \rangle = 0.321$ m/s within which cap bubbles were observed, both two drag coefficient models still maintain considerably better prediction at the adjacent of pipe wall; however, void fraction at the core of pipe has been under-predicted (Figure 4.5 h). One of the possible reasons which can explain this discrepancy may be the lateral lift force since it is the major factor effecting bubble radial movement between pipe wall and core. The lift force acting on a bubble in a simple unbounded shear flow are dominated by bubble deformation; void fraction and relative velocity between two phases. As reported by Tomiyama (1998), bubble will migrate toward the pipe centre when bubble is larger than 5.5 mm for bubbly upward air-water system and his lift force correlation has been adopted in this study. Since the predicted time average sauter mean bubble diameters for both drag coefficient models (see Figure 4.5) are lower than this migration standard, the numerical higher void fraction at the centre of pipe is considerably difficult to be simulated. Another possible reason for inaccurate prediction may be due to Tomiyama (1998) lift force conducted from single bubble behaviour in infinite stagnant liquid system. It may have been challenged when it has been adopt into flow conditions involving extremely significant influence from closely package neighbour bubbles.

4.4.2 Sauter mean bubble diameter

The predicted and measured Sauter mean bubble diameter distributions are illuminated in Figure 4-6. The potential tendency of small bubbles migrating towards the wall provides considerable possibility for highly concentrated bubbles to merge together to form slightly larger bubbles. Therefore, the Sauter mean bubble diameter distributions profiles appeared characteristics with almost equal value along the radial direction with

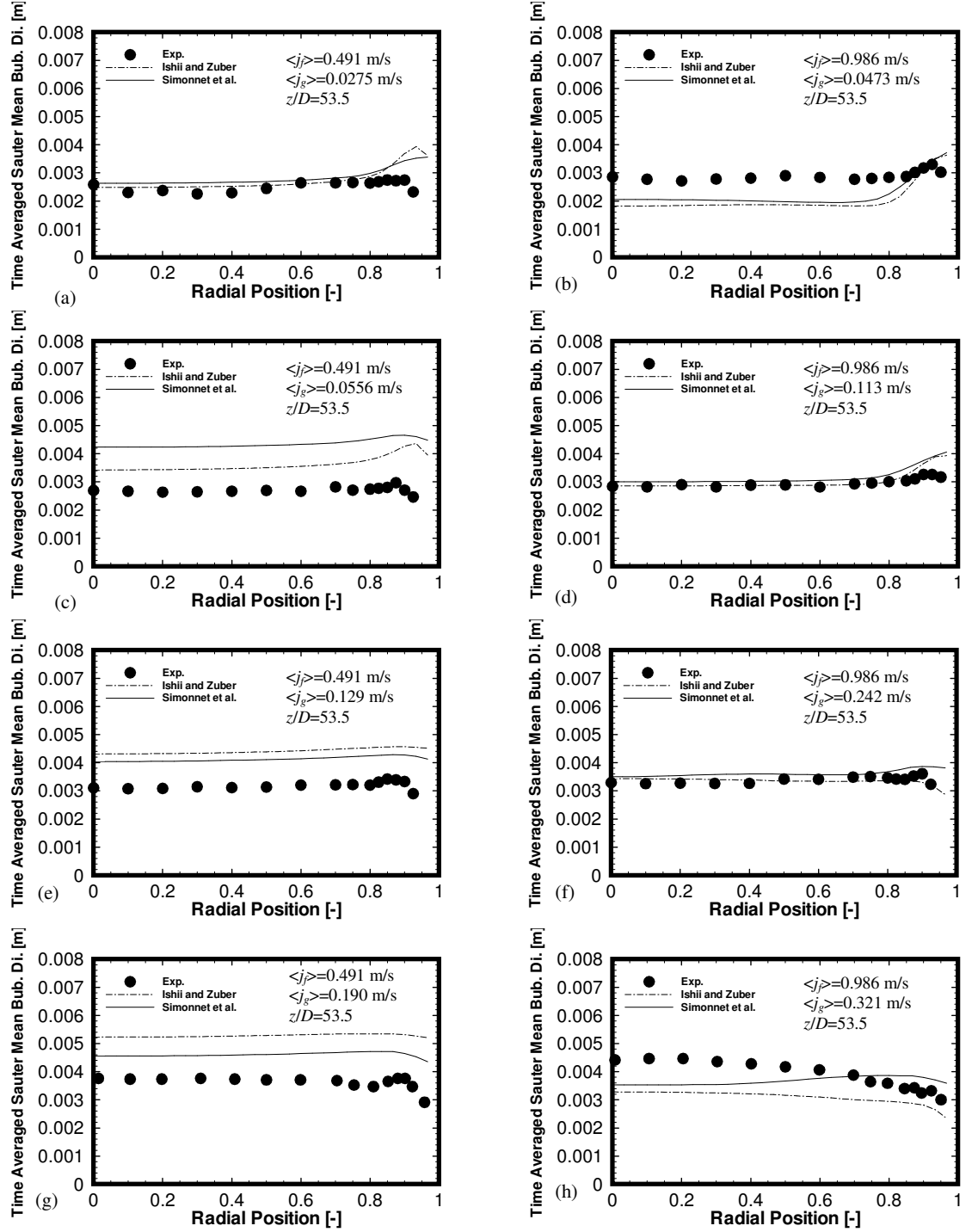


Figure 4-6 Predicted Sauter mean bubble diameter distribution and experiment data of Hibiki et al. (2001).

slim larger value near the wall for most cases except for the flow condition of $\langle j_f \rangle = 0.986 \text{ m/s}$ and $\langle j_g \rangle = 0.321 \text{ m/s}$. When the size of formed large bubbles beyond certain critical standard (5.5 mm for bubbly upward air-water system), the large bubble intend to move towards to pipe centre and deform to cap bubble shape. And the flow

condition of $\langle j_f \rangle = 0.986$ m/s and $\langle j_g \rangle = 0.321$ m/s is a typical example demonstrating this migration and observation of cap bubbles were reported by Hibiki et al. (2001). Furthermore, cap bubble has weak entrainment phenomenon by absorbing small following bubbles in its weak area to form even larger bubble, which consequently increase sauter mean diameter at pipe centre and enlarge the range of the sauter mean diameter distribution. Generally speaking, these two numerical models reasonably well predicted bubble size distribution for all cases except flow condition of $\langle j_f \rangle = 0.986$ m/s and $\langle j_g \rangle = 0.321$ m/s. both two drag correlations under-predicted Sauter mean bubble diameter at the core but reasonably predicted in the vicinity of the wall area (Figure 4.6 h). These discrepancies might caused by population balance model since ABND model only presenting average sauter bubble diameter. It might be difficult when it has been adapt to flow conditions with a wide range of bubble size distribution (Cheung et al. 2007 a and b). Moreover, ignoring the wake entrainment phenomenon in Yao and Morel (2004) model may be another reason for the discrepancies between predicted results and measured data.

4.4.3 Time-averaged gas velocity

The measured and predicted radial profiles of the time-averaged air velocity at the measuring station of $Z/D=53.5$ at the vicinity of pipe outlet are illuminated in Figure 4-7. The Simonnet et al. (2007) drag coefficient correlation by introducing local void fraction has considerably better prediction of the gas velocity profiles than Ishii and Zuber's (1979) drag coefficient model in most of flow cases in study. As reported in Simonnet et al. (2007), the drag force influence has the tendency to increase with the increasing of gas void fraction up to 15%; subsequently further increasing gas void fraction leads to decreasing of drag reduction phenomenon. The reasons of explanation of increased drag when gas void fraction is between 0 to 15% might be due to the accelerated liquid phase velocity. Since the space of liquid phase has been occupied by adding bubbles, the liquid phase has been forced to accelerate to pass narrowed space in order to maintain the same flow rate. When gas void fraction increased beyond certain critical value of 15%, the aspiration in the bubbles wakes started to play dominant influence on flow conditions and resulted in a decreased drag coefficient with the local void fraction. In order to further demonstrate the degree of improvement of Simonnet et

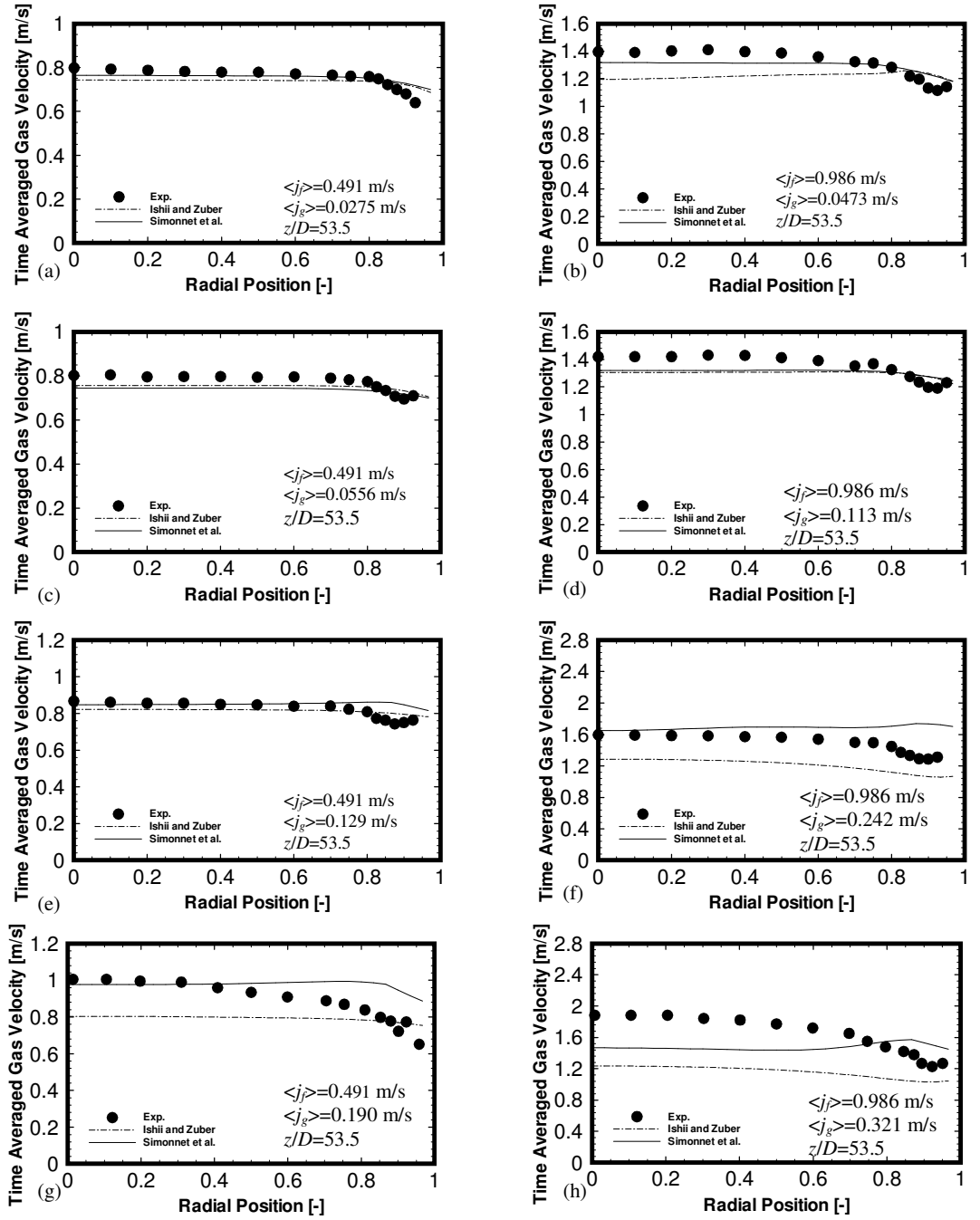


Figure 4-7 Predicted radial gas velocity profile and experiment data of Hibiki et al. (2001).

al. (2007) drag coefficient comparing with Ishii and Zuber (1979)'s model. Conception of error percentage of gas velocity is introduced as follow:

$$error = \frac{|u_g - u_g'|}{u_g} \times 100\% \quad (4.18)$$

where u_g and u_g' are predicted and experimental gas velocity, respectively. This formulate has been used to estimate the accuracy of simulation results comparing with experimental data. In Figure 4-8, the error percentage of time-averaged gas velocity are plotted against the axial position of $Z/D=6.0$ and 53.5 . The solid line indicates the prediction results of Simonnet et al. (2007) while the dash dot line illuminates that of Ishii and Zuber (1979), respectively. As shown in Figure 4-8, the Simonnet et al. (2007) model shows low error percentage values along axial position for most of cases comparing with Ishii and Zuber (1979) model and can provide considerably better predictions in time averaged gas velocity for major flow conditions.

4.5 Conclusions

Two drag mechanisms proposed by Simonnet et al. (2007) and Ishii and Zuber (1979) were implemented into Eulerian-Eulerian two-fluid model coupled with ABND model to handle the isothermal gas-liquid bubbly flow conditions. Particular research focus has been centered on investigation of bubbly-to-slug transition regime. The performances of these two models were validated against experimental measurement reported by Hibiki et al. (2001) under various flow scenarios. Local radial distributions of primitive variables: void fraction, Sauter mean bubble diameter and gas velocity, are chosen to be three aspects to assess these two drag models' performances. In general, both of the drag coefficient correlations provide fair prediction agreement with experimental results. Due to drag force compared with other interfacial force is the primary and fundamental parameter reflecting liquid/gas velocity; Simonnet et al. (2007) model in terms of local void fraction provides comparatively better prediction in gas velocity comparing with correlation of Ishii and Zuber (1979).

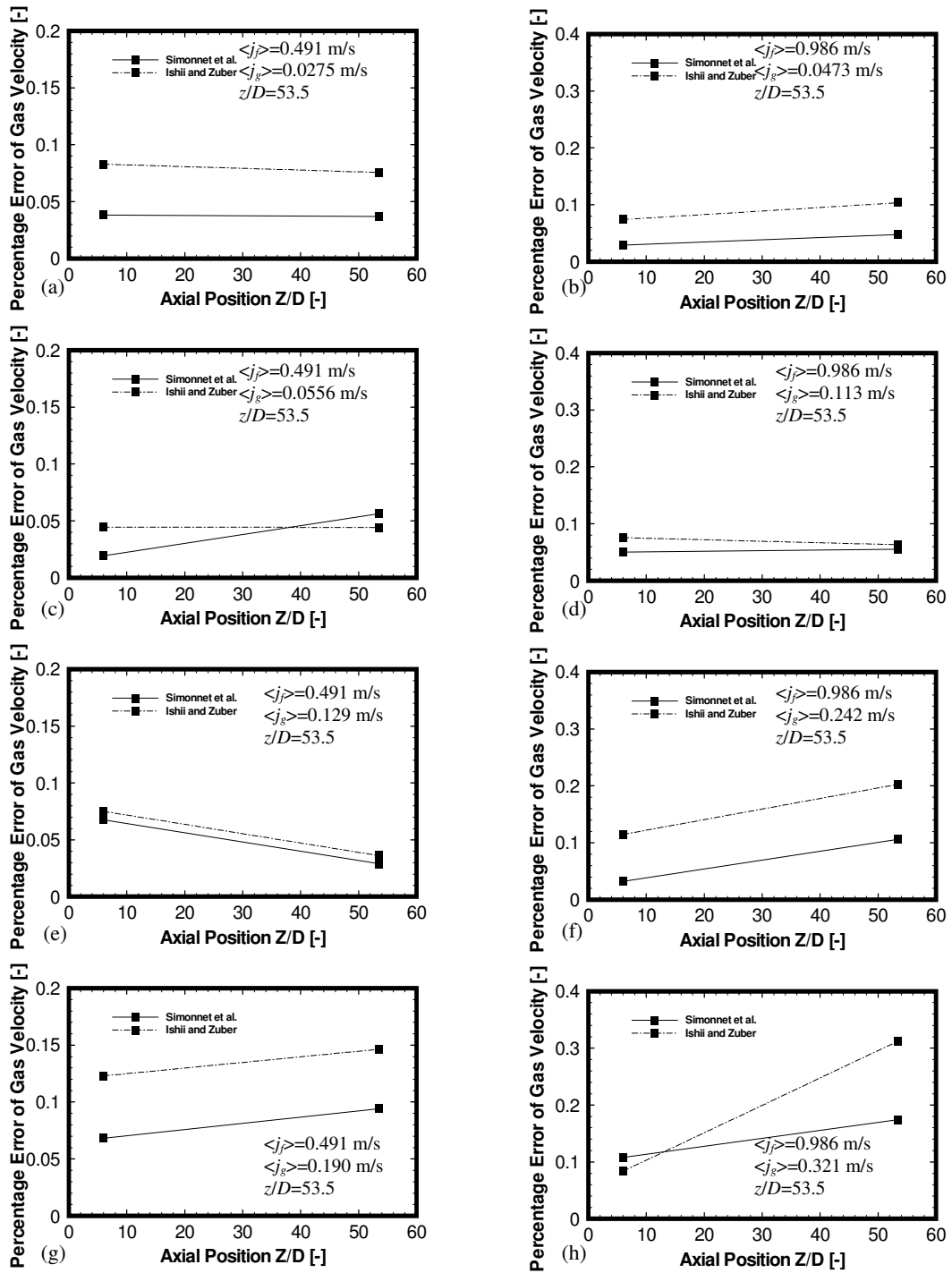


Figure 4-8 Error percentage of predicted time averaged gas velocity comparing with experimental data of Hibiki et al. (2001).

Chapter 5 On Modelling Horizontal Gas-liquid Bubble Flow using Population Balance Approach

Horizontal gas-liquid bubbly flow has various industries application background; however, this flow orientation received less attention than vertical bubbly flow. The migration of dispersed bubbles towards the top due to buoyant influence causes a highly non-symmetric internal phase distribution, which increase the degree of difficulty for numerical predictions. In this study, the internal phase distributions of horizontal bubbly flow have been simulated using population balance model under four individual flow conditions with average gas volume fraction up to 20%. The predicted three local primitive variables distributions are validated against the experimental data of Kocamustafaogullari and Huang (1994 a).

5.1 Introduction

Horizontal bubbly multi-phase flow has been widely adopted in various industries because of their capability to provide large interfacial areas for heat and mass transfer in general and for attachment to bitumen in hydro-transport. As reported by Malysa et al. (1999), Luthra et al., (2003); Wallwork, (2003) and Mankowski et al., (1999), air injection not only reduce energy consumption by helping bitumen recovery at lower process temperature ($<50^{\circ}\text{C}$), but also increase the tendency for bitumen droplets attaching to the surface of air bubbles of the similar size as themselves. Since the injected air bubbles size distribution is a critical parameter dominating bitumen procession, the development of modeling and simulation capabilities of the size distribution in horizontal bubbly flow is very important for the design, operation and safety of bitumen hydro-transport system. In order to reduce the degree of complexity gas-water-solid particles three-phase numerical models, the gas-water two-phase bubbly flow system has been focused initially.

In the past, most studies of bubbly flow performance have been concerned with vertical configuration and horizontal flow orientation received less attention in the literature. In

vertical flows, buoyant acts counter against or parallel with flow main direction which mainly affects gas-water relative velocity at the axial direction instead of velocity or phase distribution asymmetry in radial direction. However, the buoyant force is cross to main flow direction in the case of horizontal flows. It not only causes a significant flow asymmetry, but also imposes an extra strong radial force. Thereby, under influence of radial and axial forces simultaneously, bubbles move neither vertically nor horizontally as demonstrated in Figure 5-1 (Li et al 2010 a and b). Furthermore, as reported by Tselishcheva et al.(2010), the buoyant force is extremely dominant lateral force comparing to lateral lift force in numerical model, which has difficulties to predict the comparatively slow radial rising velocity observed in experiment without adding new numerical models at this stage.

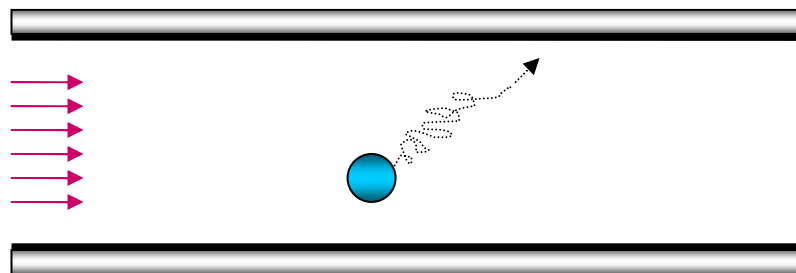


Figure 5-1 A simplified schematic bubble motions in horizontal pipe flow: Under the combination of radial and axial force, bubbles travel neither vertically nor horizontally

In the literature, several measurement technologies have been utilized to explore the horizontal bubbly flow characteristics. However, no numerical researches have been reported in this field till recent stage. Haoues et al (2009) and Talley and Kim (2010) developed drift flux model to predict the integral flow characteristics of horizontal bubbly flows, however the drift flux model could not fully describe the interactions between two phases. Tselishcheva et al (2010) applied two-fluid model coupled with interfacial forces transformation to simulate the void fraction and velocity profiles in two flow situations: in a lone straight horizontal pipe and in a horizontal pipe with 90 degree elbow, nevertheless, all the numerical research is studied under the assumption of constant bubble diameter without consideration of bubble realistic interaction

mechanisms. By consideration bubble coalescence and break-up through the interactions among bubbles as well as between bubbles and turbulent eddies in turbulent flows, Ekambara et al (2008) applied computationally expensive population balance model –Multiple Size Group (MUSIG) approach to investigate internal phase distribution of horizontal bubbly flow. With the purpose of reduce computational cost, an averaged simple population balance model - Average Bubble Number Density (ABND) approach has been applied to simulate the internal phase distributions of air-water bubbly flow in a 50.3mm i.d. horizontal pipeline in this study. With the aim of assessing the model performance under wide range of flow scenarios, four individual flow conditions with average gas volume fraction from 4.4% to 20% have been considered. The predicted local radial distributions of void fraction, Interfacial Area Concentration (IAC) and gas velocity are validated against the experimental data of Kocamustafaogullari and Huang(1994 a).

Table 5-1 Flow scenarios and its inlet boundary condition details in simulation of Kocamustafaogullari and Huang (1994 a) experiment.

Kocamustafaogullari and Huang (1994)				
Superficial liquid velocity $\langle j_f \rangle$ (m/s)	Superficial gas velocity $\langle j_g \rangle$ (m/s)			
4.67 m/s	0.213 m/s	0.419 m/s	0.788 m/s	1.21 m/s
$[\alpha_g]_{z/D=0.0}$ (%)	[4.4]	[8.5]	[14.6]	[20.46]
$[D_s]_{z/D=0.0}$ (mm)	[3.0]	[3.0]	[3.0]	[3.0]

5.2 Numerical Details

The numerical model is validated against experiments conducted by Kocamustafaogullari and Huang (1994 a) with wide range of superficial liquid velocities $\langle j_f \rangle$ and superficial gas velocities $\langle j_g \rangle$ at the location of $z/D = 253$ (see Figure 5-2 a). The computational mesh of cross section is shown in Figure 5-2 (b). At the inlet of the test section, as the diameter of the injected bubbles are unknown,

uniformly distributed superficial liquid and gas velocities, void fraction and bubble size are assumed and specified in accordance with the flow condition described. Details of the boundary conditions have been summarized in Table 5.1.

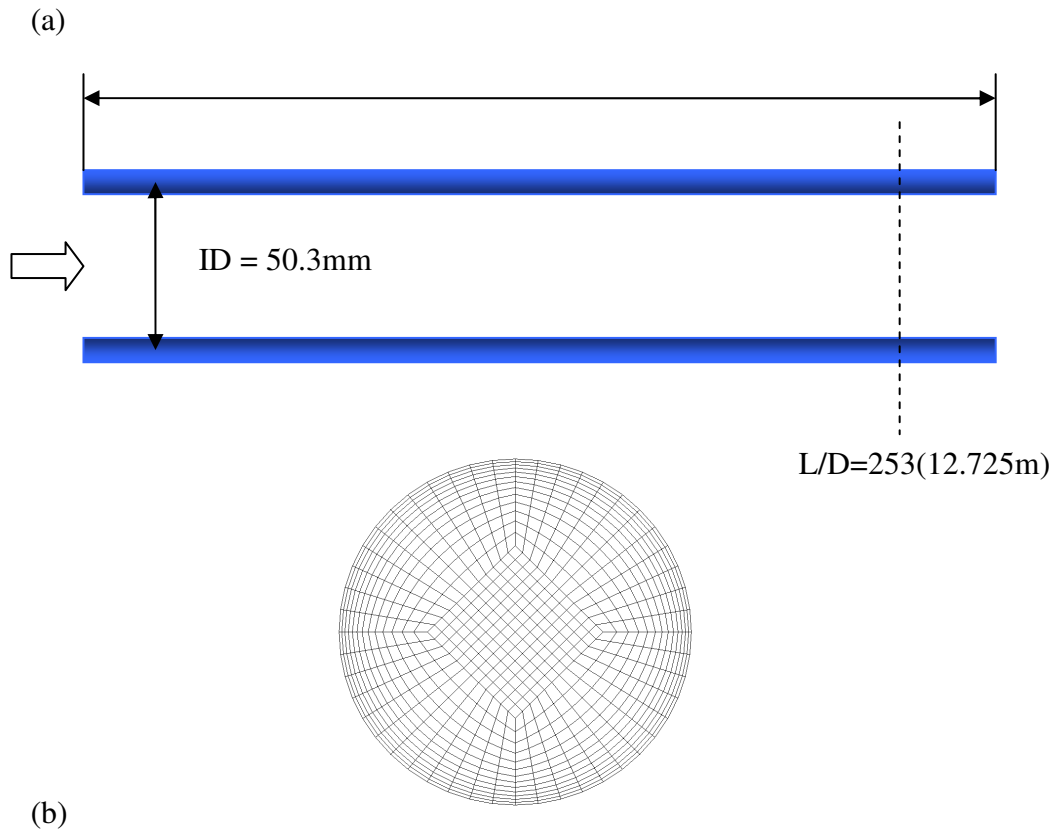


Figure 5-2 (a) Geometry details of Kocamustafaogullari and Huang (1994) experiment and (b) mesh distribution of computational model for cross section.

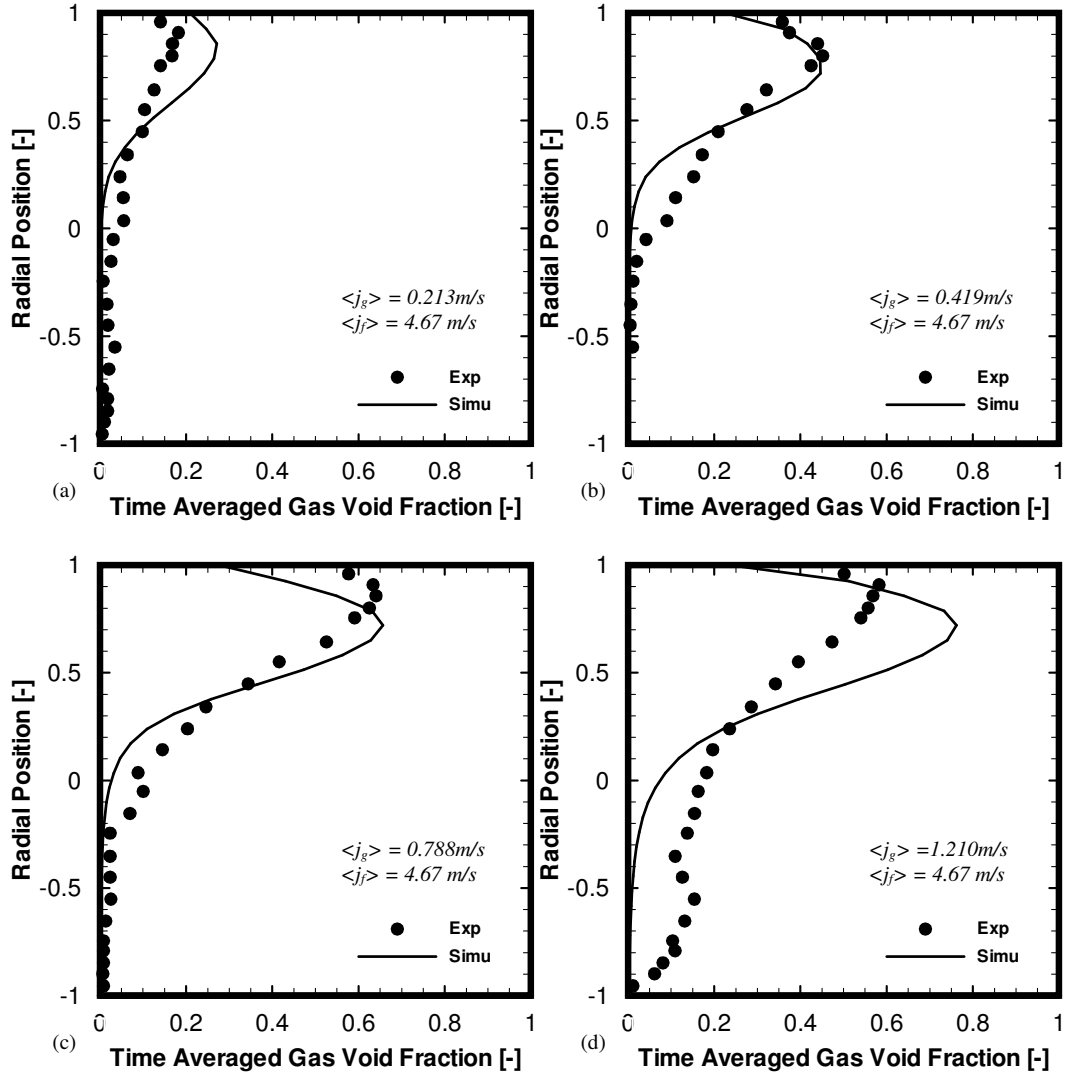


Figure 5-3 Predicted Time Averaged Gas Void Fraction distributions and experimental data of Kocamustafaogullari and Huang (1994) at location of $L/D =$

253

5.3 Results and Discussion

5.3.1 Time averaged gas void fraction

The predicted radial void fraction distribution of horizontal bubbly flow comparing with experimental data of Kocamustafaogullari and Huang (1994 a) at the dimensionless axial position $Z/D = 253$ are depicted in Figure 5-3. As demonstrated in the figures, there is peak of gas void fraction profile in the vicinity of the upper pipe area in each flow condition, which resulted from the migration of bubbles toward the upper wall due

to the influence of buoyant force. The wall lubrication force push the dispersed bubble away from the upper wall, thereby the peak is not formed directly on the upper surface of pipe wall. Form Figure 5-3 (a) to (c), the peak value of gas void fraction increases with the increasing of interfacial gas velocity under the certain of

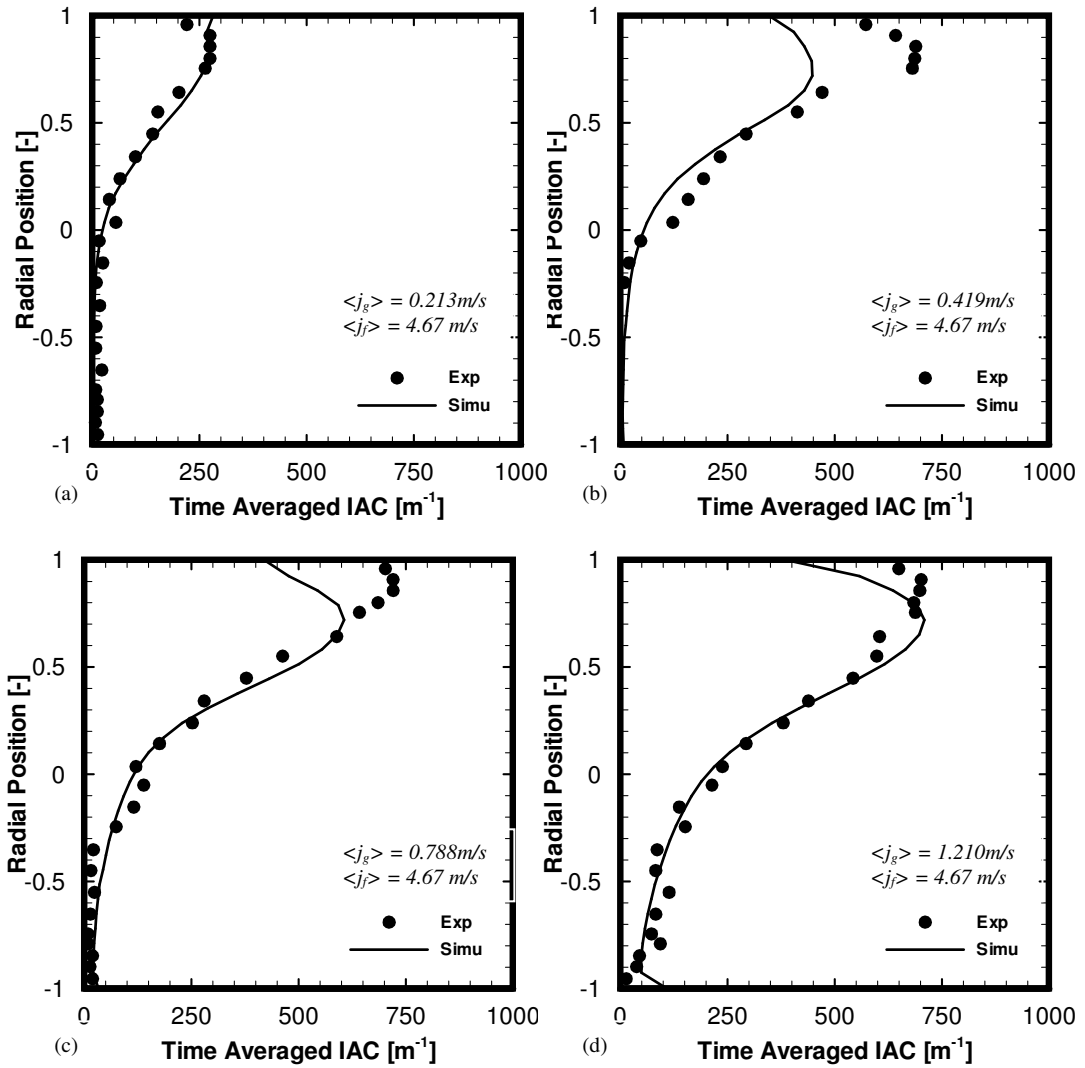


Figure 5-4 Predicted Time Averaged Interfacial Area Concentration (IAC) distributions and experimental data of Kocamustafaogullari and Huang (1994) at location of $L/D = 253$

interfacial liquid velocity of $\langle j_f \rangle = 4.67$ m/s, however, when the interfacial gas velocity accelerate to $\langle j_g \rangle = 1.210$ m/s (Figure 5-3 d), the peak value maintains at the level of around 60% and local gas void fraction at other locations start to increase. Generally speaking, the numerical model gives considerably reasonable good agreement with

experimental value for most of flow conditions. For the flow condition of $\langle j_f \rangle = 4.67$ m/s and $\langle j_g \rangle = 1.210$ m/s, the numerical model performs considerably good profile

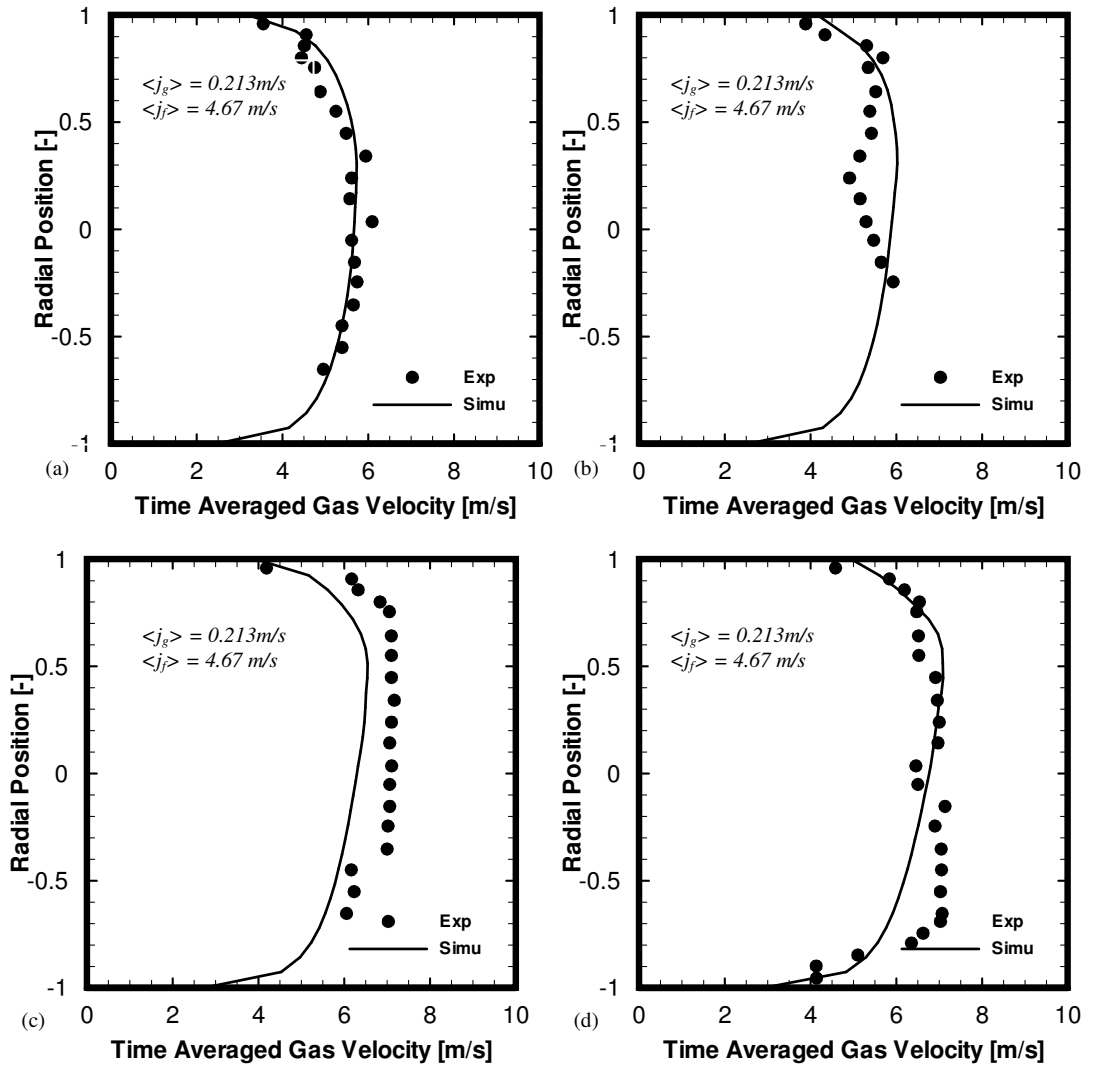


Figure 5-5 Predicted gas velocity distributions and experimental data of Kocamustafaogullari and Huang (1994) at location of $L/D = 253$

tendency for gas void fraction, however, underestimation is noticed at the lower radial position of pipe. One of the possible reasons may be that the bubbles are dispersed by strong liquid turbulence and eddies under such high liquid velocity of $\langle j_f \rangle = 4.67$ m/s, where there are no reasonable numerical models to describe it at this stage.

5.3.2 Time averaged Interfacial Area Concentration (IAC)

Predicted and measure Interfacial Area Concentration (IAC) distributions are illuminated in figure 5-4. With the assumption that bubble are spherically shaped, the Interfacial Area Concentration (IAC) a_{if} is proportion to local void fraction α_g . Thereby, the IAC has similar distribution profile of void fraction. Generally speaking, numerical results give reasonable prediction when comparing with experimental data except for the underestimation of IAC peak at the vicinity of the wall at the flow condition of $\langle j_f \rangle = 4.67$ m/s & $\langle j_g \rangle = 0.419$ m/s and $\langle j_f \rangle = 4.67$ m/s & $\langle j_g \rangle = 0.788$ m/s. It might be caused by under estimation of turbulence. According to the research of Kocamustafaogullari et al. (1994 b), the bubble sizes are generally determined by the turbulence in the core. The under estimated turbulence magnitude leads to more interaction time for coalescence between bubbles. Consequently formed larger bubbles result to the reducing of interfacial surface.

5.3.3 Time averaged gas velocity

Figure 5-5 shows the comparison of predicted and experimental data of axial components of gas velocity profiles for various gas injection rates under fixed superficial liquid velocity of $\langle j_f \rangle = 4.67$ m/s. The experimental data indicates that the velocity profile has been symmetrically distributed along radial direction regardless of highly asymmetrical distribution in gas void fraction and IAC. As suggested by Beattie (1972) there is no evidence to suggest a strong proportionate correspondence between void fraction and velocity profiles. And similar phenomena are observed in vertical bubbly flow. In vertical bubbly flow condition, bubble accelerates under the strong buoyant driving force, thereby gas bubbles rise faster than liquid; However, in horizontal bubbly flow condition, the buoyant force which is perpendicular to flow axial direction have less contribution of pushing bubble to move along axial direction than that have in vertical bubbly flow condition. According to the research of Kocamustafaogullari and Huang (1994 a) liquid velocities are slightly greater than the

bubble velocities and the bubbles are accelerated by liquid inertia in a very short distance after injection and closely follow the local liquid phase velocities. Generally speaking, numerical results give reasonable prediction about gas velocity profile compared to experimental data.

5.4 Conclusion

In this study, the internal phase distributions of air-water horizontal bubbly flow in a 50.3mm i.d. have been simulated by two-fluid model coupled with Average Bubble Number Density (ABND) approach. With the aim of assessing the model performance, the predicted local radial distributions of three primitive variables are validated against the experimental data of Kocamustafaogullari and Huang (1994 a) under wide range of flow scenarios up to 20% of average gas volume fraction.

In general, satisfactory agreements between predicted and measured results are achieved. The results indicate that ABND population balance model has reasonable performance to predict the parameter distributions of horizontal bubbly flow, in which the observed local void fraction can reach 0.65-0.70 whereas the peak interfacial area concentration can go up to 700-800 m^2/m^3 . Some slight discrepancies are found between the numerical and experimental results at certain locations of pipe, where turbulent model which can describe strong turbulence physical phenomena in horizontal bubbly flow or other interfacial force such as bouncing force among bubbles may need to be considered to further improve the prediction performance.

Chapter 6 On Modelling Vertical Gas-liquid Bubble Flow using Direct Quadrature Method of Moments (DQMOM) Approach

This chapter firstly introduced the Method of Moments and its extended methods. Then the information of experimental setup and numerical details of MTLOOP and TOPFLOW have been mentioned. Discussion has focused on the comparison between performances of DQMOM model and experimental measurements. The conclusion is provided at the end of this chapter.

6.1 Introduction and Mathematical Formulations

Nowadays, numerous industrial equipments run under the two-phase bubbly flow condition in order to obtain large interfacial area for heat transfer or particles attachment. With the purpose of representing the distribution changes of interfacial area concentration in bubbly two phase flow, the population balance model which tracks bubble number changes in a finite space has been widely used in industrial applications and academic researches. The Monte Carlo method has superiority of simulation accuracy however it has limitation of application background. It tracks each gas particle individually in three-dimensional system; thereby this method has less computational affordability and only can be applied in certain flow conditions with considerably less particles. Class Methods (CM), which divides bubble size range into about 20 to 50 groups and focus on the statistic changes of bubble number in each size group instead of tracking each individual bubbles, can be considered as a gratification compromising between prediction accuracy and computational cost and has been extensively applied in certain small industrial or lab scale processions. Nevertheless, the computational time is not bearable and pleased when it comes to simulate complex industrial procession where the turbulent modeling has already undertaken computational efforts. The recently developed Method of Moments (MOM) and its extensional methods, which

only use general 4 to 6 of scalars and abundantly shrink computational time, can be considered as a promising approach for solving complex industrial simulation in future.

The Method of Moments (MOM) was firstly proposed by Hulburt and Katz (1964). It has beautiful invention of transformation particle size distribution (PSD) problem into its lower-order moments question. The k th integer moments of the PSD are defined as

$$m^{(k)}(X, t) = \int_0^\infty f(\xi, X, t) \xi^k d\xi \quad (6.1)$$

For a particle population with distribution $f(\xi, X, t)$ in some size variable ξ , the zero order moment ($k = 0$), is the number of particles in the system, usually expressed as number concentration. When ξ is particle volume, the first order moment ($k = 1$), represents the particle volume fraction which is proportional to the mass concentration. Conventional MOM model demands less computational efforts, however it has a severe restriction in its applications in to those systems for which the set of moment equations is closed (McGraw, 1997). A certain type of source and sink terms which can be completely convened into a function of moments even with different orders is required when it is handled by this method. One example of MOM application is to solve the growth law source term in General Dynamic Equation (GDE) which is suitable for describing aerosol formation in complex flow fields. With the aid of certain linear format of particle growth law $\phi(\xi) = a + b\xi$, the growth term can be fully transformed to an expression of moments which calls closure problem (Hulburt and Katz, 1964).

$$k \int \xi^{k-1} \phi(\xi) f(\xi) d\xi = ak \int \xi^{k-1} f(\xi) d\xi + bk \int \xi^k f(\xi) d\xi = akm^{(k-1)} + bm^{(k)} \quad (6.2)$$

However, not every source and sink terms can follow such format type and can be completely closed with an expression of moments only. When this moment operator applies to the PBE, the moment equations are open and a number of closure approaches with reformation of bubble density function have been searched and explored. Hulburt and Katz (1964) expressed the bubble density function as a truncated series of some orthogonal polynomials, while Williams (1986) assumed the bubble density function shape. However, this assumption and reformation of bubble density function adds not only additional computational effort but also extra error in the calculations for bubbly flow simulation.

In order to avoid the closure problem, McGraw (1997) proposed a modification of the MOM by means of a quadrature approximation with abscissas ξ_i and weights w_i and named it as quadrature method of moments (QMOM), thereby this method can be utilized in broad applications regardless the formats of source and sink terms. For n - point Gaussian quadrature, the moments can be written

$$m^{(k)}(X, t) = \int_0^\infty f(\xi, X, t) \xi^k d\xi \approx \sum_{i=1}^n \xi_i^k w_i(X, t) \quad \text{for } k = 0 \text{ to } 2n-1 \quad (6.3)$$

and the growth law source term in General Dynamic Equation (GDE) which is mentioned before can be simply approximated as follow without consideration of the format of particle growth law $\phi(\xi)$.

$$k \int \xi^{k-1} \phi(\xi) f(\xi) d\xi \approx k \sum_{i=1}^n \xi_i^{k-1} \phi(\xi_i) w_i(X, t) \quad \text{for } k \geq 1 \quad (6.4)$$

As the result, the essence of quadrature-based closure shifts from restricting source term formats to searching the proper abscissas ξ_i and weights w_i . The methods of product-difference (PD) algorithm (McGraw, 1997) and Jacobian matrix transformation (JMT) (McGraw and Wright, 2003) are introduced for calculating abscissas ξ_i and weights w_i . The QMOM has recently been implemented into a CFD code and validated against numerous experimental data by Marchisio et al (2003a, b, and c). It shows satisfactory improvements for prediction of particle size distribution (PSD). However, as pointed by Marchisio and Fox (2005), there are two main disadvantages by using the QMOM method: (1) it could not be applied to multi-variate distributions due to the loss of simplicity and efficiency when it is applied, and (2) it could not represent the sensitive inter-actions between the internal characteristics and phase velocities because of the tracking of moments only instead of variables.

With the purpose of overcoming these limitations, the Direct Quadrature Method of Moments (DQMOM) is proposed by Marchisio and Fox (2005) by using a summation of multi-dimensional Dirac delta functions. Thereby, the variables, instead of the moments of the PSD, appear in the quadrature approximation and can be tracked directly. In order to assess the performance of DQMOM in prediction of bubbly flow, the DQMOM model has been implemented into the ANSYS CFX-11 through subroutine programming and validated against the two experimental measurements with

lab scale pipe size conducted by Lucas et al. (2005) and with industrial scale size executed by Prasser et al. (2007).

6.2 Mathematical models

6.2.1 DQMOM models

The fundamental and critical equation of importance in DQMOM is formulation of PSD with Dirac delta function which can be written as:

$$f(\xi, X, t) = \sum_{i=1}^n \delta[\xi - \xi_i(X, t)] w_i(X, t) \quad (6.5)$$

When it has been substituted into the PBE given in equation (3.1), the new formulation can be written as follow after manipulations of these transport equations and introduction of weighted abscissas $\zeta_i = w_i \xi_i$.

$$\sum_{i=1}^n \{ \delta[\xi - \xi_i(X, t)] + \delta'[\xi - \xi_i(X, t)] \xi_i(X, t) \} a_i - \sum_{i=1}^n \delta'[\xi - \xi_i(X, t)] b_i = S_\xi(\xi) \quad (6.6)$$

Where a_i and b_i are source terms to the transport equations as follow:

$$\begin{aligned} \frac{\partial w_i}{\partial t} + \frac{\partial}{\partial x_\alpha} (u_\alpha(\xi) w_i) - \frac{\partial}{\partial x_\alpha} (D_x \frac{\partial w_i}{\partial x_\alpha}) &= a_i \\ \frac{\partial \zeta_i}{\partial t} + \frac{\partial}{\partial x_\alpha} (u_\alpha(\xi) \zeta_i) - \frac{\partial}{\partial x_\alpha} (D_x \frac{\partial \zeta_i}{\partial x_\alpha}) &= b_i \end{aligned} \quad (6.7)$$

As can be seen from these manipulations and transformations, the substitution not only results a transport equations system coupled by summation across N phases and satisfied by PBE, but also leads to new functions δ' and δ'' which are the first and second derivatives of the Dirac delta function which can be removed in certain process of moment transformation since Dirac delta function has the characteristics as follow (Marchisio and Fox, 2005):

$$\begin{aligned} \int_{-\infty}^{+\infty} \xi^k \delta[\xi - \xi_i(X, t)] d\xi &= \xi_i^k(X, t) \\ \int_{-\infty}^{+\infty} \xi^k \delta'[\xi - \xi_i(X, t)] d\xi &= -k \xi_i^{k-1}(X, t) \end{aligned} \quad (6.8)$$

$$\int_{-\infty}^{+\infty} \xi^k \delta''[\xi - \xi_i(X, t)] d\xi = k(k-1) \xi_i^{k-2}(X, t)$$

Substituted Equation (6.8) into Equation (6.6), we obtain:

$$(1-k) \sum_{i=1}^n \xi_i^k a_i + k \sum_{i=1}^n \xi_i^{k-1} b_i = S_k^{-(n)} \quad (6.9)$$

Where the moment source terms are approximated by

$$S_k^{-(n)} = \int_{-\infty}^{+\infty} \xi^k S_\xi(\xi) d\xi \quad (6.10)$$

The matrix for solution has the simple form of equation (6.9)

$$A\phi = d \quad (6.11)$$

where the $2n \times 2n$ coefficient matrix $A=[A_1 \ A_2]$ is given by:

$$A_1 = \begin{bmatrix} 1 & \cdots & 1 \\ 0 & \cdots & 0 \\ -\xi_1^2 & \cdots & -\xi_n^2 \\ \vdots & \ddots & \vdots \\ 2(1-n)\xi_1^{2n-1} & \cdots & 2(1-n)\xi_n^{2n-1} \end{bmatrix} \quad (6.12)$$

$$A_2 = \begin{bmatrix} 0 & \cdots & 0 \\ 1 & \cdots & 1 \\ 2\xi_1 & \cdots & 2\xi_n \\ \vdots & \ddots & \vdots \\ (2n-1)\xi_1^{2n-2} & \cdots & (2n-1)\xi_n^{2n-2} \end{bmatrix}$$

The $2n$ vector of unknowns ϕ is defined by:

$$\phi = [a_1 \cdots a_M \ b_1 \cdots b_M]^T = \begin{bmatrix} a \\ b \end{bmatrix} \quad (6.13)$$

and the source on the RHS is:

$$d = [\bar{S}_0 \cdots \bar{S}_{2n-1}]^T \quad (6.14)$$

The source term for the k^{th} moment \bar{S}_k is defined by:

$$\bar{S}_k(r, t) = \int_0^\infty \xi^k S(\xi, r, t) d\xi \quad (6.15)$$

It can be resolved with straightforward Gaussian elimination. Once generated through matrix process, the a_i and b_i can be the source and sink terms for solution of the transport equations (6.7). Consequently, the unknown weight w_i and abscissas ξ_i will be

discovered and represent the shape of particle size distribution (Marchisio and Fox, 2005).

6.2.2 Source and Sink terms for DQMOM models

In the research of DQMOM, more complicated coalescence and breakage kernels are applied in current study. For coalescence, the Prince and Blanch (1990) film drainage model has been applied which considered three stages of occurring for the merging of bubbles. Meanwhile, for breakup, the model developed by Luo and Svendsen (1996) is employed for the break-up of bubbles in turbulent dispersions.

The coalescence rate proposed by Prince and Blanch (1990) considered the turbulent collision and can be expressed as relating to the time required for coalescence:

$$\Psi(\xi'; \xi) = [\eta_{turb}(\xi'; \xi) + \eta_{buo}(\xi'; \xi) + \eta_{shear}(\xi'; \xi)] \nu(\xi'; \xi) \quad (6.16)$$

Where η_{turb} , η_{buo} and η_{shear} are turbulent contributions to collision frequency, buoyancy contribution to collision frequency and shear contribution to collision frequency, respectively. In this current research, only collisions induced by turbulence are considered, thus the equation (6.16) can be simplified as:

$$\Psi(\xi'; \xi) = F_c \frac{\pi}{4} [\xi_i + \xi_j]^2 (u_{ti}^2 + u_{tj}^2)^{0.5} \exp\left(-\frac{t_{draine}(\xi'; \xi)}{t_{contact}(\xi'; \xi)}\right) \quad (6.17)$$

Luo and Svendsen (1996) assumed bubble breakage equally occurs in all directions under turbulent flow condition and developed the bubble breakage rate which can be obtained as:

$$\Omega_{tur}(\xi'; \xi) = 0.923 F_B \left(1 - \alpha_g \left(\frac{\varepsilon}{\xi_j^2}\right)^{1/3}\right) \int_{\xi_{min}}^1 \frac{(1 + \varsigma)^2}{\varsigma^{11/3}} \times \exp\left(-\frac{12c_f \sigma}{\beta \rho_l \varepsilon^{2/3} \xi^{5/3} \varsigma^{11/3}}\right) d\varsigma \quad (6.18)$$

More detailed information of equations (6.17) and (6.18) can be found in Chapter 3.

6.3 Description of the experiment setup

The two individual sets of experiments (namely MTLOOP and TOPFLOW) which are utilized to validate DQMOM model in this study have been briefly described in this section. The most important flow phenomenon which is worth to be noticed is the main configuration details of each experiment and their resulted dominate force leading to bubble coalescence or breakup processes (Duan et al., 2011).

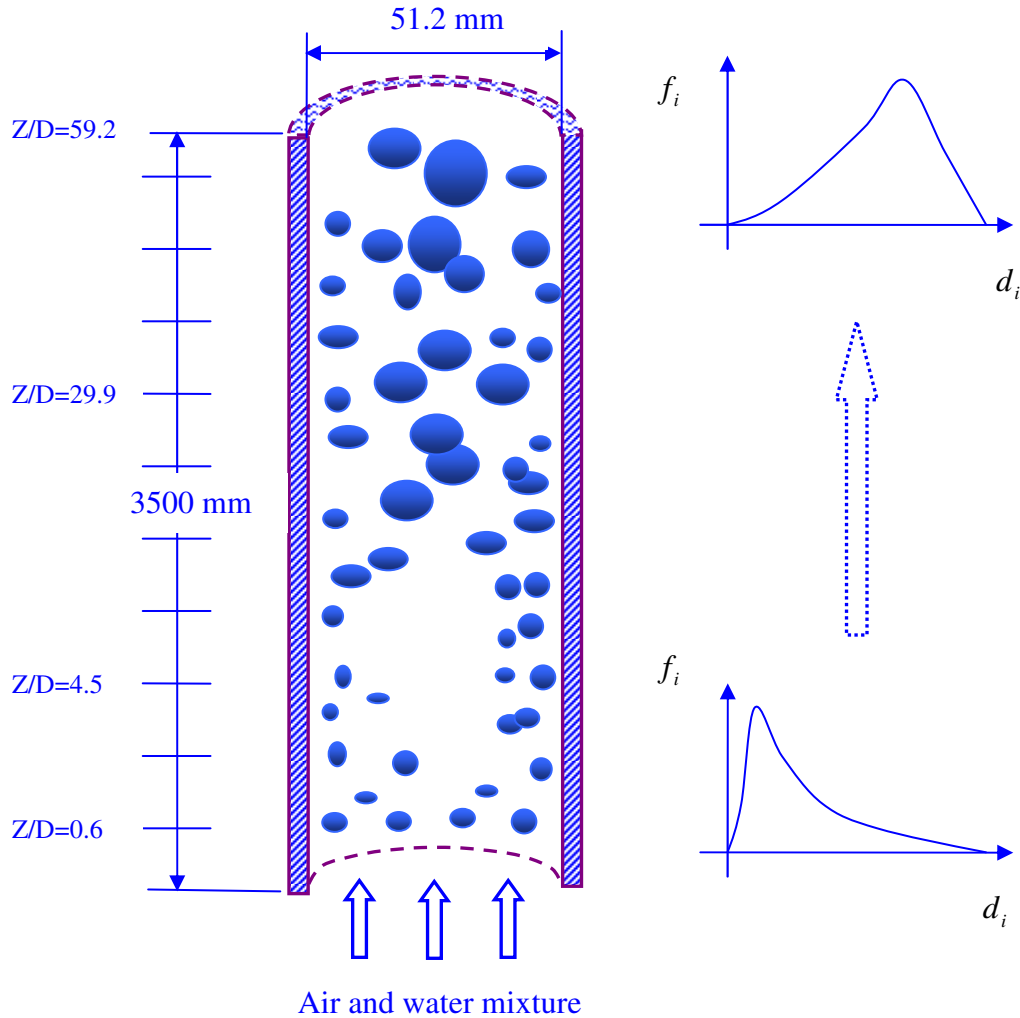


Figure 6-1 Schematic Illustration of MTLOOP experiment

6.3.1 Descriptions of the MTLOOP and TOPFLOW Experimental Setup

Figure 6.1 and Figure 6.2 depict the schematic diagrams of the MTLOOP and TOPFLOW, respectively. Both of them were designed and performed by the same

research group in the Forschungszentrum Dresden-Rossendorf FZD facility. In the experiment of MTLOOP (designed by Lucas et al. 2005), a lab scale tube with inner

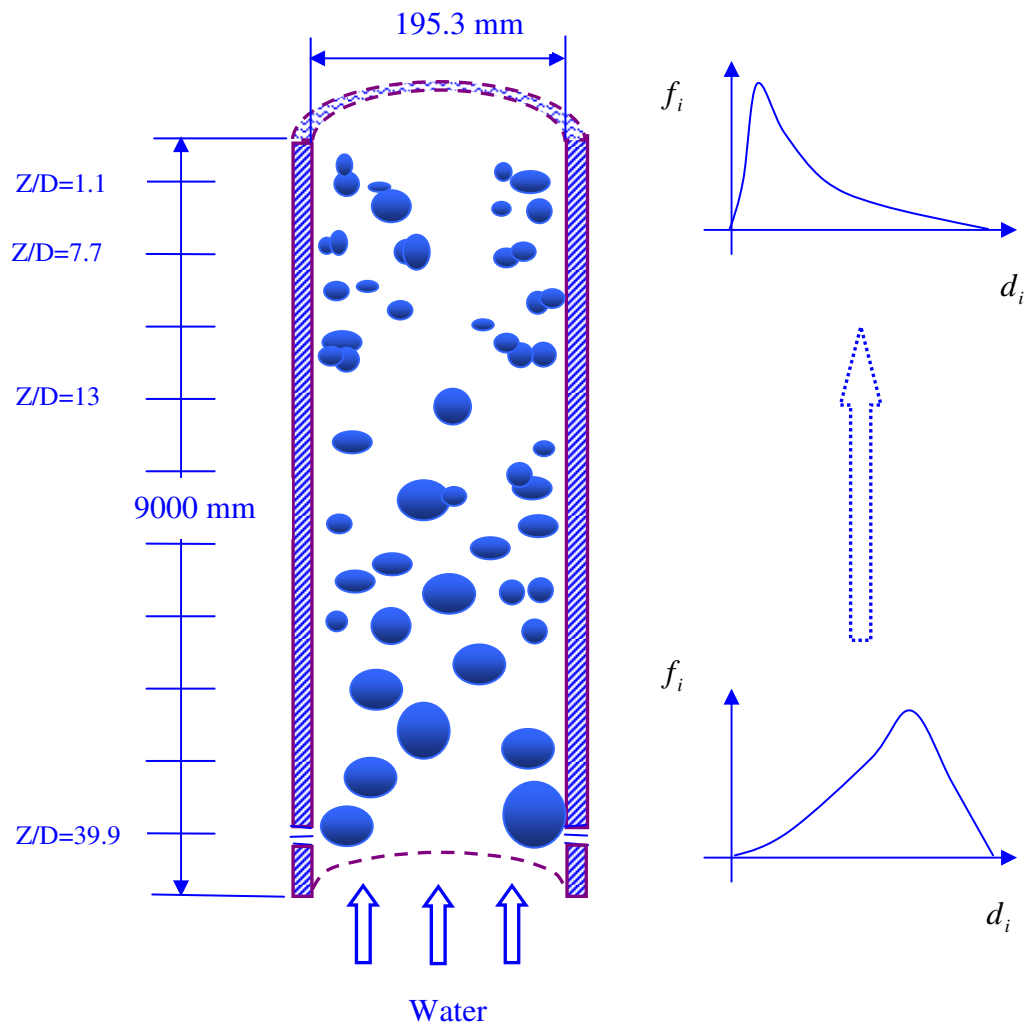


Figure 6-2 Schematic Illumination of TOPFLOW experiment

diameter of 51.2mm and length of 3.5m was built up. The air-water mixture maintained at 30°C by a heating system was injected from the bottom of this vertical tube and the phenomenon of bubbles' coalescence and breakup was observed along this tube. However, a large industrial size tube with inner diameter of 195.3 mm and height 9000 mm was considered in TOPFLOW in order to search the two-phase flow characteristics in practice. Different from the traditional gas injection system at the bottom of tube, a novel gas injection device was adopted (Prasser et al. 2007). There were 18 gas injection units with 3 levels of chambers installing along this tube at different positions

along this tube from $Z/D = 1.1$ to 39.9. In order to satisfy the purpose of injections of different size bubbles, 72 orifices of 1 mm diameter were annular distributed at the up and down level chambers while 32 annularly distributed orifices of 4 mm diameter are manufactured at the central chamber. In both experiments, wire-mesh sensor technology was applied to measure radial profiles of void fraction for a given range of bubble diameters as well as its distributions under about 100 combinations of gas and liquid volume flow rates. Nevertheless, the air fixedly was injected at inlet and the wire-mesh sensor was moved up to 10 different locations from inlet to record the flow phenomenon along the tube in MTLOOP experiment. While in TOPFLOW experiment, the measurements of bubbles' coalescence and breakup were performed with the wire-mesh sensor fixed at the exit of the tube and flexible air injection units at different axial locations along the tube.

6.3.2 *Different bubble size evolution caused by different injection methods*

As reported by Duan et al. (2011), these two experiments were comparatively exhibited the different processes of bubble coalescence and breakup. In MTLOOP, bubble coalescence mechanism was observed to be stronger than breakup actions. The mixed gas bubbles and liquid phase are injected through equally distributed capillaries, these bubbles showed a single-peaked radial distribution profile next to the tube wall with narrow bubble diameter range from size 2mm to 10 mm. Bigger bubbles were further formed through coalescence as they rise up towards exit resulting extended bubble size at outlet location of tube. Unlike the coalescence mechanism was performed to be the major influence factor in MTLOOP, it was found out that bubble breakup was stronger than bubble coalescence in TOPFLOW. In the TOPFLOW experiment, larger bubbles with various bubble size ranges between 0 to 40mm were formed immediately from the merging of fully packed swarm of bubbles since bubbles were injected straightforward from orifices on the wall of tube and highly concentrated within the wall proximity. In the travelling up to the outlet of tube, such large bubbles were easily broken down to small size due to liquid turbulence, interfacial surface instability and so on.

6.4 Numerical Details

For the two-fluid model, the conservation of mass and momentum for each phase were solved through transport equations built in the ANSYS Inc, CFX 11. Extra efforts were conducted to code transport equations governing 4 sets of weights and abscissas with the evaluation of the source terms through the use of a user subroutine incorporated within the CFD computer code. For the purpose of computational efficiency, the numerical simulations only performed on a 60 degree radial sector of the pipe under the assumption of radial symmetry. Four sets of experiment data under two different flow conditions – hereafter denoted as case M107, M118, T107 and T118 – were selected from both experiments. Inlet conditions were assumed to be homogeneous superficial liquid and gas velocities and uniformly distributed bubble size. Detailed information of geometrical size as well as inlet flow conditions of MTLOOP and TOPFLOW is described in Table 6.1.

Table 6-1 Information of inlet flow conditions employed in simulation of MTLOOP and TOPFLOW experiment

MTLOOP Experiment		M107	M118
	$[\langle j_l \rangle]_{Z/D=0}$ (m/s)	1.017	1.017
	$[\langle j_g \rangle]_{Z/D=0}$ (m/s)	0.140	0.219
	$[\alpha_g]_{Z/D=0}$ (%)	[12.1]	[17.72]
TOPFLOW Experiment	$[D_s]_{z/D=0}$ (mm)	[5.14]	[6.38]
		T107	T118
	$[\langle j_l \rangle]_{Z/D=0}$ (m/s)	1.017	1.017
	$[\langle j_g \rangle]_{Z/D=0}$ (m/s)	0.140	0.2194
	$[\alpha_g]_{Z/D=0}$ (%)	[12.1]	[17.72]
	$[D_s]_{z/D=0}$ (mm)	[20.18]	[23.28]

6.5 Discussion

As mentioned before, DQMOM solves the primitive variables appearing in the quadrature approximation which eliminates the closure problem and tracks moments of the distribution explicitly. The prediction with 4 moments were compared through the axial development of the measured area averaged bubble size distribution and void fraction at the measuring stations of $Z/D = 4.5$ and 60 for MTLOOP and $Z/D = 1.7$ and 39.9 for TOPFLOW.

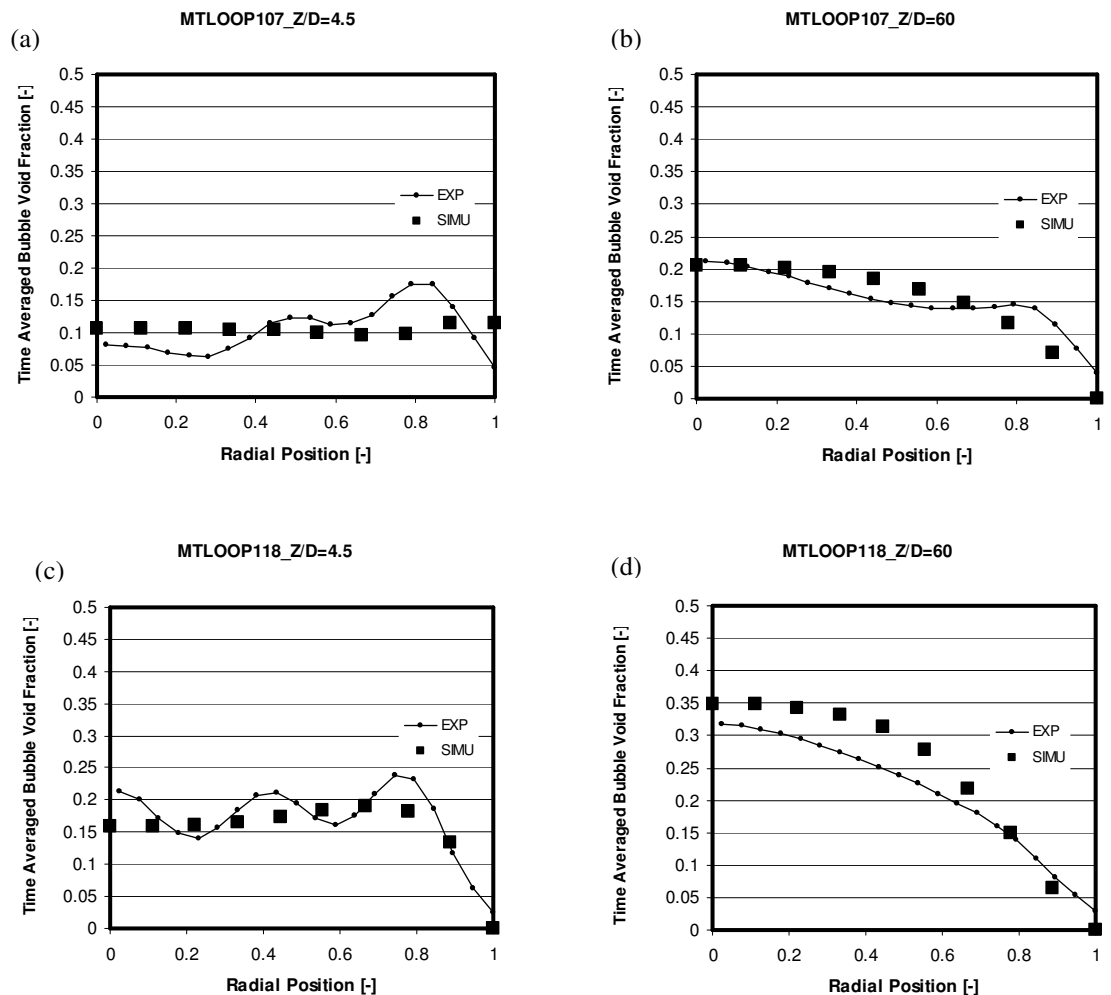


Figure 6-3 Predicted radial void fraction distribution and experiment data of MTLOOP measured by Lucas et al., (2005).

6.5.1 Bubble void fraction distribution

In Figure 6-3, the performance of DQMOM model to predict the bubble void fraction distribution profile at dimensionless axial position of $Z/D=4.5$ and 60 under the flow conditions of cases M107 and M118 is assessed against experimental data of MTLOOP. The thin line with small dots represent the experimental measurements while the comparatively larger square dots delegate the numerical prediction. As demonstrated in Figure 6-3, the DQMOM model has the capability to capture the shape changes of gas volume fraction distribution profile to “core peak” at $Z/D=60$. The adopted interfacial lift force successfully described the lateral motion of bubbles. However, the DQMOM model over-predicted the summit of gas volume fraction in the tube centre at the axial location of $Z/D=60$ as depicted in Figure 6.3 (d).

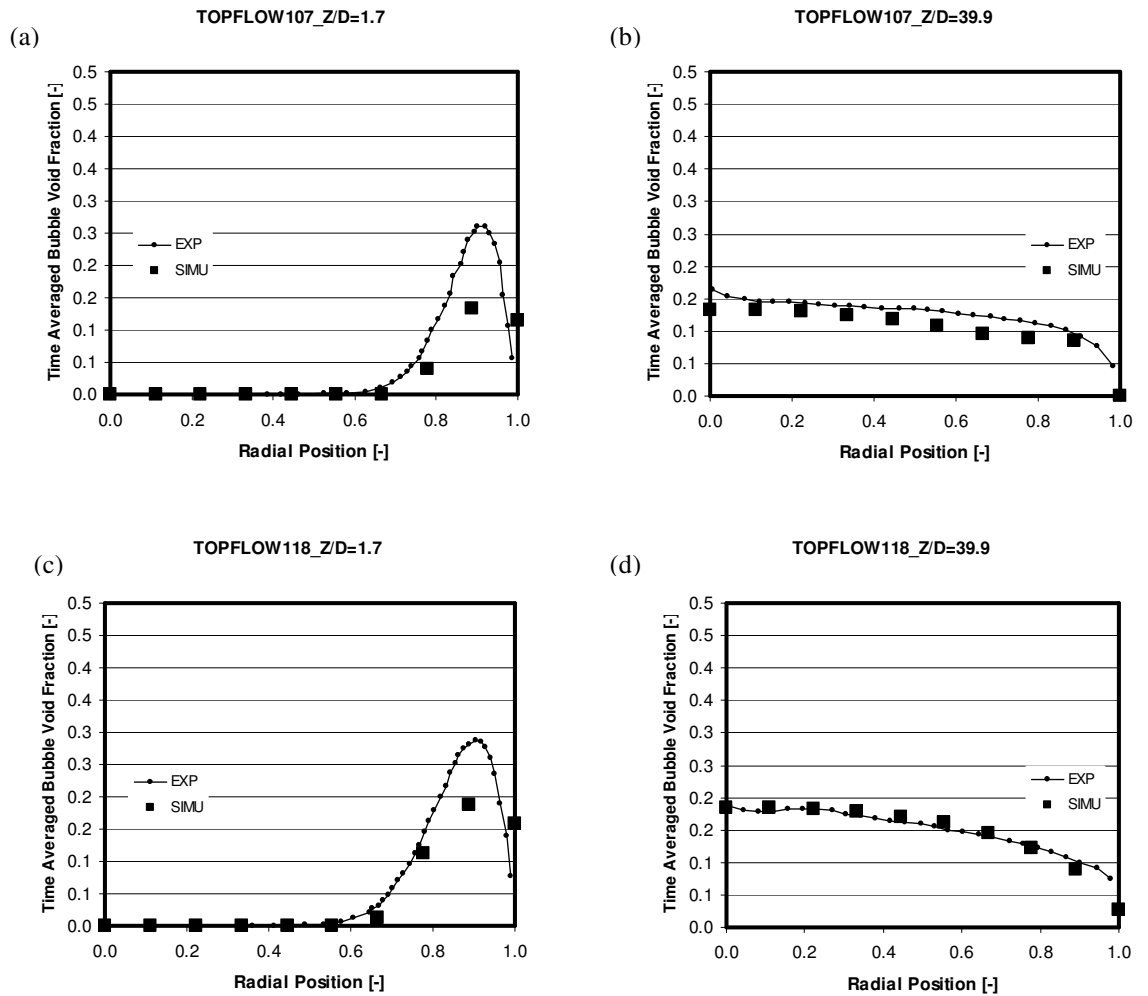


Figure 6-4 Predicted radial void fraction distribution and experiment data of TOPFLOW measured by Prasser et al (2007).

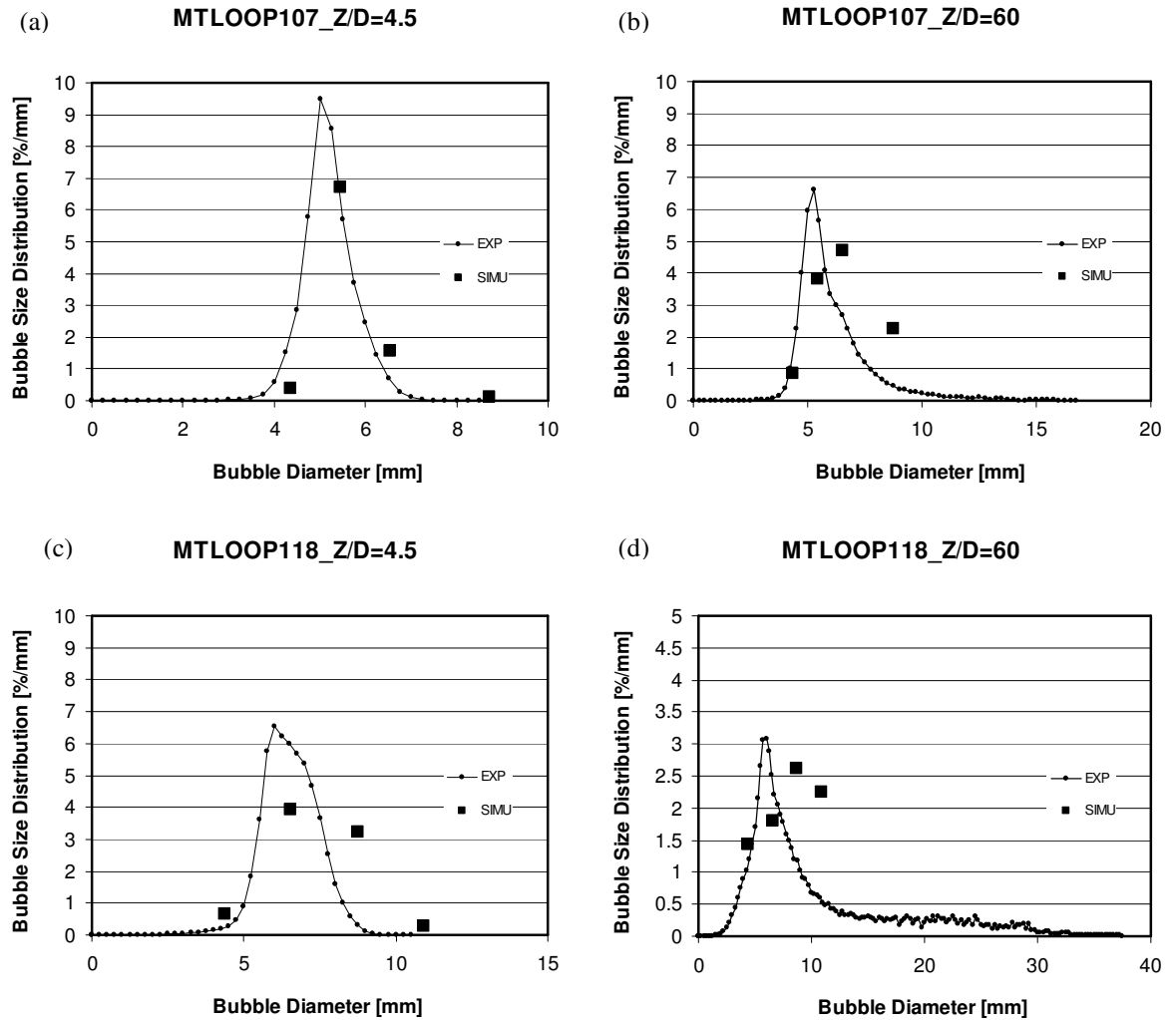


Figure 6-5 Predicted bubble size distribution and experiment data of MTLOOP measured by Lucas et al., (2005).

The comparison between the predicted volume fraction distributions simulated by DQMOM model and experimental data of TOPFLOW measured by Prasser et al., (2007) for flow condition of T107 and T118 at the location of $Z/D = 1.7$ and $Z/D = 39.9$ has been depicted in Figure 6.4. Similar to MTLOOP, the dynamical changes from “wall peak” to “core peak” bubble behaviours were successfully described by the DQMOM model. The numerical model gives reasonable prediction at location of $Z/D = 39.9$ for both flow conditions, nonetheless, the wall peaks at $Z/D = 1.7$ for both flow conditions is under-predicted. This error might come from the interfacial forces which are generally developed from the mechanics that bubbles were injected from the bottom and travelled upwards to the top. The interfacial forces model might not be suitable for the

flow condition in TOPFLOW with bubble injections on the wall. The same tendency was not observed in the flow conditions of MTLOOP.

6.5.2 Bubble Size Distribution

Figure 6.5 illustrates the comparison between prediction results and experimental data of bubble size distribution for MTLOOP experiment at location $Z/D = 4.5$ and 60 under flow conditions of M107 and M118. The dynamical changes of these profiles indicated the evolution of bubble size and interfacial area concentration influenced by the dominant coalescence mechanism. At the location of $Z/D = 4.5$ close to inlet, the initial bubble size are considerably small and size distribution are comparatively narrow, as depicted in Figure 6.5 (a) and (c) for both flow conditions of M107 and M118. As bubbles rise up to outlet, a significantly widened bubble size distribution has been observed. In M107, the original range of bubble size was from 0 to 10 mm; however, it has been extended to from 0 to 20 mm at the vicinity of outlet. Similar phenomenon has been noticed for the flow condition of M118. In such flow rates, the bubble size ranged from 0 to 40 mm which achieved almost four times its initial size range (Duan et al 2011). For these flow conditions with such widely ranged bubble size distribution, extremely abundant efforts are required by using traditional Class Method (CM). By using CM method, considerably amount size groups are necessarily classified to cover these wide bubble size ranges and consequently extensive transport equations are required to solve through extra computational calculation. However, as can be seen from these figures, the DQMOM model with only 4 moments gave reasonable prediction of the dynamical changes of bubble size distribution profile at different radial position with affordable computational effort. This can be considered as an alternative approach to solve population balance model within certain simulation cost. As a recently proposed simulation solution for population balance model, plenty of validation should be further carried on to overcome the limitation of the adopted coalescence and break-up kernels, which might be the reasons of some discrepancies between measurement and prediction found in Figure 6.5 (b) and (d).

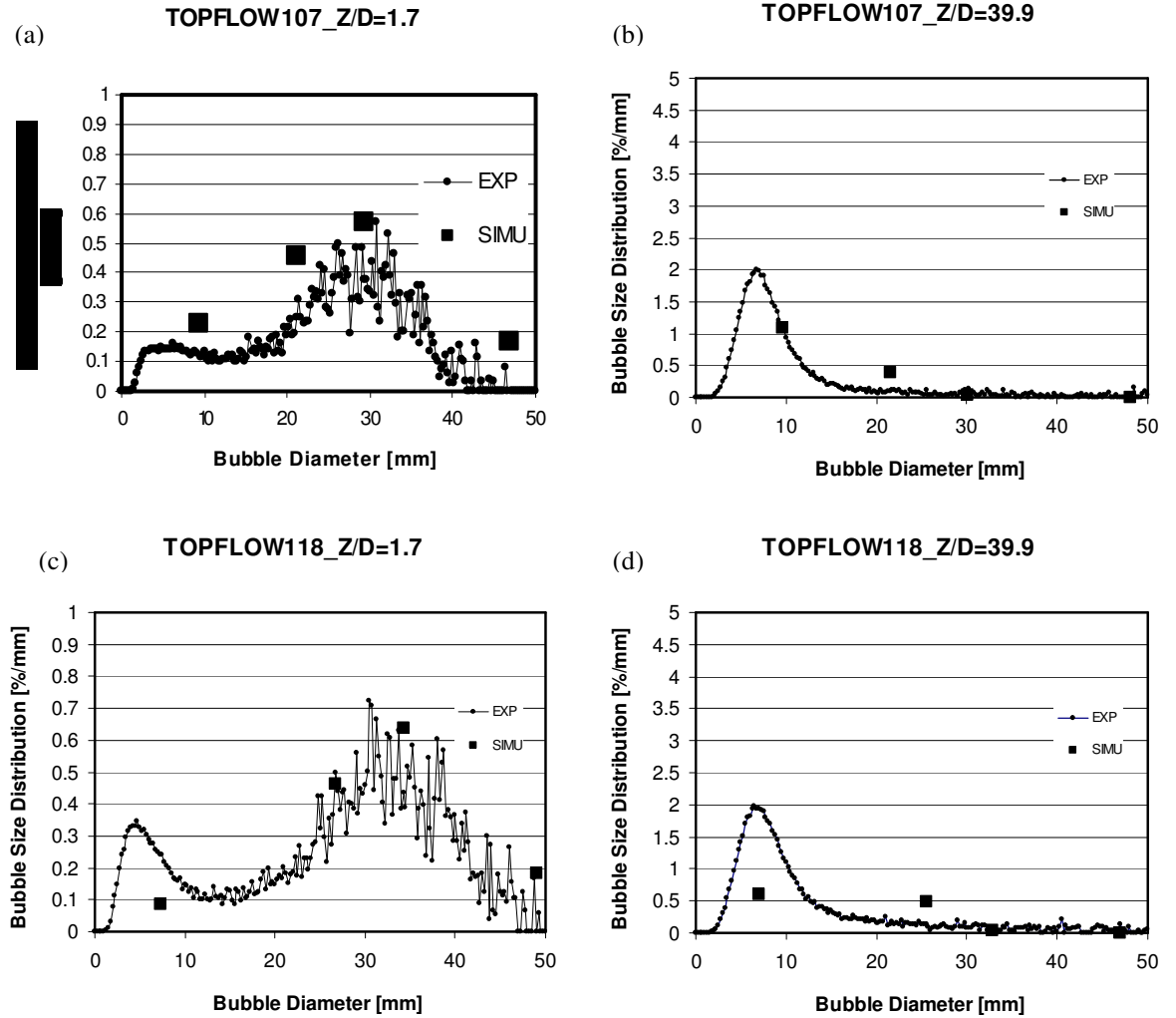


Figure 6-6 Predicted bubble size distribution and experiment data of TOPFLOW measured by Prasser et al (2007).

Figure 6.6 shows the predicted bubble size distribution by applying DQMOM model with $n=4$ and its comparison against TOPFLOW experimental measurements. As depicted in Figure 6.6 (a) and (c), the bimodal bubble size distributions are observed in experiments with wall injection system. Through the wall injection method, the injected small bubbles are highly concentrated in the vicinity of the wall to form the first peak (around 5mm) of bubble size distributions. Meanwhile, the closely packaged bubbles have a tendency to merge together and move towards to the centre of the pipe to form the second peak (around 30mm) of bubble size distribution. Under the dominant break-up flow mechanism, large distorted/cap bubbles break down to small bubbles to narrow the range of bubble size distribution with single-peaked shape. As demonstrated in

Figure 6.6, the DQMOM model with $n=4$ conservatively caught up the transformations of the bubble size distribution and considerably provided satisfactory performance in prediction in TOPFLOW. Generally speaking, it can be considerably suggested as an alternative approach to solve population balance model in simulation of bubbly flows because of its affordable computational cost as well as acceptable accuracy in prediction.

6.6 Conclusion

A two-fluid model coupled with DQMOM has been presented in this chapter to handle isothermal gas-liquid bubble flows. The evaluation of the source terms and the incorporation of an appropriate set of equations for the abscissas and weights were implemented with the CFD code ANSYS Inc., CFX-11 to determine the temporal and spatial geometrical changes of the gas bubbles. The assessment of the DQMOM model has been validated with the experimental data of Lucas et al. (2005) and Prasser et al. (2007) measured in Forschungszentrum Dresden-Rossendorf FZD facility. Because of different pipe sizes and gas injection systems between these experiments, opposite flow phenomenon were discovered. In the MTLOOP experiment with lab scale pipe size (Lucas et al., 2005), the bubble coalescence prevailed as the dominant feature while bubble break-up is the major characteristic in the TOPFLOW experiment with large pipe size for industrial application purpose (Prasser et al., 2007). Reasonably good agreement for the bubble void fraction and bubble size distribution was achieved between the DQMOM two-fluid model and measurements. Although the above encouraging results had already demonstrated the prospect of the DQMOM two-fluid model for bubbly flow applications, further validation or sensitivity studies are still required to assess the performance of DQMOM against a wider range of flow conditions.

Chapter 7 Experimental Setup and Digital Image Data Procession

The common question regarding CFD technology is how accurate the numerical model can describe practical flow phenomenon. In order to answer this question, the work of comparisons between numerical prediction and experimental measurement, referred as verification and validation, are necessary and important. The primary aim of this chapter is to introduce the experimental research of bubbly two-phase flow in current work. Firstly, the background information regarding main measurement approaches for local bubble size distribution has been introduced and particularly intensive interest has focused on the photograph research methods in the present study. Then the experimental setup has been described and its improvement with side-light illumination method with two flashes has been proposed by this study. After the attaining of the experimental image data, the research interesting has centered on the image process algorithm of abstracting useful mathematical distribution information from monotonous picture pixels with value of neither 1 nor 0 in finalized black and white testing pictures. After brief introduction of image process background, the Overlapped Object Recognition (OOR) method by finding joint points through convolution has been investigated in detection of bubbles in gas-liquid bubbly flow. This method was initially proposed by Ruan and Zhao (2005) to recognize the coal particles. Finally, the results of improvement by side-light illumination method with two flashes and image data analysis based on Overlapped Object Recognition (OOR) method are discussed and concluded at the end of this chapter.

7.1 Experimental Methods for Measuring Local Bubble Diameter Distributions

Computational fluid dynamics (CFD) is a very helpful research tool in the design of multi-phase flow reactors. However, the assessment of its prediction accuracy generally requires verification and validation against experimental data, which extensively

depends on measurement technology. On the other hand, the description and design of gas-liquid reactors is, to a large extent, still reliant on empirical rules and correlations, which in turn are based on measurements made under conditions as close as possible to industrial practice. In such scenarios, reasonable accurate measuring techniques are required in order to rationally describe and design multiphase reactors. Depending on the aim of the analysis, measurement techniques can be classified as different types. Distinguish between time-averaged and transient measurements and between local and global measurements are the generally applied types classification. According to this common classification, the following types of values or characteristics are measured in multiphase flow reactors (Boyer et al. 2002):

- Global steady-state characteristics of the reactor (gas or liquid void fraction, pressure drop, flow regime, minimum fluidization velocity, etc)
- Local time-averaged characteristics
- One-dimensional space: cross-section-averaged values at a given level of a reactor
- Two-dimensional space: local averaged values over a reactor cross-section (tomographic techniques)
- Three-dimensional space
- Local and transient characteristics of the flow field

With the aim of verifying and validating the population balance model in numerical research of gas-liquid two-phase flow, greater interest has been focused on measurements of local characters, such as interfacial area concentrations or bubble size distributions. As far as the author's knowledge, there are three major approaches for measuring the local interfacial area concentrations at this stage, namely conductivity sensor probe, wire-mesh sensor and photographic method.

The conductivity sensor probe by using conductivity probe method based on the fundamental difference in conductivity between the two phases has been one of the most widely used measurement techniques in obtaining local two-phase flow parameters. In case of a water-air two-phase flow, the water phase is slightly conducting, while the gas phase is practically an ideal insulator. The sensor probe proposed by Neal

and Bankoff (1963) was basically used as a phase identifier of the two-phase mixture. Currently, there exist two types of conductivity probes which are developed by Professor Ishii's group in Purdue University, America (namely the double-sensor conductivity probe and the four-sensor conductivity probe). And their experimental data of bubbly column by using this measurement technology have been widely utilized in verification and validation of the accuracy of CFD codes in gas-liquid two-phase flow field.

Recently, wire-mesh sensors were proposed by the Forschungszentrum Dresden-Rossendorf (FZD), Germany. Similar to the conductivity sensor probe, the wire-mesh is based on the same physical principle of conductivity difference between two fluids; however, as highlighted in Prasser et al. (1998), the wire-mesh sensors has advantages of testing areas instead of individual location points as well as attaining information simultaneously and can be considered as one of the most promising technology in future. Comparing with the sensor probe approach which only can investigate single spatial point, the wire mesh sensor can provide information of whole 2D area of cross-section at test locations at the same time. Similar advantages have been observed by many literatures. As reported by Manera et al. (2009), this method has the capability not only to provide smoother parameters distributions profiles due to numerous measuring locations but also to detect more accurate interfacial area density because of capturing actual bubble shape. And most importantly, there is no bubble missing since the wire-mesh sensor covers entire cross-section, thereby better statistical information and full mapping of the interfacial area density can be achieved. It is worthy to mention that a full 3D reconstruction of gas bubbles can be realized with the wire-mesh sensor with the recording information of a sound to recognize different bubble sizes. However, this wire-mesh sensor technology has a limitation of observation of bubble shapes since the mesh destroy the bubbles.

The direct photographic technique is a useful visualization measuring methods which also maintain the advantage of wire-mesh sensor measurement with fewer disturbances. Nevertheless, there are still many challenges to apply this method even till current stage, including limitation of observed bubbles only at the vicinity of the wall at high gassing rates and specified requirements of a transparent wall and a transparent liquid. At current stage, bubble size distributions are most commonly measured using Doppler

Anemometry (PDA), Interferometer Particle Imaging (IPI), and Capillary Suction Probe (CSP) or Direct Imaging (DI) techniques. When the first two techniques have been performed under flow investigations of bubbly flow with less and smaller dispersed objects, these two methods have reasonable high prediction accuracy. But the accuracy of prediction decreases with the increment of bubble number in flow. The CSP technique only can measure a relatively small dynamic range of bubble size and its performance is sensitive to flow conditions at the probe inlet. The DI technique which is utilized in current experimental study is the direct method to get original information of bubbly flow characteristics.

7.2 Experimental Setup and its Improvement by using Side-light illumination method with two flashes

7.2.1 Experimental Setup Details

An experimental facility was designed to measure the relevant two-phase parameters necessary for developing constitutive models for the two-fluid model in isothermal vertical bubbly flow. The two-phase flow experiment was performed by using a flow loop construction at the Process Science and Engineering Division, Commonwealth Scientific and Industrial Research Organization (CSIRO). Figure 7-1 shows the experimental facility layout. The water supply was held in the holding tank which was opened to the atmosphere through a separator tank. Water was pumped with a positive displacement, eccentric screw pump, capable of providing a constant head with minimum pressure oscillation. For the isothermal air-water flow experiment, porous spargers with the pore size of 10 μ m were used as air injection. The water, which flows through a magnetic flow meter, was divided into four separate flows and can then be mixed with air before it was injected into the test section to study isothermal air-water bubbly flow. The test section was a tube geometry that is formed by a clear polycarbonate tube with 2670mm length and 38.1mm inner diameter. A square transparent image box with 50mm*50mm*80mm has been located at the test point which is 2 m far from the injection. In order to compensate the refraction of light through tube, glue water was filled into the space between the image box and tube.

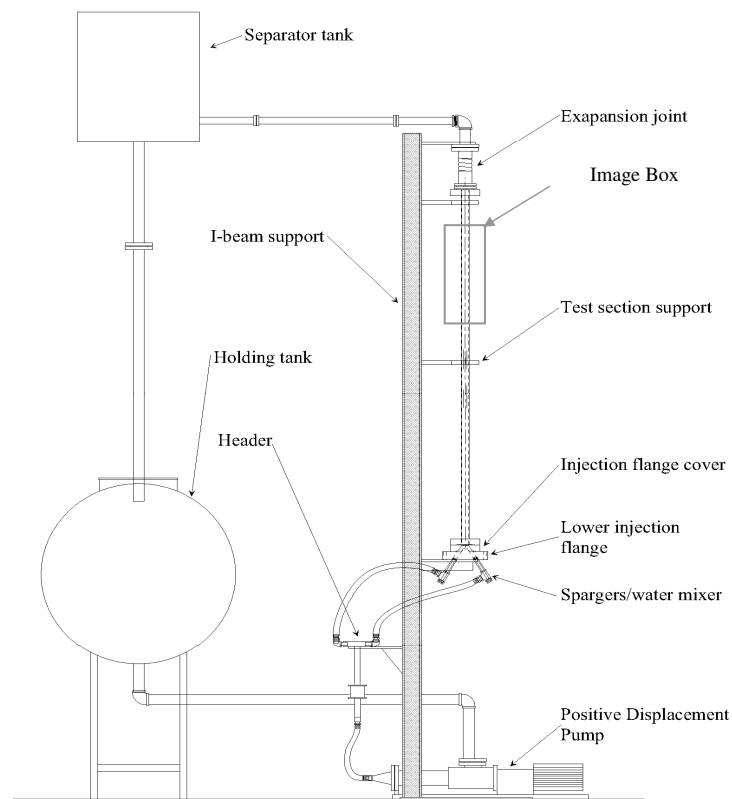


Figure 7-1 Schematic drawing of experimental setup

7.2.2 Experimental Setup Improvement

7.2.2.1 Back-light illumination Configuration

To some extent, the illumination method for target plays a critical role in obtaining information in multi-phase flow experiment within application of the Direct Imaging (DI) techniques. The method of back-light configuration can be considered as one of the most widely utilized illumination approaches in visualization of multiphase flow because of its maximization of the light entering into the lenses of camera. As illustrated in Figure 7-2 (a), a flash was located at the back of the bubble column whereas the camera was positioned at the front of the bubble column; thereby nearly whole energy of light fully

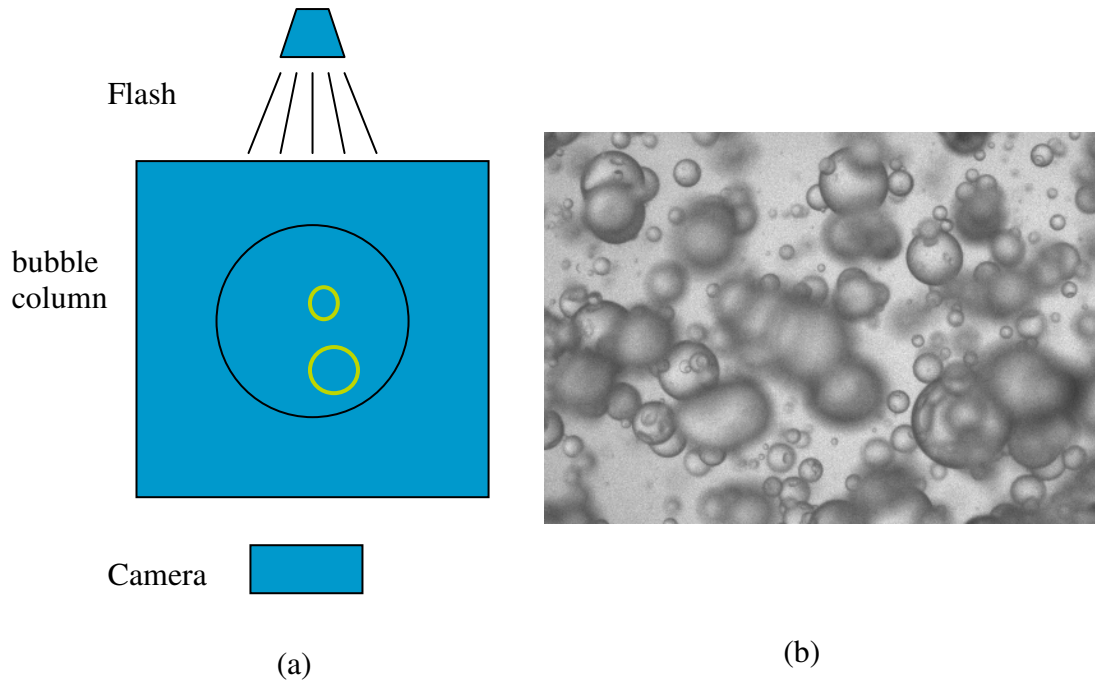


Figure 7-2 Schematic drawing of back-light illumination method

sweep entire cross-section of pipe and finally reached the lenses of camera. Through this arrangement, the energy of light has been maximally utilized to illuminate objects; however overlapped bubbles images are unexpected observed by using this method as shown in Figure 7-2 (b) since the light sweeps each individual bubbles in cross-section. The massive overlapped objects images decrease the possibility of edge identification of each single bubble and consequently increase the difficulties to obtain the identical information such as bubbles locations and diameters. With the purpose of diminishing or at least reducing the percentage of overlapped bubbles in the obtained experimental pictures, the side-light illustration method with only one flash was investigated and reported in some literatures of experimental visualization of two-phase flow.

7.2.2.2 Side-light illumination with one flash Configuration

The original idea behind the side-light illumination method is only making the necessary bubbles bright instead of all bubbles in entire tube by lighting only the axial plane sheet through a window on the side of image box. In such case, only the bubbles in the axial plane sheet are illuminated. In this method, the illuminant light was not

travel straight from the illumination source towards to the lenses; however the diffusible light from bubbles is strong enough to be recorded by the camera. In order to organize the light which is expected to enter cross-section, the image box was covered by black papers only leaving 2mm gap on the left side wall of bubble column as an lighting window which is demonstrated in Figure 7-3 (a). The diffusible light of bubbles entered the lenses of camera through a square uncovered window with 50*80 on the front wall on image box. The results by using side-light configuration are demonstrated Figure 7-3 (b). Comparing Figure 7-3 (b) with the Figure 7-2 (b), some differences and improvements are easily observed. Firstly the background of side-light illumination method is black while the background of back-light illumination method is white. It can be simply explained that in side-light illumination method with covered image box there was no light from the back of image box; however in back-light method the light source located at the back of image box. Additionally, the reducing of the bubble numbers was observed in side-light illumination method as shown in Figure 7-3 (b). In the Figure 7-3 (b), the brightened and recorded bubbles were no longer densely packaged with each other since only few bubbles in axial plane of tube were illuminated; therefore, the chance of bubble overlapping is significantly decreased.

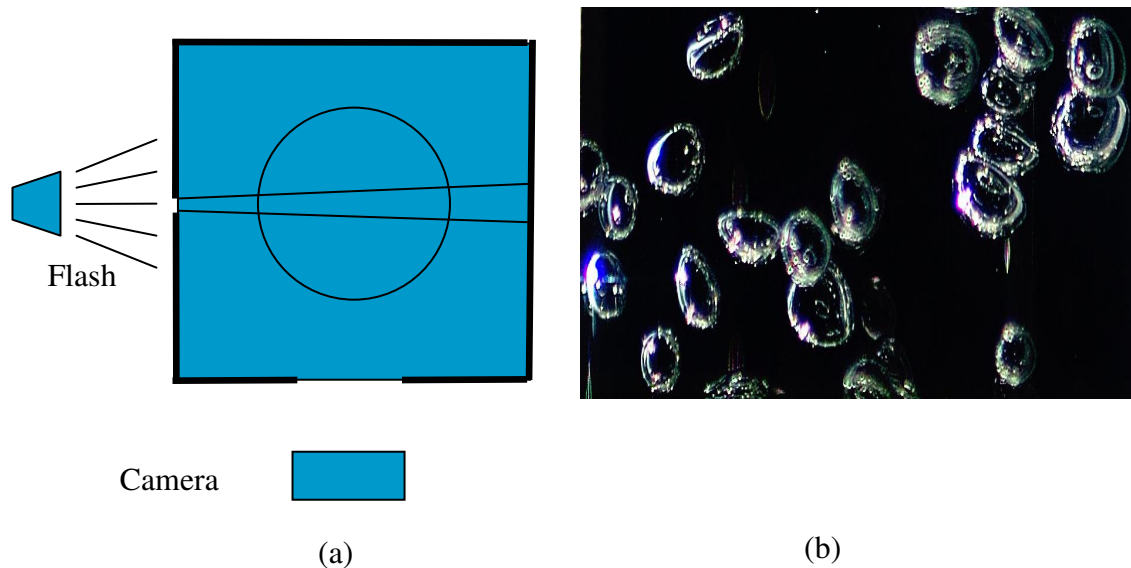


Figure 7-3 Side illumination methods with one flash

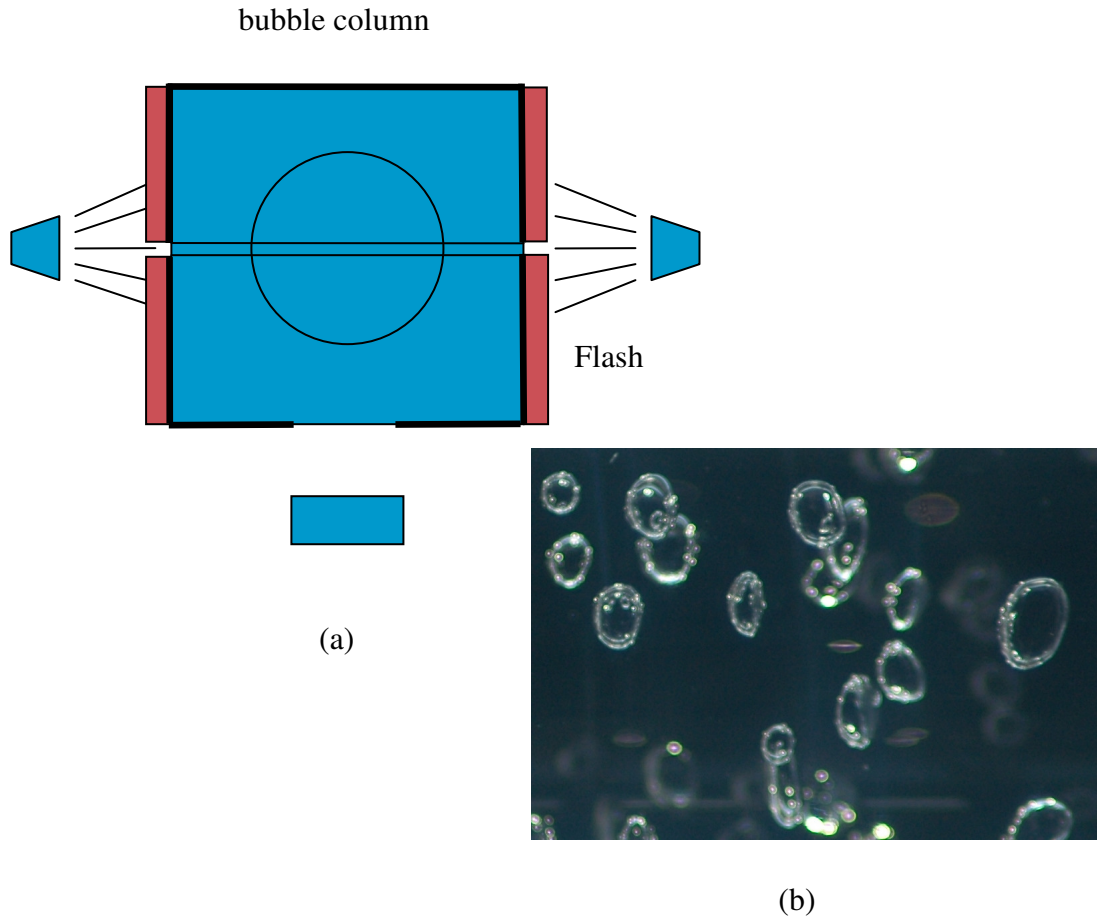


Figure 7-4 Side illumination methods with two flashes

Nevertheless, some limitations have been observed by using side-light illumination method with single flash. As can be seen in Figure 7-3, the intensities of bubble edges were unbalanced with stronger brightness on the left side than the right side of bubble edges. This unbalance of light intensities is caused by the only single flash has been located and utilized on the left side of bubble column. In additional, the diffusion of the flash lights causes unequal thickness of light sheet, as shown in Figure 7-3 (a). The diffusion of light diffusion led to over-measured bubble numbers on the left side of bubble column from the top view due to such unexpectedly over involved lighted volume. In order to overcome this shortage, the side-light illumination method with two flashes was proposed by the current research.

7.2.2.3 *Side-light illumination with two flashes Configuration*

The experimental illumination method of side-light with two flashes was proposed in this visualization measurement study of two-phase flow. As demonstrated in Figure 7-4 (a), two flashes with same bright energy have been posited at each side of the bubble column, thereby the each side of bubbles was equally accepted similar light intensities. With the purpose of reducing light diffusion, four wood blocks with a thickness of 3 mm were installed by the side of the 2 mm gap windows as shown in Figure 7-4 (a). As a result, only the light of straight direction from flash has possibility to go into the bubble column while the light of other direction were filtered by such arranged blocks. The improved image results were shown in Figure 7-4 (b) by applying side-light illumination method with two flashes. Comparing with Figure 7-3 (b), the intensities of bubble edge were equally distributed in Figure 7-4 (b), which greatly reduced the difficulty degrees for abstracting mathematical information of bubble size distribution in next stage of image procession. Furthermore, the reduction of light diffusion helpfully increases the accuracy of measurement results.

7.3 Image Procession

In order to automatically batch process the transformation of experimental images information to capably utilized mathematical distribution data through computer characteristic ability, a computational image procession technique is required. Following the significant development of computer power, the image procession technique has been extensively manufactured by various physical devices, including video camera, x-ray devices, electron microscopes, radar and ultrasound and manipulated for a variety of purposes, such as entertainment, security, business (e.g. documents), military (e.g. target identification), civil (e.g. traffic) and medical.

Generally speaking, the original images taken from such physical devices could not straightforward suit the scientific or industrial purpose and extra efforts are required for information transformation from plane images to mathematical numbers. These extra efforts which commonly referred as image analysis and procession are challenging jobs since there are numerously involved difficulties and struggles amid computational

singulars recognition of only 0 or 1 (black or white) and realistic multi-degree gray existing between black and white.

Commonly, a digital image is made up of pixels (array of small elements in a two-dimensional grid) that can store information such as signal position and intensity in a digital memory (MediaCybernetics, image-Pro Plus 7.0, User Manual). As demonstrated in Figure 7-5 (a), the pixels location start to mark from the first top left one as the pixel 0.0, then the others will be marked consequently

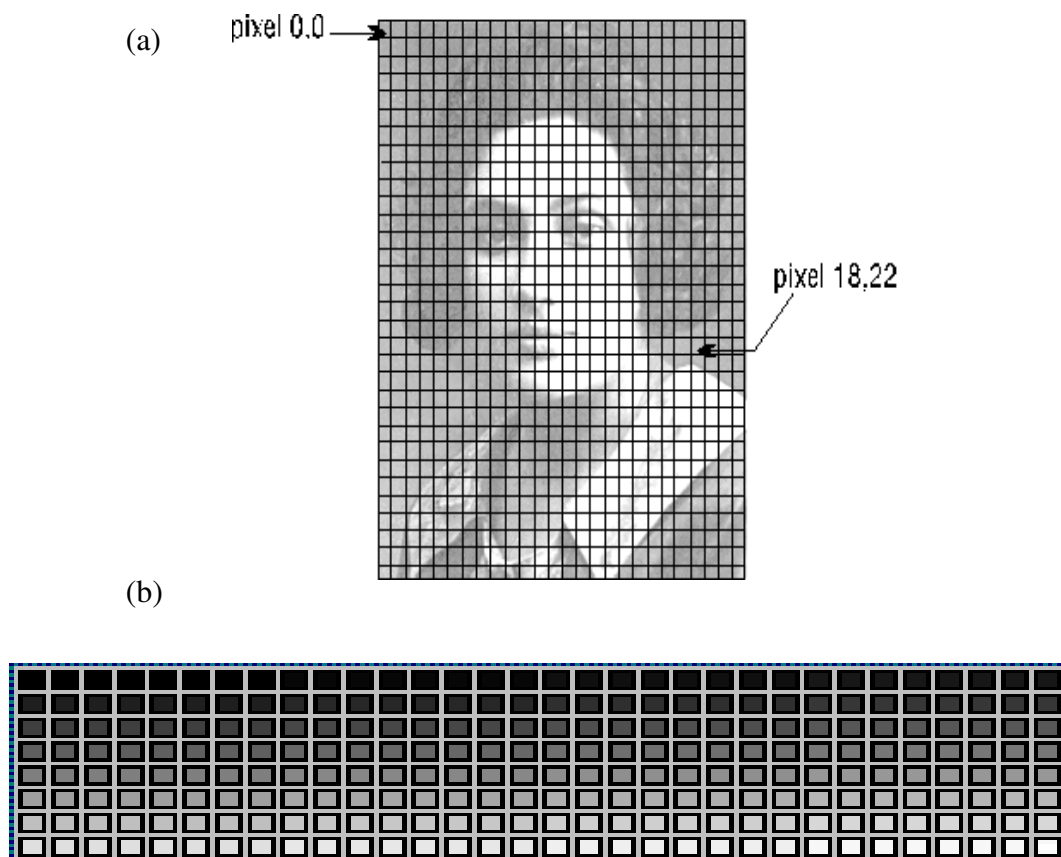


Figure 7-5 Pixel definition (MediaCybernetics, image-Pro Plus 7.0, User Manual)

in this two-dimensional digital image grid. Except the location information, each pixel also represents the ‘brightness’ or signal intensity. In an 8-bit gray-scale image, the range of intensity is from 0 to 255 value, such that they represent the colors black to white in their extreme ends. The figure 7-5 (b) shows the intensity value range from 0 (black) to 255 (white) in an 8-bit gray-scale image.

In the image analysis and procession of two-phase flows pictures where bubbles are densely packaged with each other, the image profiles are consisted by multi segments from different and overlapped bubbles in stead of typical ellipse shape representing individual bubble. If a common grey-scale thresholding method (Chigier, 1991) is applied, such profiles would be mistakenly detected as only a single big irregular shape object without recognition of its consisting of multi segments from different bubbles. Thereby, to large extension errors occur in identification the distributions of diameters, interfacial area concentrations and velocities of studied objects. The aim of this study is to present algorithms which have capabilities to distinguish individual in-focus bubbles from image sequences of rather dense multiphase suspensions, where the bubbles are densely overlapping in the image.

7.3.1 Literature review of identification algorithms of overlapped objects

The arcs identification and segmentation are the task of recognizing and classifying elements of a curve consisted of multi-sections according to some criteria. Seeking solutions concerning these problems is continuously research interesting in the fields of image process, pattern recognition and computer vision for decades (Shen et al. 2000). Nevertheless, as pointed out in the literature of Melen and Ozanian (1993), there is no unique one which can be considered the best algorithm suitable for all cases since the completion of task is decided by the purpose of the segmentation, characteristics of objects as well as the qualities of images.

In earlier stage, the number of round objects in an image was limited and their sizes were almost the same. After image procession of thresholding/binarzing, the edges of research targets were detected by some conventional approaches, such as Hough Transformation. Similar reports can be found in literature of Duda and Hart (1972), Kierkegaard (1992) and Pei and Horning (1995). However, such conventional approaches possibly could not to be considered as efficient algorithms to segment densely overlapped objects and to be expected to provide satisfactory results. The procession results of Hough Transformation on images of fully packed bubbles in current experimental studies are shown Figure 7-6. As can be seen from the Figure 7-6

(b), Hough Transformation only abstracted irregular shape profiles of bubble groups instead of identifying individual ellipse shape bubbles. Additional, as reported by Shen et al. (2000), a number of points which had to be accumulated in the parameter space in order to construct peaks and well-defined peaks are often hard to obtain when applying Hough Transformation method. Furthermore, Yuen and Feng (1996) also pointed out that the Hough Transformation suffered from the storage problem. Such lack of these capabilities reduces the possibility of applying Hough Transformation method on images with overlapped objects in order to achieve reasonable results of identification and segmentation.

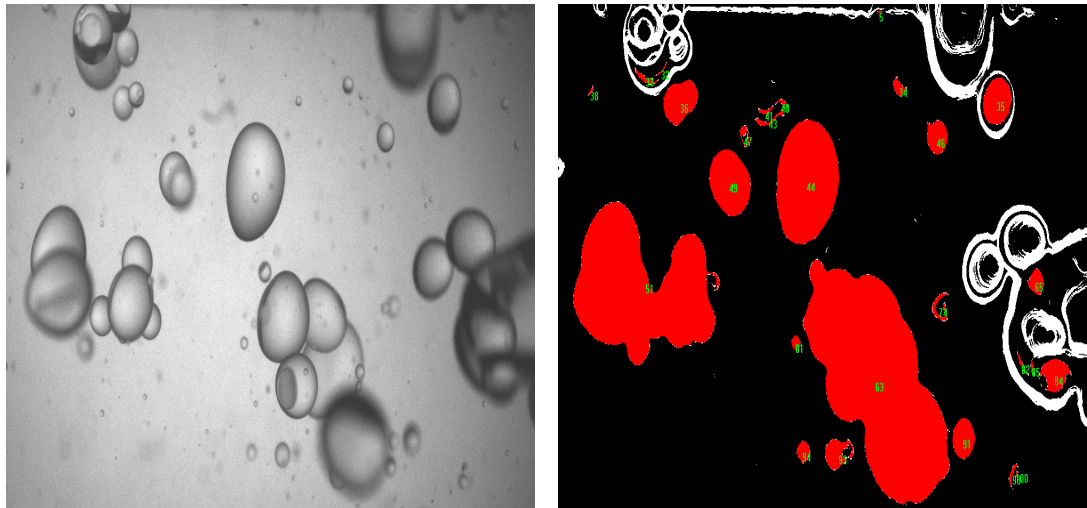


Figure 7-6 Results of Hough Transform: Hough Transform could not identify individual bubble from its group

Besides conventional approaches, another method, referred as iterative method, has been frequently reported in numerous literatures, such as Sakaue (1982), Dakaue and Takagi (1983), and Rosin and West (1995). The advantages of iterative method include non-parametric, invariant to transformations, simple and generic; however, too many sub-divided segments cost more computational efforts due to the increased difficulty degrees of clustering elements of same group at later stage (Shen et al. 2000).

The image procession method by detection of joint point (connection points of different arcs segments on a curve) is recently mentioned by many scientists. As reported by Lim et al. (1995) and Pla (1996), most of joint point detection methods are under the principle of identification of curvature extreme. But most of these methods have the disadvantages of sensitivity to background noise and of dependence on parameters that are chosen empirically (Shen et al. 2000). In digital images, the contours of objects are consisted by pixels; thereby the contours of round objects are not smooth and continuous curve but separated and individual dots. Consequently, it is almost impossible to accurately calculate the curvature of a curve. In order to calculate the approximate curvature, a curve smooth procession is requested initially before the calculation of the curvature. Unfortunately, to large extension the joint points on the curve would become blunt on curve and difficult to detect in next stage.

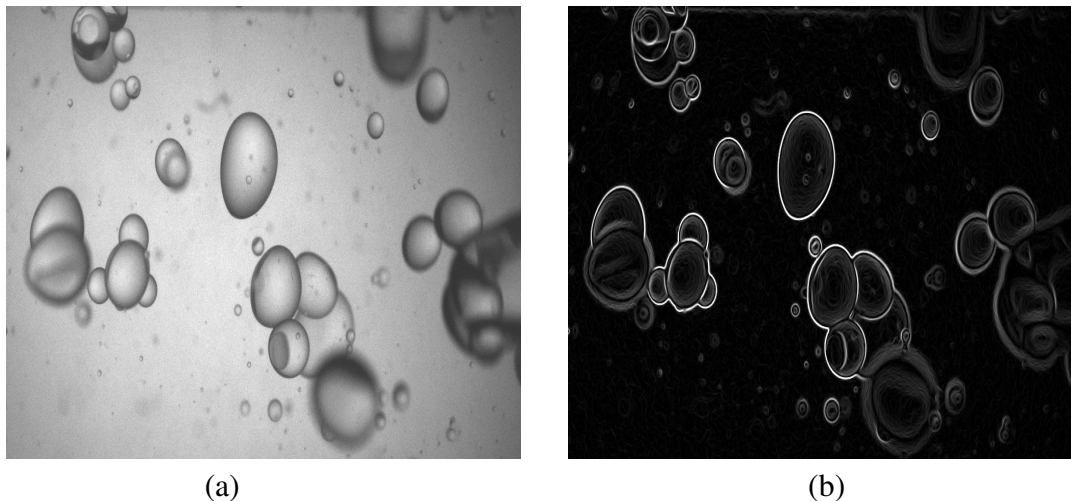


Figure 7-7 image procession result of the Canny edge detection

In the current study, a effective image procession method propose by Ruan and Zhao (2005) to recognize overlapped coals has been assessed in identify overlapped bubbles in two-phase flow. The overlapped Object Recognition (OOR) method includes the following five process processes:

- recognizing the edge of overlapped bubbles
- threshold
- finding the joint point
- tracing circular arcs segments from joint point

- grouping the arcs of the same circle

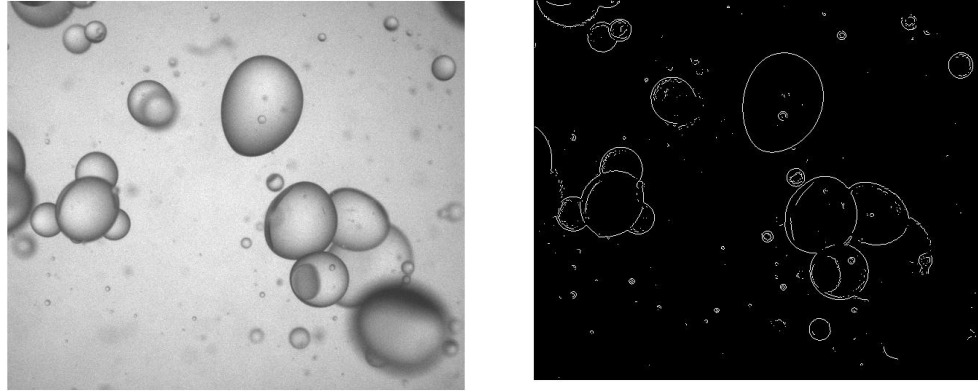


Figure 7-8 Results of threshold

Firstly, the Canny's edge detection method (Canny, 1986) and threshold were adopted to detect the contours of overlapped bubbles, as shown in Figure 7-7 and Figure 7-8. The current study focuses on the third process step of detection of joint points. With this purpose, this method utilized a method of matrix convolution instead of searching approximation of curvature of a curve. After the joint point has been detected, an image process algorithm has been conducted to trace the circular arcs from the joint point. Finally, the area correlation algorithm is utilized to group the circular arcs which belong to the same bubble.

7.3.2 Overlapped Object Recognition (OOR) Method

7.3.2.1 *Edge Detection*

Edge detection has been research topics for decades. Feature detection (e.g. face critical) and feature extraction (e.g. pattern analysis) are some examples of this typical applications in this field. It is an image process algorithms aimed at capturing important events and changes in a digital image at locations whereby the image brightness undergoes sharp changes or even more formally discontinuities (MediaCybernetics, image-Pro Plus 7.0, User Manual). Edge detection is not always possibly fortunate to

obtain such perfect edges from practical life images since the edge detection algorithm is to large extension dependent on the quality of an image. Poor edge detection may causes serious issues such as missing edge segments, false edges as well as discontinuity of edges.

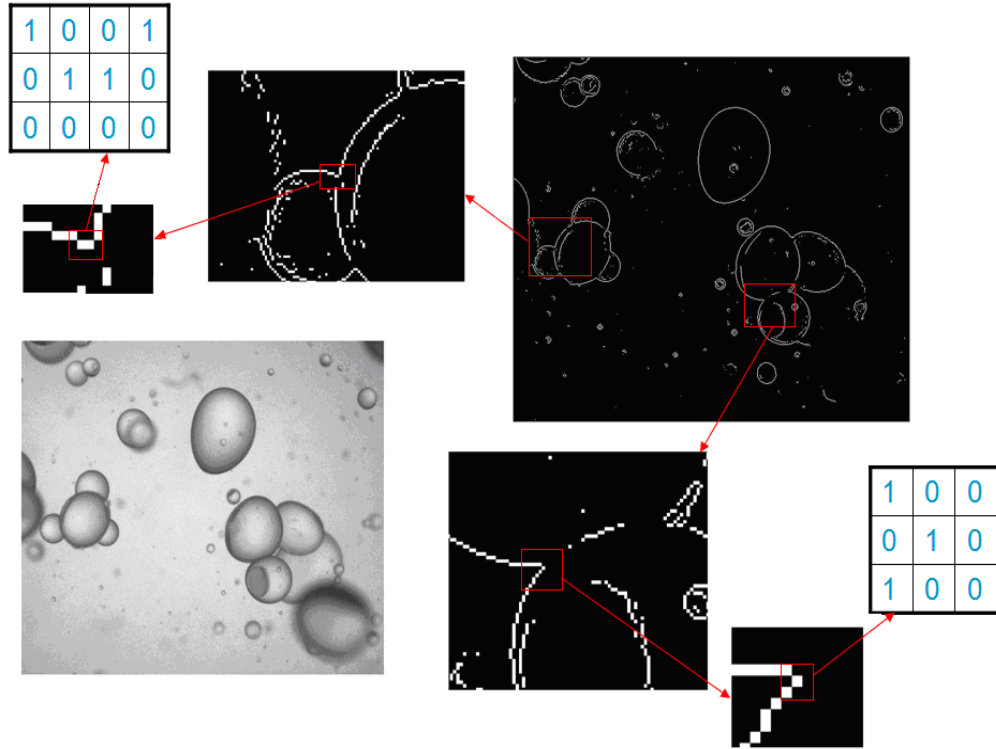


Figure 7-9 Connections between “black” and “white” in binary image and local pixel values of “1” or “0” in its magnified local position.

Since the edge detectors have been an essential part of many computational image processes, numerous research investigations have been carried on in this area to exploit the best method to segment contours of objects. Among them, the Canny edge detection operator can be considered as the most widely used one in commercial software. The Canny edge detection operator developed by John F. Canny in 1986 applies a multi-stage algorithm to detect a wide range of edges in images. The principle of edge detection is exploiting the spatial position where sharply changes of image intensity occur. Thereby mathematically these points can be capturing as a local maximum of the first derivative of the image intensity I with respect to the perpendicular direction \vec{n} , or

as zero of the second derivation of I with respect to \vec{n} . In most of situations, the image intensity is not always continuously distributed and consequently filters or convolution matrixes are initially required to remove the background noises and smooth the intensity distribution (Ruan and Zhao 2005). Canny edge detection utilizing Gaussian G as a filter can be expressed as

$$\frac{\partial^2}{\partial \vec{n}^2} (G * I) = 0 \quad (7.1)$$

Where the two-dimensional Gaussian G filter is defined as

$$G = \exp\left(-\frac{x^2 + y^2}{2\delta^2}\right) \quad (7.2)$$

Where x and y are the coordinates of pixel to be processed, and δ is the standard deviation of the coordinates in a considered domain. Usually δ is selected as 1 or 2.

The perpendicular direction of an edge, \vec{n} known a priori can be decided by

$$\vec{n} = \frac{\nabla(G * I)}{|\nabla(G * I)|} \quad (7.3)$$

7.3.2.2 Threshold

The threshold refers to algorithms which aimed at simply identifying the “object” and “background” by converting other scale images (e.g. gray scale image) to binary images. During the threshold procession, every pixel value of the image is re-set to an extreme where it is greater or smaller than a critical value. After conversation, the extreme new pixel values would represent the interested objects (typically set as binary “1”) or the background region (set as binary “0”) depending on their definition. In general, the binary image outcome is perceived as black and white and may be used for further processing depending on the nature of the image analysis. Figure 7-8 demonstrates the image procession of threshold.

7.3.2.3 Detection of Joint Point

After edge detection and thresholding, the gray scale image becomes to a binary image with pixel value either “1” (it means completely white) or “0” (it means absolutely

black). Figure 7-9 illustrates connections between “black” and “white” in binary image and local pixel values of “1” or “0” in its magnified local position. From Figure 7-9, it can be seen that boundary segmentation is made up of a series of curves which contain more than two arcs. In order to identify the boundary of overlapped individual bubbles and sequentially obtain mathematical information of bubbles size and their distributions, separation these connected arcs in a curve is required and grouping them belonging to same bubble is possibly needed as well in later stage depending on the purpose. Thereby, how to locate the joint points or connection points among these arcs becomes to the initial and critical question.

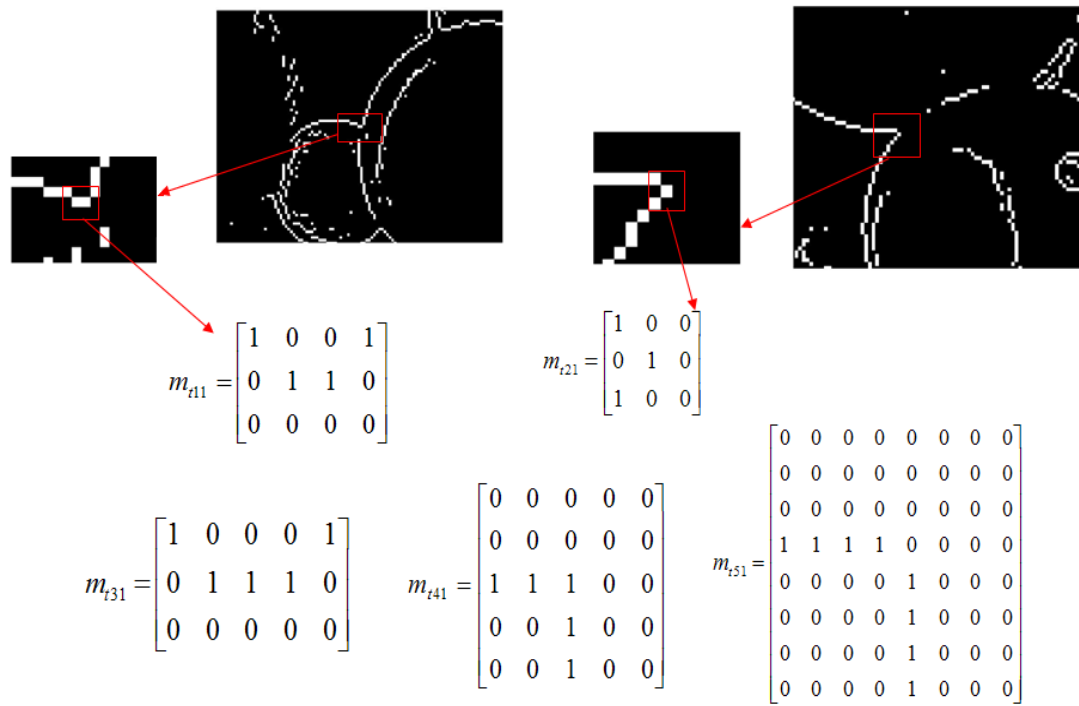


Figure 7-10 The distributions of local pixels values can be represented as these five types of matrixes and their symmetrical matrixes

Through the observations and investigations of pixel value map of these processed binary images, it was discovered that the joint point can be characterized as 5 types of matrixes and their symmetrical matrixes. As some examples illustrated in Figure 7-10, the distributions of local pixels values can be represented as these five types of matrixes and their symmetrical matrixes. These five types of matrixes can be concluded as follow:

$$\begin{aligned}
m_{t11} &= \begin{bmatrix} 0 & 0 & 0 & 0 \\ 0 & 1 & 1 & 0 \\ 1 & 0 & 0 & 1 \end{bmatrix} \quad m_{t21} = \begin{bmatrix} 0 & 0 & 0 \\ 0 & 1 & 0 \\ 1 & 0 & 1 \end{bmatrix} \quad m_{t31} = \begin{bmatrix} 1 & 0 & 0 & 0 & 1 \\ 0 & 1 & 1 & 1 & 0 \\ 0 & 0 & 0 & 0 & 0 \end{bmatrix} \\
m_{t41} &= \begin{bmatrix} 0 & 0 & 0 & 0 & 0 \\ 0 & 0 & 0 & 0 & 0 \\ 1 & 1 & 1 & 0 & 0 \\ 0 & 0 & 1 & 0 & 0 \\ 0 & 0 & 1 & 0 & 0 \end{bmatrix} \quad m_{t51} = \begin{bmatrix} 0 & 0 & 0 & 0 & 0 & 0 & 0 & 0 \\ 0 & 0 & 0 & 0 & 0 & 0 & 0 & 0 \\ 0 & 0 & 0 & 0 & 0 & 0 & 0 & 0 \\ 1 & 1 & 1 & 1 & 0 & 0 & 0 & 0 \\ 0 & 0 & 0 & 0 & 1 & 0 & 0 & 0 \\ 0 & 0 & 0 & 0 & 1 & 0 & 0 & 0 \\ 0 & 0 & 0 & 0 & 1 & 0 & 0 & 0 \\ 0 & 0 & 0 & 0 & 1 & 0 & 0 & 0 \end{bmatrix}
\end{aligned}$$

Each matrix has its other three symmetrical matrixes. Take matrix m_{t41} for example, it has three symmetrical matrixes.

$$\begin{aligned}
m_{t42} &= \begin{bmatrix} 0 & 0 & 1 & 0 & 0 \\ 0 & 0 & 1 & 0 & 0 \\ 0 & 0 & 1 & 1 & 1 \\ 0 & 0 & 0 & 0 & 0 \\ 0 & 0 & 0 & 0 & 0 \end{bmatrix} \quad m_{t43} = \begin{bmatrix} 0 & 0 & 0 & 0 & 0 \\ 0 & 0 & 0 & 0 & 0 \\ 0 & 0 & 1 & 1 & 1 \\ 0 & 0 & 1 & 0 & 0 \\ 0 & 0 & 1 & 0 & 0 \end{bmatrix} \quad m_{t44} = \begin{bmatrix} 0 & 0 & 1 & 0 & 0 \\ 0 & 0 & 1 & 0 & 0 \\ 1 & 1 & 1 & 0 & 0 \\ 0 & 0 & 0 & 0 & 0 \\ 0 & 0 & 0 & 0 & 0 \end{bmatrix}
\end{aligned}$$

In this current study, convolution between the namely matrixes pairs has been applied to detect the joint points in binary images. The matrixes pairs refer as a matrix and its coordinately symmetrical matrix, which are normally called as original matrix and testing matrix. The roles of original matrix and testing matrix can be exchanged depending on detecting purpose. Take the m_{t4} for example, the m_{t41} and m_{t42} , m_{t43} and m_{t44} are matrix pairs, respectively. And the m_{t41} can be the test matrix of m_{t42} , while the m_{t42} is also the test matrix of m_{t41} depending on the situations.

Name the binary image matrix as I , and its size is $M \times N$. It is worthy to be reminded that the matrix I is consisted by random distributions of these five types' matrixes and their symmetrical matrixes. In order to detect the joint points represented in a matrix e.g. m_{t41} , the testing matrix of J (e.g. m_{t42}) with the size of $m \times n (5 \times 5)$ is utilized. Within the convolution between I and J , a new matrix of K is created with the size

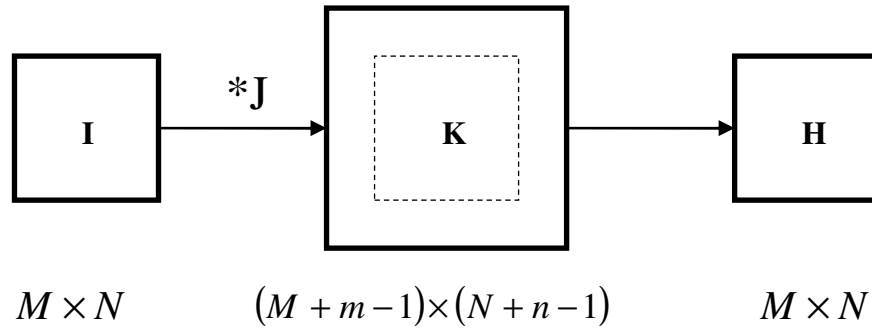


Figure 7-11. Implementation of matrix convolution

of $(M + m - 1) \times (N + n - 1)$. After cutting the extra pixel of image edges, where the pixel value is “0”, the matrix H with the same size of original matrix I has been obtained, as shown in Figure 7-11. Then the resulted new matrix H was ready to be searched for the maximum pixel value wherein the locations represent the joint points of connected arcs in curves.

7.3.2.4 Tracing the Boundaries

Even though the locations of the joint points have been detected, the identification of object boundary required more information to calculate the radius and centre location (X_c, Y_c) . The boundary trace algorithm has been used to find the location (X, Y) of each pixel which possibly belongs to the same bubble. The principle of boundary trace algorithm is searching nearby pixel, whose value is “1” from joint point, then looking for the next neighbor pixel with value “1” from the new pixel, and continuously repeating the same process till certain steps set up experientially. Since the initial search direction for the next pixel is unknown, possible 8 initial directions have been exploited. The Figure 7-12 demonstrates all the possible initial search directions. In order to maximize the accuracy of the calculation of radius and centre location, it is important to search as many points belonging to the same bubble as possible. On other hand, this

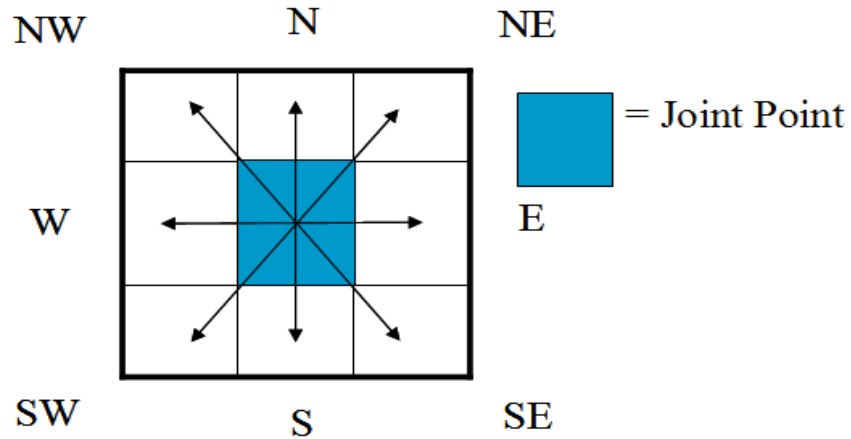


Figure 7-12 image procession of tracking form the joint point towards 8 directions

algorithm might provide fake information by mistakenly track random background noises when the only certain points are caught up. Thereby an experiential criterion of searching steps is needed to set up to classify the random background noises and real bubble edge pixels. In this current research, the experiential value of 20 has been set up as a filtering criterion. In other words, if the 20 connected points have been traced, these pixels are considered as presentation of bubble edges which is ready to be use for next grouping process; otherwise, the traced points are regarded as background noise in the image. After obtaining as many as possible information of pixel locations on the bubble edges, the radius and the center of the circle can be decided by locations of any three pixels on the circle edge as demonstrated in Figure 7-13.

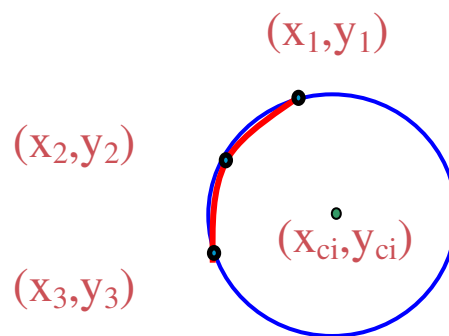


Figure 7-13 image procession of tracking form the joint point towards 8 directions

7.3.2.5 Clustering Algorithms

After the bubble radius and circle center have been calculated by using information of any three pixels, it is worth to be noticed that plenty of circles from any combinations of three pixels possibly represent the same single bubble in practice. Thereby the clustering algorithm is required to simplify the over-predicted data. Within this clustering algorithm applied in current study, initially each circle is considered to be with its own individual group. An iterative procedure is performed, and then two circles are compared and decided if they represent the same bubble or not depending on their distance function which defined as follow is small enough or not. The iteration is carried out until the all circles are completely compared. Here the distance function D is defined as

$$(D_{ij} = \sqrt{(x_{ci} - x_{cj})^2 + (y_{ci} - y_{cj})^2} \leq \varepsilon_c) \wedge (|R_i - R_j| \leq \varepsilon_r) \quad (7.4)$$

Where x_c and y_c are the coordinates of the circle centre of the i -th arc, R is the radius, ε_c and ε_r are the selected tolerances, the indexes i, j are the coordinates of pixels in x and y directions, respectively. In the present research, we selected ε_c as 2-pixels and ε_r as 1-pixel.

7.4 Discussion and Conclusion

With the purpose of reducing the overlapped chance of bubbles in experimental images, a side-light illumination method with two flashes was improved in this study. And an efficient image analysis method called Overlapped Object Recognition (OOR) method was assessed in process pictures of bubbly flow.

7.4.1 Illumination methods with two side flashes

The Figure 7-14 illustrated the comparisons between these three illumination methods in bubbly two-phase flow experiments. As shown in Figure 7-14 (a), bubbles are closely

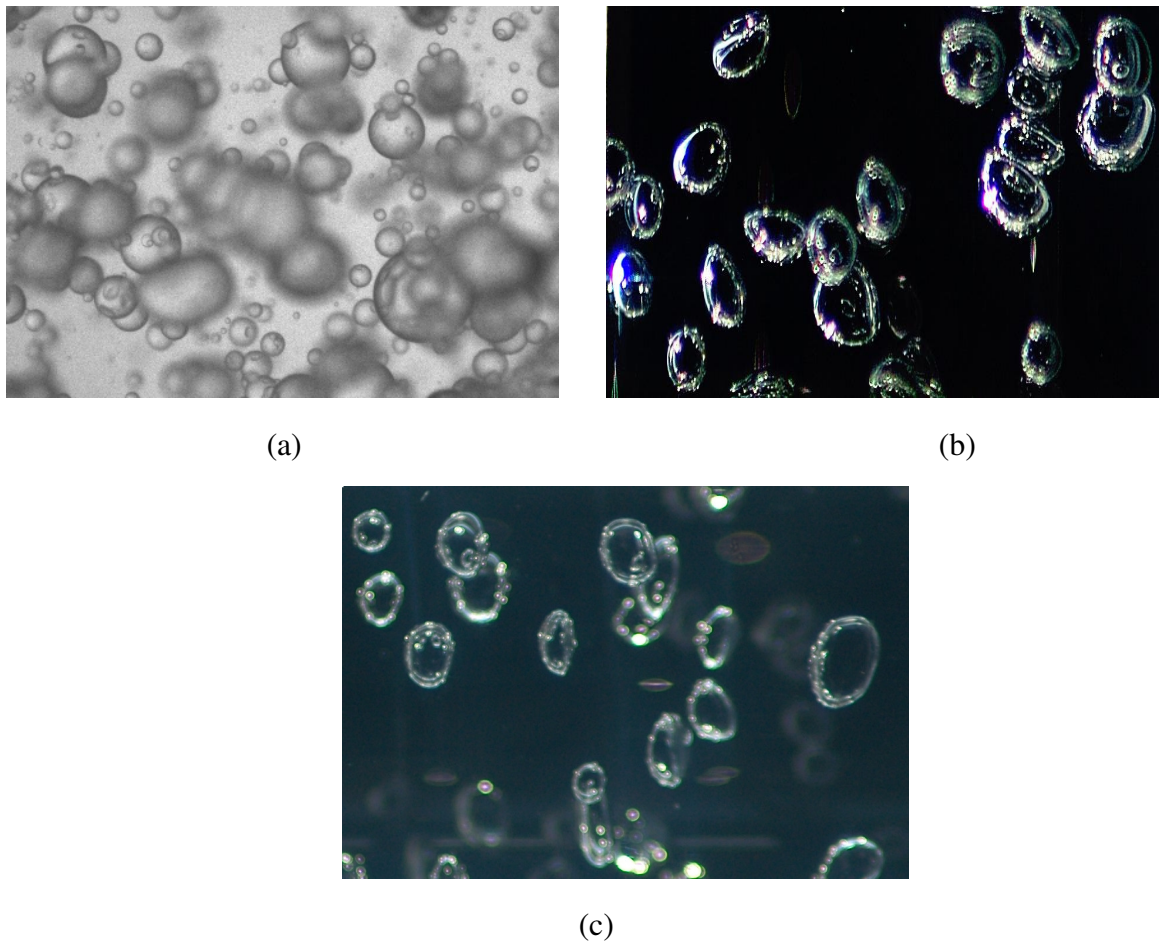


Figure 7-14 the comparison between difference illumination methods: (a) back-light illumination method; (b) Side-light illumination method with one flash; (c) Side-light illumination method with two flashes

packaged with each other and highly overlapped since the flash lights located at the back of bubble column by which the lights come across whole bubble column from back to front and illuminated every individual bubble. The objects recognition algorithm of images with such highly overlapped bubbles involving complex Edge detection, massive background noise threshold, numerous algorithm transformation and difficult individual bubble identification makes it almost impossible to abstract mathematical information of bubbles sizes and their distributions. Moreover, the most of research interests are only focus on the bubble mechanisms from inlet to outlet on axial plane. In order to only illuminate the axial plane, a side-light illumination method was reported

by literature and tested in current study. The results are shown in Figure 7-14 (b). However, only one flash was initially proposed by literature in this method. Through assessment in this current study, there were some shortcomings came to be author's notice. As can be seen from the Figure 7-14 (b), the brightness intensity did not equally distributed along the bubble edges leaving the left side of bubbles is brighter than the right side since the flash was located on the left side of bubble column. Consequently, it led to wide range of pixel values; thereby it increased the difficulties of classify the background noises and bubble edge pixels and possibly some of pixels with low intensity value can be mistakenly filter out as background noises in algorithm transformation. With the purpose of balance the intensity values around the bubble edges, the side-light illumination method with two flashes is proposed in current work. The test results are shown in Figure 7-14 (c). As can be see in Figure 7-14 (c), this new method efficiently reduced bubble overlapped chance by illumination only axial plane comparing with Figure 7-14 (a) with background illumination method. Furthermore, this method also controlled the intensity of bubbles edges varying a narrow range by simultaneously using two flashes, which provided considerably higher possibility to computationally batch image data.

7.4.2 Overlapped Object Recognition

Currently most of image algorithms are still under investigation of testing small lab scale experimental research images and seldom reported in massive industrial application at current stage. Within even highly qualities of experimental image significantly improved by using side-light illumination method with two flashes, the algorithm transformations to abstract mathematical distribution information from planar images are still a challenging research topic at this stage. The following work regarding algorithm transformations, namely Overlapped Object Recognition (OOR) algorithm is an effort to conquer the corner of this challenge.

The result of the Overlapped Object Recognition (OOR) algorithm is illustrated in Figure 7-15. As can be seen from Figure 7-15 (a), most of joint points have been successfully detected after complex algorithm transformation by using OOR algorithm. Then dividing procession in edges for packaged bubbles from the joint point provides

the platform for the next step to identify the single edges and to abstract mathematical distribution information. After tracing arcs from joint points, some individual bubbles are identified from overlapped objects. Therefore, the local parameters, such as bubble locations, centre points and diameters, have the possibility to be abstracted out and recorded.

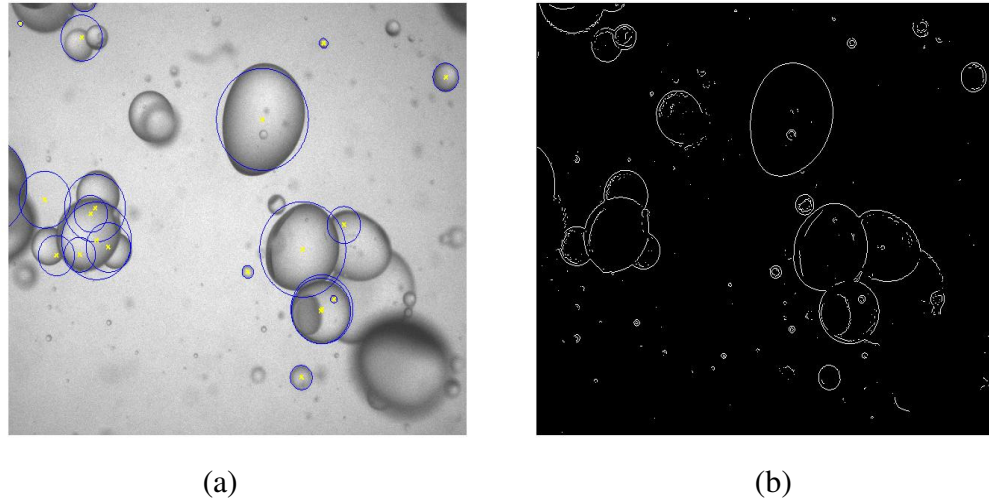


Figure 7-15 Image Processing Results

Some inaccuracies between algorithm edges prediction and physical bubble boundaries are observed in Figure 7-15 (a). In the area of bottom right in of Figure 7-15 (a), the blurring in bubble shape caused by the inexistence of bubble on the focus plane of the camera lens could not reach critical sensitive standards of edge detection and did not recognized by algorithms in this study. The principle behind the edge detection is to search the sharp gradient of image intensity. The smooth gradient of the blur object could not trigger the certain sensitivity of edge detection algorithm to recognize the bubble boundaries. Although the algorithm sensitivity can be reduced, more background noise might be introduced with low sensitivities. Another raised problem is that some bubbles are computationally over-counted more than once with different diameters, which cause over-prediction of void fraction in experimental results. In order to reduce this inaccuracy, the sensitivity of clustering algorithm can be tested in future to optimize tracing steps, selected tolerance and computational cost. Furthermore, more complex

algorithm formation for irregular bubble shape should be considered in order to apply this research to realistic flow conditions.

Chapter 8 Conclusion

During the course of this research, the two-phase bubbly flow in vertical and horizontal pipes has been investigated. Particular interesting has been focused on better understanding interfacial driving force and population balance equations to close the two-fluid model. There are four major contributions from this study: (1) an experimental drag coefficient correlation in terms of local void fraction formulated by Simonnet et al., (2007) has been investigated under various bubbly flow conditions and compared with drag coefficient model proposed by Ishii and Zuber (1979); (2) The Population Balance Approach with Averaged Bubble Number Density (ABND) model has been applied to predict the bubble flow conditions in horizontal pipes where a highly asymmetric internal phase distribution occurs; (3) the performance of an alternative Population Balance Approach, named Direct Quadrature Method of Moments (DQMOM) model has been assessed in simulation of bubbles' behaviors in medium and large sized pipes and validated against experimental data of MTLOOP and TOPFLOW; (4)

8.1 Numerical Investigation of Influence of Interfacial Force on Bubble Flow

The primary aim of this research is to estimate the prediction capabilities of a recently proposed experimental drag coefficient formulation by Simonnet et al. (2007) by validation against experimental results of isothermal gas-liquid bubbly flow in a vertical pipe performed by Hibiki et al. (2001). This experimental model in terms of local void fraction by considering the influence of neighbour bubbles has been also compared with commonly applied Ishii and Zuber (1979) model which classifies flow phenomenon into five categories and describes drag reduction in each categories individually. Coupled with the ABND model (Cheung et al. 2007 a and b), the experimental drag coefficient correlation of Simonnet et al., (2007) has been implemented into ANSYS CFX commercial software via the CFX Expression Language (CEL) to predict the local bubble distribution particularly in bubbly-to-slug transitional regime where cap-bubbly

were observed. In general, both drag force models achieved satisfactory agreements between predicted and measured results. The latest coefficient model of Simonnet et al. (2007) provides reasonable better performance since it considers the reduction of drag forces incurred by neighbouring bubbles.

Among these eight cases under investigation, notable discrepancies are found between the numerical prediction and experimental results in bubbly-to-slug transitional flow condition of $\langle j_f \rangle = 0.986$ m/s and $\langle j_g \rangle = 0.321$ m/s. The usage of one group equation to present averaged Sauter mean bubble diameter in ABND model may be one of the reasons for these discrepancies. Moreover, the ignoring of wake entrainment phenomenon in Yao and Morel (2004) model for ABND equations source and sink terms may also result in inaccuracy. Finally, Tomiyama (1998) lift coefficient model only considered the behaviour of single distorted bubble under stagnant flow condition. The lift force in multi-bubble system requires further development.

8.2 On Modelling Horizontal Gas-liquid Bubbly Flow using ABND based Population Balance Approach

In practical industrial application, there are many appliances are running under horizontal gas-liquid bubbly flow since it can provide large interfacial area for heat and mass transfer comparing to other flow condition (such as slug flow, annular flow) under certain gas volume. Nonetheless, this flow orientation received less attention in the literature than vertical bubbly flow. It might be due to the difficulty of the highly asymmetric internal phase distribution. This asymmetry is caused by the buoyant influence which drives the dispersed bubbles towards the top in horizontal pipe. In this study, the internal phase distributions of air-water bubbly flow in a 50.3mm i.d. horizontal pipeline have been simulated using population balance model based on Average Bubble Number Density (ABND) approach. With the aim of assessing the model performance under wide range of flow scenarios, four individual flow conditions of Kocamustafaogullari and Huang (1994 a).with average gas volume fraction from 4.4% to 20% have been modeled.

Generally, satisfactory agreements between predicted and measured results are achieved. The ABND population balance model shows its performance and capability to predict the highly asymmetrical distributed parameters in horizontal bubbly flow (the observed local void fraction can up to 0.65-0.70 and the interfacial area concentration can up to 700-800 m^2/m^3). Some slight inaccuracies are found between the numerical and experimental results at certain locations of pipe. These might due to the numerical turbulent model which could not describe the realistic turbulence physical phenomena. Additional interfacial force such as bouncing force among bubbles may be one of the reasons causing the discrepancies and it needs to be considered to further improve the prediction performance.

8.3 On Modelling Vertical Gas-liquid Bubble Flow using Direct Quadrature Method of Moments (DQMOM) Approach

In order to obtain detailed information regarding bubble size distribution, population balance model (PBM) has been widely applied to track the changes of bubble number. Comparing with traditional Class Method (CM) in PBM such as MUSIG model breaking the bubble size range down into series of groups (commonly into 20 groups) and describing each group with a set of transport equation, the recently developed DQMOM has the advantages of affordable computational cost by transforming the particle size distribution (PSD) into few moments (general into 4 or 6 moments). In this study, the performance of DQMOM coupled with two-fluid model has been investigated to handle isothermal gas-liquid bubble flows. The evaluation of the source terms and the incorporation of appropriate set of equations for the abscissas and weights were implemented with the CFD code ANSYS Inc., CFX-11 to determine the temporal and spatial geometrical changes of the gas bubbles. In this current research, these predicted local radial distributions of bubble void fraction and bubble size distribution are validated against experimental data of MTLOOP measured by Lucas et al. (2005) and TOPFLOW measured by Prasser et al. (2007).

The results of satisfactory agreement between the numerical simulation and experimental measurement shows that the DQMOM model has the capability to predict the detailed bubble size distribution and can be considered as one promising population balance approach. Since it shows the capability to achieve reasonable simulation results under affordable computational time, it shows the prosperous blueprint of utilization in real industrial application where flow conditions are more complicated than the one in lab scale. However, further validation or sensitivity studies are still required to assess the performance of DQMOM against wider range of flow conditions.

8.4 Side-light Illumination Method with Two Flashes and Overlapped Object Recognition (OOR) Method

The dictation of the information of the intensive packed bubbles is continuously a headache in gas-liquid two phase flow experimental design. Since limited information of two-phase flow under flow condition of high gas void fraction where bubbles are close to each other can be provided to develop simulation models, till this stage the capacity of CFD has been stagnant only on simulation of flow conditions with low gas void fraction, up to 30% of gas void fraction to my best knowledge. However, most of industrial applications are running under high gas void fraction flow condition which may be difficult to simulate under current capacity of CFD. Thereby, the breakthrough of experimental method of dictation of the information of the intensive packed bubbles is very important for CFD to be applied to industrial background. In this study, a side-light illumination method with two flashed and Overlapped Object Recognition (OOR) method have been proposed and tested.

Comparing with the traditional photograph methods where illumination resource is generally located at the back of the research objects, the proposed method arranges the illumination resource locating at the sides of the research objects. The shortcoming of the traditional back illumination method is that a large number of bubbles are overlapped in the pictures since the lights travels from the back to the front lenses and brightens all the bubbles in the pipe. This causes massive computational workload for

the bubble detection in the next process stage called image procession. However, with the side-illumination method, only a thin sheet in the pipe has been brightened and only the bubbles in this sheet are captured by the lenses. Thereby, the computational workload has been reduced significantly in recognition of bubble information such as bubble locations and diameters. Even though a side-illumination method with only one flash has been proposed before, it suffered the imbalanced image intensities and incompleteness on the bubble edges which cause difficulties to recognize bubble information. The side-illumination method with two flashes successfully has resolved this problem and contributed to the image dictation.

A recently proposed image process method named Overlapped Object Recognition (OOR) method has been tested in the two-phase field. This algorithm focuses on the dictation of overlapped objects by using a matrix convolution to search the joint points. The results of the Overlapped Object Recognition (OOR) algorithm are positive. Most of joint points have been successfully detected after complex algorithm transformation by using this algorithm which provides the platform for identification of individual bubble and abstract the information such as bubble locations and diameters. Some inaccuracies have been observed in the picture. The blurring of the bubble shape may be one of the reasons to cause these inaccuracies. Additionally, the sensitivities of sub-algorithms including tracing, clustering etc. should be further tested in the future in order to optimize the algorithm and achieve the best performance.

8.5 Recommendations on CFD Development and Future Researches on Two-phase Flow

Population balance model has been widely utilized to statistically describe the distribution information of bubble size and interfacial area in order to understand bubbles' behaviors and provide better designs. However, this research shows some bubbles' behaviors, particularly in horizontal bubbly flow, could not be described by the currently utilized interfacial driving forces. Thereby, more researches are needed to discover additional interfacial driving forces in the future. In addition, the computational cost is a continuous limitation to obstruct the development of CFD. The

recently proposed DQMOM model successfully reduces the computational workload; however, more sensitivities test of this model should be researched in order to confidently apply this model. Furthermore, due to the difficulties of recognition and identification on the overlapped bubbles in experiments, the limited information which provided by experiments hinders the CFD application in industries. More work should be carried on the experimental designs and improvements to reduce the chance of overlapped bubbles. Algorithms of identification individual object from overlapped bubbles are also important and should be focused in the future researches.

References

ANSYS. *CFX-11 User Manual*. ANSYS-CFX, 2006.

Antal S.P., Lahey Jr R.T., Flaherty J.E., (1991), “Analysis of phase distribution in fully developed laminar bubbly two-phase flow”. *International Journal of Multiphase Flow*, **17**, 635.

Andreussi, P., A. Paglianti, et al. (1999), “Dispersed bubble flow in horizontal pipes”. *Chemical Engineering Science*, **54**, 1101.

Bannari R., Kerdouss F., Selma B., Bannari A., Proulx P. (2008). “Three dimensional mathematical modelling of dispersed two phase flow using class method of population balance in bubble columns”. *Computational Chemical Engineering*, **32**, 3224.

Beattie D.R.H., (1972) “2-phase flow structure and mixing length”, *Nuclear Engineering Design*, **21**, 46.

Behzadi A., Issa R. I., Rusche H. (2004). “Modelling of dispersed bubble and droplet flow at high phase fractions”, *Chemical Engineering Science*, **59**, 759.

Bendjaballah, N., Dhaouadi, H., Poncin, S., Midoux, N., Hornut, J. M., & Wild, G. (1999). “Hydrodynamics and flow regimes in external loop airlift reactors”. *Chemical Engineering Science*, **54**, 5211.

Bertola F., Baldi G., Marchisio D., Vanni M. (2004). “Momentum transfer in a swarm of bubbles: estimates from fluid-dynamic simulations”, *Chemical Engineering Science*, **59**, 5209.

Bhaga D, Weber M.E. (1981). “Bubble in viscous liquids: shapes, wakes and velocities”, *Journal of Fluid Mechanism*, **105**, 61.

Bhole M. R., Joshi J. B., Ramkrishna D. (2008). “CFD simulation of bubble columns incorporating population balance modelling”. *Chemical Engineering Science*, **63**, 2267.

Boyera, C., Duquenneb, A., Wild, G., (2002) “Measuring techniques in gas–liquid and gas–liquid–solid reactors”, *Chemical Engineering Science*, **57**, 3185.

-
- Burns, A. D., Frank, T., Hamill, I. and Shi, J., (2004), "The Favre Averaged Drag Model for Turbulent Dispersion in Eulerian Multiphase Flow", *Proceedings of the Fifth International Multiphase Flow, Yokohama, Japan*.
- Camarasa, E, Vial, C., Poncin, S., Wild, G., Midoux, N., & Bouillard, J. (1999), "Influence of coalescence behaviour of the liquid and of gas sparging on hydrodynamics and bubble characteristics in a bubble column". *Chemical Engineering and Processing*, **38**, 329.
- Canny, J., (1986), "A computational approach to edge detection", *Transaction on Pattern Analysis and Machine Intelligence PAMI-8*, 679.
- Chesters A.K. Hoffman G., (1982), "Bubble coalescence in pure liquids", *Applied Scientific Research*, **38**, 353.
- Chesters, A.K., (1991),
"The Modeling of Coalescence Processes in Fluid-Liquid Dispersion: A Review of Current Understanding", *Trans. I. Chem. Eng.*, **69**, 259.
- Chen p., Sanyal J., Dudukovic M. P. (2005). "Numerical simulation of bubble columns flows: effect of different breakup and coalescence closures". *Chemical Engineering Science*, **60**, 1085.
- Cheung S.C.P., Yeoh G.H., Tu J.Y. (2007 a), "On the modelling of population balance in isothermal vertical bubbly flows – average bubble number density approach". *Chemical Engineering Process*, **46**, 742.
- Cheung S.C.P., Yeoh G.H., Tu J.Y. (2007 b), "On the numerical study of isothermal vertical bubbly flow using two population balance approaches". *Chemical Engineering Science*, **62**, 4659.
- Cheung S.C.P., Yeoh G.H., Tu J.Y. (2008), "Population balance modelling of bubbly flows considering the hydrodynamics and thermomechanical processes", *AIChE Journal*, **54**(7), 1689.
- Cheung S.C.P., Yeoh G.H., Tu J.Y. (2009 a), "A review of population balance modelling for isothermal bubbly flows", *Journal of Computational Multiphase Flows*, **1**(2), 161.
- Cheung S.C.P., Yeoh G.H., Tu J.Y. (2009 b), "Direct Quadrature Method of Moments for Isothermal Bubbly Flows", *The 7th International Conference on*

-
- Computational Fluid Dynamics in the Minerals and Process Industries, December 2009, Melbourne, Australia.*
- Chigier N., (1991) "Optical image of sprays" *Progress Energy Combustion Science*, **17**, 211.
- Churchill S. W. (1989). "A theoretical structure and correlating equation for the motion of single bubbles", *Chemical Engineering Process*, **26**, 269.
- Clift R., Grace J. R., Weber M. E. (1978), "Bubble, Drops, and Particles", *Academic Press*, New York.
- Coulaloglu, C.A., (1975), "Dispersed phase interactions in an agitated flow vessel" Ph.D. Dissertation, Illinois Institute of Technology, Chicago.
- Coulaloglu, C.A., Tavlarides, L.L., (1977), "Description of interaction processes in agitated liquid-liquid dispersions", *Chemical Engineering Science*, **32**, 1289.
- Davidson J. F., Harrison D. (1966). "The behaviour of a continuously bubbling fluidised bed". *Chemical Engineering Science*, **21**, 731.
- Dorao C.A., Jakobsen H.A., (2006), "Numerical calculation of the moments of the population balance equation". *Journal of computational and applied mathematics*, **196**, 619.
- Dorao C.A., Lucas D., Jakobsen H.A., (2008), "Prediction of the evolution of the dispersed phase in bubbly flow problems". *Applied mathematical modelling*, **32**, 1813.
- Doublié L., (1991), "The drainage and rupture of a non-foaming liquid film formed upon bubble impact with a free surface", *International Journal of Multiphase Flow*, **17**, 783.
- Duineveld P.C., (1994), "Bouncing and coalescence of two bubbles in water", Ph.D. Dissertation, University of Twente, The Netherlands.
- Drew D.A., Lahey Jr., R.T. (1979). "Application of general constitutive principles to the derivation of multidimensional two-phase flow equation". *Int. J. Multiphase Flow*, **5**, 243.
- Duan X.Y., Cheung S.C.P., Yeoh G.H., Tu J.Y., Krepper E. and Lucas D., (2011), "Gas-liquid flows in medium and large vertical pipes", *Chemical Engineering Science*, **66**, 872.

-
- Duda, R.O., Hart, P.E., (1972), "Use of the Hough transformation to detect lines and curves in pictures". *Communications of ACM*, **15**, 11.
- Ekambara, K., Sanders, R. S., Nandakumar, K., Masliyah, J. H., (2008), "CFD simulation of bubbly two-phase flow in horizontal pipes". *Chemical Engineering Journal*, **144**, 277.
- Finlayson, B.A., (1972), "The method of weighted residuals and variational principles", *Mathematics in Science and Engineering*, **87**, Academic Press, New York.
- Frank T., Shi J., Burns A.D., (2004), "Validation of Eulerian multiphase flow models for nuclear safety application", in: *Proceeding of the Third International Symposium on Two-Phase Modelling and Experimentation*, Pisa, Italy.
- Fredrickson A.G., Ramkrishna D., Tsuchiya H.M., (1967), "Statistics and dynamics of procaryotic cell population". *Mathematical Bioscience*, **1**, 327.
- Friedlander S. K. (1977), "Smoke, dust, and haze", *Wiley. New York*.
- Friedlander S. K. (2000), "Smoke, dust, and haze: foundationals of aerosol dynamics" (2nd Edition). *Oxford: Oxford University Press*.
- Fu X.Y., Ishii M., et al., (2002) "Two-group interfacial area transport in vertical air-water flow I, mechanistic model", *Nuclear Engineering Design*, **219**, 143.
- Gordon R.G., (1968), "Error bounds in equilibrium statistical mechanics". *Journal of Mathematical Physics*, **9**, 655.
- Grace, J. R. (1973), "Shapes and velocities of bubbles rising in infinite liquids". *Trans. Chem. Eng.*, **51**, 116
- Grace, H. P. (1982), "Dispersion phenomena in high viscosity immiscible fluid systems and application of static mixers as dispersion devices in such systems", *Chemical Engineering Communication*, **14**, 225.
- Grienberger J., Honfmann H. (1992). "Investigations and modelling of bubble columns". *Chemical Engineering Science*, **47**, 2215.
- Haoues, L., Olekhnovitch, A., Teyssedou, A., (2009), "Numerical study of the influence of the internal structure of a horizontal bubbly flow on the average void fraction". *Nuclear Engineering Design*, **239**, 147.
- Hibiki T., Ishii M. (2000), "One-group interfacial area transport of bubbly flows in vertical round tubes", *International Journal of Heat and Mass Transfer*, **43**, 2711.

- Hibiki T., Ishii M., Xiao Z., (2001), "Axial interfacial area transport of vertical bubble flows", *International Journal of Heat and Mass Transfer*, **44**, 1869.
- Hibiki T., Ishii M., (2002), "Development of one-group interfacial area transport equation in bubbly flow systems", *International Journal of Heat and Mass Transfer*, **45**, 2351.
- Hibiki T., Ishii M. (2007), "Lift force in bubbly flow systems". *Chemical Engineering Science*, **62**, 6457.
- Hidy G. M., and Broke J. R., (1970) "The dynamics of aerocolloidal systems", *Pergamon*.
- Ho M.K., Yeoh G.H., (2005). "Phenomenological investigation of gas-liquid flows". *Trans. American Nucl. Soci.*, **93**, 408.
- Howarth W. J., (1964). "Coalescence of drops in a turbulent flow field". *Chemical Engineering Science*, **19**, 33.
- Hulburt H.M., Katz S., (1964), "Some problems in particle technology: A statistical mechanical formulation". *Chemical Engineering Science*, **19**, 574.
- Ishii M. (1975). "Thermo-Fluid Dynamic Theory of Two-Phase Flow", Chapter IX and X, Eyrolles, Paris, or Scientific and Medical Publication of France, N.Y.
- Ishii, M., Zuber, N., (1979), "Drag coefficient and relative velocity in bubbly, droplet or particulate flows". *AIChE J.*, **25**, 843
- Ishii, M., Kin, S. and Uhle, J., (2002), "Interfacial Area Transport: Model Development and Benchmark Experiments", *International Journal of Heat and Mass Transfer*, **45**, 3111.
- Jamialahmadi M., Branch C., Muller-Steinhagen H., (1994). "Terminal bubble rise velocity in liquids". *Chemical Engineering Research and Design*, **72**, 119.
- Kendoush A.A. (2001). "Hydrodynamic model for bubbles in a swarm", *Chemical Engineering Science*, **56**, 235.
- Kendoush A.A., Mohammed T. J., Abid B. A., Hameed M. S. (2004). "Experimental investigation of the hydrodynamic interaction in bubbly two-phase flow", *Chemical Engineering and Processing*, **43**, 23.
- Kennard E.H., (1938). "Kinetic theory of gases". *McGraw-Hill, New York*.

-
- Kierkegaard P., (1992), "A method for detection of circular arcs based on the Hough transform". *Machine Vision and Applications*, **5**, 249.
- Kim S., Park J. H., Kojaosy G., Kelly, J. M., Marshall, S. O., (2007), "Geometric effects of 90-degree Elbow in the development of interfacial structures in horizontal bubbly flow". *Nuclear Engineering Design*, **237**, 2105.
- Kim S., Callender, K., Kojasoy, G., (2009), "Interfacial area transport in horizontal bubbly flow with 90-degree elbow", *Nuclear Technology*, **167**, 20.
- Kocamustafaogullari G., Wang Z., (1991), "An experimental study on local interfacial parameters in a horizontal bubbly 2-phase flow. *International Journal of Multiphase Flow*, **17**, 553.
- Kocamustafaogullari G., Huang W. D., (1994 a), "Internal structure and interfacial velocity development for bubbly 2-phase flow. *Nuclear Engineering and Design*, **151**, 79.
- Kocamustafaogullari G., Huang W. D., Razi J., (1994 b), "Measurement and modeling of average void fraction, bubble size and interfacial area". *Nuclear Engineering and Design*, **148**, 437.
- Kocamustafaogullari G., Ishii M., (1995) "Foundation of the interfacial area transport equation and its closure relations". *International Journal of Heat and Mass Transfer*, **38**, 481.
- Krepper E., Lucas D., Prasser H., (2005), "On the modelling of bubbly flow in vertical pipes". *Nuclear Engineering and Design*, **235**, 597.
- Kuboi R., et al., (1972) "Collision and coalescence of dispersed drops in turbulent liquid flow", *Journal of Chemical Engineering of Japan*, **5**, 423.
- Lahey Jr., R.T., Sim S., Drew D.A., (1979). "An evaluation of interfacial drag models for bubbly two-phase flow". In: *Chen, J.C., BankoE, S.G., (Eds.), ASME 18th National Heat Transfer Conference, New York, USA, 11*.
- Lage P. L. C., & EspLosito, R. O. (1999). "Experimental determination of bubble size distributions in bubble columns: Prediction of mean bubble diameter and gas hold up". *Powder Technology*, **101**, 142.
- Lee C.H., et al. (1987), "Bubble breakup and coalescence in turbulent gas-liquid dispersions", *Chemical Engineering Communications*, **59**, 65.

-
- Lehr, F., Mewes, D., Millies, M., (2002), "Bubble-size Distribution and Flow Fields in Bubble Columns", *AIChE Journal* **42**, 1225.
- Levich, V.G. Physicochemical Hydrodynamics., (1962), "Prentice-Hall, Englewood Cliffs", NJ, USA.
- Lo S. (1996), "Application of the MUSIG model to bubbly flows". *AEAT-1096*, AEA Technology.
- Lopez de Bertodano, M., (1992), "Turbulent Bubbly Two-Phase Flow in a Triangular Duct", *PhD Dissertation, Rensselaer Polytechnic Institute, New York*.
- Lopez de Bertodano, M., (1998), "Two-Fluid Model for Two-phase Turbulent Jet", *Nuclear Engineering Design*, **179**, 65.
- Li C., Yeoh G.H., Cheung Sherman C. P. and Tu Jiyuan, (2010 a) "Modelling Horizontal Gas-Liquid Flow using Averaged Bubble Number Density Approach", *Journal of Computational Multiphase Flows*, **2(2)**, 89.
- Li C., Cheung Sherman C. P., Yeoh G.H., and Tu Jiyuan, (2010 b) "On Modelling Horizontal Gas-liquid Bubbly Flow using Population Balance Approach" *The 17th Australasian Fluid Mechanics Conference, December, Auckland, New Zealand*.
- Li C., Cheung Sherman C. P., Yeoh G.H., and Tu Jiyuan, (2009 a) "A study of drag force in isothermal bubbly flow" *Journal of Computational Multiphase Flows*, **1(4)**, 295.
- Li C., Cheung Sherman C. P., Yeoh G.H., and Tu Jiyuan, (2009 b) "Influence of drag forces of a swarm of bubbles in isothermal bubbly flow conditions" *The 7th International Conference on Computational Fluid Dynamics in the Minerals and Process Industries, December 2009, Melbourne, Australia*.
- Li C., Cheung Sherman C. P., Tu Jiyuan, and Yeoh G.H., (2008) "3-D Numerical simulation of isothermal upward bubbly flow: A study of drag force in multi-bubble system based on ABND model" *2008 ANSYS Australia User Conference, November 2008, Sydney, Australia*
- Liao Y. X., Lucas D., (2009), "A literature review on theoretical models for drop and bubble breakup in turbulent dispersions", *Chemical Engineering Science*, **64**, 3389.
- Liao Y. X., Lucas D., (2010), "A literature review on mechanisms and models for the coalescence process of fluid particles". *Chemical Engineering Science*, **65**, 2851.

- Lim, K., Xin, K., Hong, G., (1995), "Detection and estimation of circular segments". *Pattern Recognition Letters*, **16**, 627.
- Lin, T.J., Tsuchiya, K., & Fan, L.S. (1998), "Bubble flow characteristics in bubble columns at elevated pressure and temperature". *American Institute of Chemical Engineers Journal*, **44**, 545.
- Liu Y., Hibiki T., Ishii M., Kelly J. M. (2008). "Drag coefficient in one-dimensional two-group two-fluid model". *International Journal of Heat Fluid Flow*, **29**, 1402.
- Lucas D., Krepper E., Prasser H.M., (2005), "Development of co-current air-water flow in a vertical pipe". *International Journal of Multiphase flow*, **31**, 1304.
- Luo H., (1993), "Coalescence, breakup, and liquid circulation in bubble column reactors". *Ph.D Dissertation, the Norwegian Institute of Technology, Trondheim*.
- Luo H., Svendsen H., (1996), "Theoretical model for drop and bubble break-up in turbulent dispersions". *AIChE Journal*, **42**, 1225.
- Luthra M., Lopetinsky R.J.G., Sander R.S., Nandakumar K., Masliyah J.H., (2003), "A new device to determine oil sands processability under hydrotransport condition", *Canadian Journal of Chemical Engineering*, **82**, 752.
- Manera A., Ozar B., Paranjape S., Ishii M. and Prasser H.M. (2009), "Comparison between wire-mesh sensors and conductive needle-probes for measurements of two-phase flow parameters", *Nuclear Engineering and Design*, **239**, 1817.
- Mabrouk R., Chaouki J., Guy C. (2007). "Effective drag coefficient investigation in the acceleration zone of an upward gas-solid flow". *Chemical Engineering Science*, **62**, 317.
- Magnaudet J., Eames I. (2000). "The motion of high-Reynolds-Number Bubbles in Inhomogeneous flows". *Annu. Rev. Fluid Mech.*, **32**, 659.
- Malysa K., Ng S., Cymbalisty L., Czarnecki J., Masliyah J., (1999), "A method of visualization and characterization of aggregate flow inside a separation vessel, Part I: Size, shape and rise velocity of the aggregates", *International Journal of Mineral Process.*, **55**, 171.
- Mankowski P., Ng S., Siy R., Spence J., Stapleton P., (1999), " Syncrude's low energy extraction process: commercial implementation", *Proceeding of 31st Annual Meeting of Canada Mineral Processing, Ottawa*, 153.

-
- Marchisio D.L., Vigil D.R., Fox R.O., (2003a), “Quadrature method of moments for aggregation-breakage processes”. *Journal of Colloid Interface Science*, **258**, 322-324.
- Marchisio D.L., Pikturna J.T., Fox R.O., Vigil R.D., (2003b), “Quadrature method for moments for population-balance equations”. *AIChE Journal*, **49**, 1266.
- Marchisio D.L., Vigil D.R., Fox R.O., (2003c), “Implementation of the quadrature method of moments in CFD codes for aggregation-breakage problems”. *Chemical Engineering Science*, **58**, 3337.
- Marchisio D.L., Fox R.O., (2005), “Solution of population balance equations using the direct quadrature method of moments”. *Journal of Aerosol Science*, **36**, 43.
- MediaCybernetics, *image-Pro Plus 7.0, User Manual*, MediaCybernetics Image-pro Plus, 2010.
- Mei R, Klausner JF, Lawrence CJ. (1994). “A note on the history force on a spherical bubble at finite Reynolds number”. *Phys. Fluids* **6**, 418.
- Melen T., Ozanian T., (1993), “A fast algorithm for dominant point detection on chain-coded contours”, *In: Fifth International Conference on Computer Analysis of Images and Patterns, LNCS 719, Springer, Berlin*, 245.
- Menter, F. R., (1994), “2-equation eddy-viscosity turbulence models for engineering applications”. *AIAA J.*, **32**, 1598.
- McCoy B.J., Madras G., (2003), “Analytic solution for a population balance equation with aggregation and fragmentation”. *Chemical Engineering Science*, **58**, 3049.
- McGraw R., (1997), “Description of aerosol dynamics by the quadrature method of moments”. *Aerosol Science and Technology*, **27**, 255.
- McGraw R., Wright D.L., (2003), “Chemically resolved aerosol dynamics for internal mixtures by the quadrature method of moments” *Journal of Aerosol Science*, **34**, 189.
- Mishima K., Ishii M., (1984) “Flow regime transition criteria for upward two-phase flow in vertical tubes”, *International Journal of Heat and Mass Transfer*, **27**, 723.
- Miyahara, T., Hamaguchi, M., Sukeda, Y., & Takahashi, T. (1986). “Size of bubbles and liquid circulation in a bubble column with a draught tube and a sieve plate”. *Canadian Journal of Chemical Engineering*, **64**, 718.

- Moore DW. (1965). "The velocity of rise of distorted gas bubbles in a liquid of small viscosity", *Journal of Fluid Mechanism*, **23**, 749.
- Moraga, F.J., Larreteguy, A.E., Drew, D.A., Lahey, R. T. Jr., (2003), "Assessment of Turbulent Dispersion Models for Bubbly Flows in the Low Stokes Number Limit", *International Journal of Multiphase Flow*, **29**, 655.
- Neal L.G., Bankoff B.G., (1963), "A high resolution resistivity probe for determination of local void properties in gas-liquid flow", *AIChE J.*, **9**, 490.
- Olmos E., Gentric C., Vial Ch., Wild G., Midoux N., (2001), "Numerical simulation of multiphase flow in bubble column. Influence of bubble coalescence and break-up". *Chemical Engineering Science*, **56**, 6359.
- Oolman, T., Blanch, H.W., (1986 a), "Bubble coalescence in air-sparged bioreactor". *Biotechnology*, **28**, 578.
- Oolman, T., Blanch, H.W., (1986 b), "Bubble coalescence stagnant liquids". *Chemical Engineering Communication*, **43**, 237.
- Park J.Y., Blair L.M., (1975), "The effect of coalescence on drop size distribution in an agitated liquid-liquid dispersion", *Chemical Engineering Science*, **30**, 1057.
- Pei, S., Horng, J., (1995), "Circular arc detection based on the Hough transform". *Pattern Recognition Letters*, **16**, 615.
- Peterson, D. A., Tankin, R. S., & Banko3, S. G. (1984). "Holographic measurements of bubble size and velocity in three-phase systems". In J.M. Delhay & G. Cognet (Eds.), *Measuring techniques in gas-liquid two-phase flows (pp. 1-21)*. Berlin, Heidelberg, New York, Tokyo: Springer.
- Pla, F., (1996), "Recognition of partial circular shapes from segmented contours". *Computer Vision and Image Understanding*, **63**, 334.
- Pochorecki R., Moniuk W., Bielski P., Zdrojkwoski A., (2001), 'Modelling of the coalescence/redisperison processes in bubble columns". *Chemical Engineering Science*, **56**, 6157.
- Politano M. S., Carrica P.M., Converti J. (2003). "A model for turbulent polysidperse two phase flow in vertical channels". *Int. J. of Multiphase Flow*, **29**, 1153
- Prasser, H.M., Bo'ttger, A., Zschau, J., (1998), "A new electrode-mesh tomograph for gas-liquid flows", *Flow Measurement and Instrumentation*, **9**, 111.

-
- Prasser, H.M., Beyer, M., Carl, H., Gregor, S., Lucas, D., Pietruske, H., Schutz, P., Weiss, F.P., (2007), "Evolution of the structure of a gas-liquid two-phase flow in a large vertical pipe". *Nuclear Engineering and Design*, **237**, 1848.
- Prince M.J., Blanch H.W., (1990), "Bubble coalescence and break-up in air sparged bubble columns". *AIChE Journal*, **36**, 1485.
- Ramkrishna D., Borwanker J.D., (1973), "A puristic analysis of population balance". *Chemical Engineering Science*, **28**, 1423.
- Ramkrishna D. (1979), "Statistical models of cell populations, In: Ghose TK, Fiechter A, Blakebrough N (Eds.)", *Advances in Biochemical Engineering*, vol. 11, Berlin: Springer.
- Ramkrishna D., (1985), "The status of population balances". *Reviews in Chemical Engineering*, **3**, 49.
- Ramkrishna D., (2000), "Population balances: Theory and applications to particulate systems in engineering". New York: Academic press.
- Ramkrishna D., Mahoney A.W. "Population balances modelling, (2002), Promise for the future". *Chemical Engineering Science*, **57**, 595.
- Randolph A.D., Larson M.A. (1964), "A population balance for countable entities". *Canadian Journal of Chemical Engineering*, **42**, 280.
- Randolph A.D., Larson M.A. (1971), "The theory of particulate processes" *New York: Academic Press*.
- Rosin, P.L., West, G.A.W., (1995). "Nonparametric segmentation of curves into various representations". *IEEE Transactions on Pattern Analysis and Machine Intelligence* **17**, 1140.
- Rotta J.C., (1972), "*Turbulente Stromungen*", Teubner B.G., Stuttgart.
- Ruan X.D., Zhao W.F., (2005) "Recognizing of overlapped coal particles in microscope image", *Journal of China Coal Society*, **30**, NO. 6
- Rusche H., Issa R. I. (2000). "The effect of voidage on the drag force on particles, droplets and bubbles in dispersed two-phase flow". In *Japanese European Two-Phase Flow Meeting, Tshkuba, Japan*.
- Sakaue, K., (1982), "The application of iterative method on the image processing". *Jouhou Syori Gakkai Ronbunshuu* **23**, 641.

- Sakaue, K., Takagi, M., (1983). "Separation of images of overlapped particles by iterative method". *Jouhou Syori Gakkai Ronbunshuu*, **24**, 561.
- Sanders, R. S., Razzaque, M. M., Schaan, J., Nandakumar, K., Masliyah, J. H., Afacan, A., Shijie, L., (2004), "Bubble size distributions for dispersed air - Water flows in a 100 mm horizontal pipeline". *Canadian Journal of Chemical Engineering*, **82**, 858.
- Sato Y., Sadatomi M., Sekoguchi K., (1981). "Momentum and heat transfer in two-phase bubbly flow – I". *International Journal of Multiphase Flow*, **7**, 167.
- Scott W.T., (1968), "Analytic studies of cloud droplet coalescence". *Journal of the Atmospheric Science*, **25**, 54.
- Serizawa A., Kataoka I., (1988), "Phase distribution in two-phase flow", in: Afgan NH, *Transient phenomena in multiphase flow*, Washington, DC.
- Sevik, M., Park, S.H., (1973), "The splitting of drops and bubbles by turbulent fluid flow". *J. Fluid Eng., Trans. ASME*, **95**, 53.
- Shen L.P., Song X.Q., Iguchi M. and Yamamoto F. (2000), "A method for recognizing particles in overlapped particle images", *Pattern Recognition Letters*, **21**, 21.
- Shinnar R., Church J.M., (1960), "Predicting particle size in agitated dispersions", *Industrial and Engineering Chemistry*, **52**, 253.
- Simonnet M., Gentric C., Olmos E., Midoux N. (2007), "Experimental determination of the drag coefficient in a swarm of bubbles", *Chemical Engineering Science*, **62**, 858.
- Simonnet M., Gentric C., Olmos E., Midoux N. (2008), "CFD simulation of the flow field in a bubble column reactor: Importance of the drag force formulation to describe regime transitions", *Chemical Engineering and Processing*, **47**, 1726.
- Sovova H., (1981), "Breakage and coalescence of drops in a batch stirred vessel- II, Comparison of model and experiments", *Chemical Engineering Science*, **36**, 1567.
- Taitel Y. and Dukler A.E., (1976), "A Model for Predicting Flow Regime Transitions in Horizontal and near Horizontal Gas-Liquid Flow", *AIChE J.*, **22**, 47-55,
- Tabib M.V., Roy S. A., Joshi J. B. (2008). "CFD simulation of bubble column-An analysis of interphase forces and turbulence models". *Chemical Engineering Journal*, **139**, 589.
- Takagi, S., Matsumoto, Y., (1998), "Numerical Study on the Forces Acting on a Bubble and Particle", *Proceedings of the Third International Conference on Multiphase Flow*, Lyon, France.

-
- Talley, J. D., Kim, S., (2010), "Horizontal bubbly flow with elbow restrictions: Interfacial area transport modeling", *Nuclear Engineering Design*, **240**, 1111.
- Taylor G.I. (1934), "The formation of emulsions in definable fields of flow", *Proc. R. Soc. Lond. A* **146**, 500.
- Taylor TD, Acrivos A., (1964), "On the deformation and drag of a falling viscous drop at low Reynolds number", *Journal of Fluid Mechanism*. **18**, 466.
- Tian Z.F. (2007), "Numerical modelling of turbulent gas-particle flow and its applications", *PhD thesis*.
- Tomiyama A., (1998), "Struggle with computational bubble dynamics", in: *Proceeding of the Third International Conference on Multiphase Flow*. Lyon, France.
- Tomiyama, A. (2004). "Drag, lift and virtual mass forces acting on a single bubble". *3rd International Symposium on Two-phase Flow Modelling and Experimentation*, Pisa, 22.
- Tselishcheva, E. A., Antal, S. P., Podowski, M., (2010), "Mechanistic multidimensional analysis of horizontal two-phase flows. *Nuclear Engineering Design*, **240**, 405-415.
- Wallis G.B. (1969). "One-Dimensional Two-Phase Flow". *McGraw Hill, New York*.
- Wallwork V., (2003), "An Investigation of Oil Sand Processability", *M.Sc. Thesis, University of Alberta, Edmonton*.
- Wang, S.K., Lee, S.J., Lahey, R.T. Jr., Jones, O.C., (1987), "3-D Turbulence Structure and Phase Distribution Measurements in Bubbly Two-Phase Flows", *International Journal of Multiphase Flow*, **13**, 327.
- Wang T., et al (2005 a), "Theoretical prediction of flow regime transition in bubble columns by the population balance model", *Chemical Engineering Science*, **60**, 6199.
- Wang T., et al (2005 b), "Population balance model for gas-liquid flows: influence of bubble coalescence and breakup models", *Industrial Engineering Chemical Research*, **44**, 7540.
- Wellek, R.M., Agrawal, A.K., Skelland, A.H.P., (1966), "Shapes of Liquid Drops Moving in Liquid Media", *AIChE Journal*, **12**, 854.
- Wilcox, D.C., (1988), "Reassessment of the Scale-Determining Equation for Advanced Turbulence Models", *AIAA Journal*, **26**, 1299.

-
- Williams, M.M.R., (1986), "Some topics in nuclear aerosol dynamics", *Progress in Nuclear Energy*, **17**, 1.
- Wu, Q., S. Kim, M. Ishii, S.G. Beus, (1998), "One-group interfacial area transport in vertical bubble flow", *International Journal of Heat and Mass Transfer*, **41**, 1103.
- Yang H., Zhao T.S., Cheng P., (2004), "Gas-liquid two-phase flow patterns in a miniature square channel with a gas permeable sidewall", *International Journal of Heat and Mass Transfer*, **47**, 5725.
- Yao, W., Morel, C., (2004), "Volumetric interfacial area prediction in upward bubbly two-phase flow". *International Journal of Heat and Mass Transfer*, **47**, 307.
- Yeoh, G. H., Tu, J. Y., (2004), "Modelling Gas-liquid Bubbly Flow", *15th Australasian Fluid Mechanics Conference*, 13-17 Dec.
- Yeoh, G. H., Tu, J. Y., (2005), "A unified model considering force balances for departing vapour bubbles and population balance in subcooled boiling flow", *Nuclear Engineering and Design*, **235**, 1251.
- Yeoh, G. H., Tu, J. Y., (2006), "Numerical modelling of bubbly flows with and without heat and mass transfer", *Application of Mathematical Model*, **30**, 1067.
- Yuen, P.C., Feng, G.C., (1996), "A novel method for parameter estimation of digital arc". *Pattern Recognition Letters*, **17**, 929.
- Zhang L., Yang C., Mao Z. X. (2008), "Unsteady motion of a single bubble in highly viscous liquid and empirical correlation of drag coefficient". *Chemical Engineering Science*, **63**, 2099.
- Zuber N., F.W. Staub, G. Bijwaard, and P.G. Kroeger, (1967), "Steady state and transient void fraction in two-phase flow system". *General Electric Co. Report GEAP-5417*, **1**